Investigating the molecular mechanisms that underpin SLBP function & histone mRNA metabolism during S phase of the cell cycle

Aaron Smith

Thesis submitted in partial fulfilment of the requirements
for the degree of Doctor of Philosophy

The University of Sheffield
Faculty of Science
School of Biosciences

January 2023

Abstract

During DNA replication, newly replicated DNA strands associate with histone proteins in order to condense and form chromatin. The rate of DNA replication and the rate of histone protein synthesis are tightly coupled to maintain genomic integrity. Under conditions of replication stress, replication forks slow or stall and the intra-S phase checkpoint is activated. At the same time, histone mRNA is rapidly degraded by the histone mRNA decay pathway to inhibit the production of new histones. Müller et al. (2007) previously demonstrated that activated checkpoint sensors are required to initiate histone mRNA decay, however, the precise molecular mechanisms that link activated intra-S phase checkpoint signalling and histone mRNA decay are not clear. Recent evidence from the Smythe group suggests that residues in the N-terminus of stem-loop binding protein (SLBP), the master regulator of histone mRNA metabolism, are phosphorylated in response to hydroxyurea-induced replication stress and may be involved in the initiation of histone mRNA decay by promoting the dissociation of SLBP and histone mRNA. In data presented here, it is shown that phosphorylation of S20 and S23 does not regulate histone mRNA decay. Furthermore, the identification and characterisation of an evolutionarily conserved, multifunctional short linear motif (SLiM) in SLBP revealed an important association between residues within the SLiM and S23 that is required for the expression of histone genes in S phase. Surprisingly, the SLiM is present in only two other human proteins, RNF20 and RNF40, whose activity is essential for cell cycle progression and the expression of replication-dependent histone genes. The results presented in this thesis provide a novel insight into the regulation of histone gene expression and suggest the existence of an RYKRKL SLiM-dependent regulatory network that links cell cycle progression, histone gene transcription, histone mRNA 3'UTR processing and histone protein synthesis in vertebrate species.

This work is dedicated to the memories of

Claire Louise Hutchinson (née. Aisbitt), Michelle Briasco,

Cheryl Hughes, Susannah Braybrook, Heather McManamy,

Ruby King, Ian Bayliss and Leslie Devine.

Declaration

I declare that this thesis has been composed solely by myself and that it has not been submitted, in whole or in part, in any previous application for a degree. Except where states otherwise by reference or acknowledgement, the work presented is entirely my own.

Acknowledgements

First and foremost, I would like to express my deepest gratitude to my supervisor and previous undergraduate tutor, Professor Carl Smythe, for his unwavering support and guidance over many years. I am grateful for his trust in my abilities, his patience and for allowing me to pursue my own ideas during this project.

Additionally, I would like to thank all current and previous members of the Smythe Labs, in particular Professor Elizabeth Smythe, Dr Richard Beniston, Dr David Turton and Dr Laura Maple, for training and helpful discussion throughout my time in the lab.

Finally, I would like to thank my family (Brenda, Eric, Ashley, Chloe and baby Claire) for being there, supporting me, loving me and always believing in me. I love you and would not have been able to get through this PhD without you.

Contents

List of Figures

List of Tables

List of Abbreviations

ALK	anaplastic lymphoma kinase
ATM	ataxia-telangiectasia mutated
ATR	ATM and Rad3-related
BSA	bovine serum albumin
°C	degrees Celsius
cDNA	complementary DNA
CKII	casein kinase 2
dATP	deoxyadenosine triphosphate
dCTP	deoxycytidine triphosphate
dGTP	deoxyguanosine triphosphate
dNTP	deoxynucleotide triphosphate
dTTP	deoxythymidine triphosphate
ddH_2O	double distilled water
DMEM	Dulbecco's modified Eagle's medium
DMSO	dimethyl sulphoxide
DNA	deoxyribonucleic acid
DNA-PK	DNA-dependent protein kinase
Dox	doxycycline
DTT	dithiothreitol
E. Coli	Escherichia Coli
EDTA	ethylenediaminetetraacetic acid
EGTA	ethylene glycol tetraacetic acid
FAK	focal adhesion kinase

FBS	foetal bovine serum
FRT	flippase (Flp) recombination target
GAPDH	glyceraldehyde-3-phosphate dehydrogenase
GOI	gene of interest
HU	hydroxyurea
IgG	immunoglobulin G
kDA	kilodalton
LC-MS	liquid chromatography-mass spectrometry
M	molar
mg	milligram
mL	millilitre
mM	millimolar
mRNA	messenger RNA
MMTS	S-methyl methanethiosulfonate
MS	mass spectrometry
NMD	nonsense mediated decay
NT	non-targeting (control siRNA)
Nup54	nucleoporin 54
PBS	phosphate buffered saline
PCR	polymerase chain reaction
PP2A	protein phosphatase 2A
qPCR	quantitative PCR
RNA	ribonucleic acid
RNAi	RNA interference
RNF20	RING finger protein 20
RNF40	RING finger protein 40
rpm	revolutions per minute
SDS	sodium dodecyl sulphate
SDS-PAGE	SDS-polyacrylamide gel electrophoresis
siRNA	short interfering RNA

SLBP	stem-loop binding protein
SLiM	short linear motif
snRNP	small nuclear ribonucleoprotein
ssDNA	single-stranded DNA
TBS	tris-buffered saline
TBST	tris-buffered saline + Tween-20
TCEP	tris(2-carboxyethyl)phosphine hydrochloride
U	enzyme unit
UTR	untranslated region
μg	microgram
μL	microlitre
WB	Western blot
γH2AX	phosphorylated histone H2AX

Chapter 1

Introduction

1.1 The eukaryotic cell cycle

The eukaryotic cell cycle is a tightly regulated series of events occurring in nucleated cells that governs cell growth and leads to cell division and duplication (Harashima et al., 2013). The eukaryotic cell cycle is divided into two main stages: interphase and the mitotic phase. Interphase is itself divided into three stages: G1, S phase and G2. In G1, the cell grows and carries out normal functions. In S phase, DNA replication occurs. In G2, the cell checks for errors in the replicated DNA and makes any necessary repairs before committing to M phase and cell division (Schafer, 1998) (Figure 1.1).

Cell cycle progression is regulated by the sequential activation of cyclins and their cognate kinases, known as cyclin-dependent kinases (CDKs) (Malumbres, 2014). The expression levels of cyclins oscillate and peak throughout the cell cycle in a precise order: cyclin D in G1, cyclin E at the G1/S phase boundary, cyclin A at the end of S phase and cyclin B towards the end of G2 (Murray, 2004) (Figure 1.2). Once the cyclin expression level has crossed a threshold, the cyclins are able to activate their cognate CDK and the activated cyclin/CDK complex becomes functional and promotes the transition from one cell cycle phase to the next (Murray, 2004). Regulation of cell cycle progression is crucial to ensure proper duplication of the cell and defects in cell cycle regulation can result in uncontrolled cell growth and division, leading to the development of proliferative diseases such as cancer (Matthews et al., 2022).

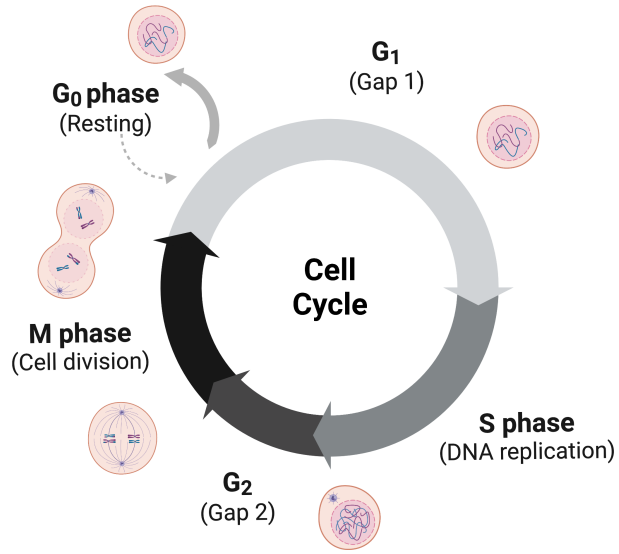

Figure 1.1: The eukaryotic cell cycle. The cell cycle is the process by which a cell grows, replicates its genetic material and then divides into two new daughter cells. The cell cycle is divided into two main stages: interphase, which includes G1 (gap phase 1), S phase (when DNA replication occurs), and G2 (gap phase 2); and the mitotic phase, which is the point at which cells physically segregate condensed mitotic chromosomes and divide into two new cells, each with a faithful copy of the original parent cell DNA. Cells commit to a full cell cycle at the restriction point in G1. Cell cycle checkpoints exist in each phase and can arrest the cell cycle if the integrity of the genetic content of the cell is compromised.

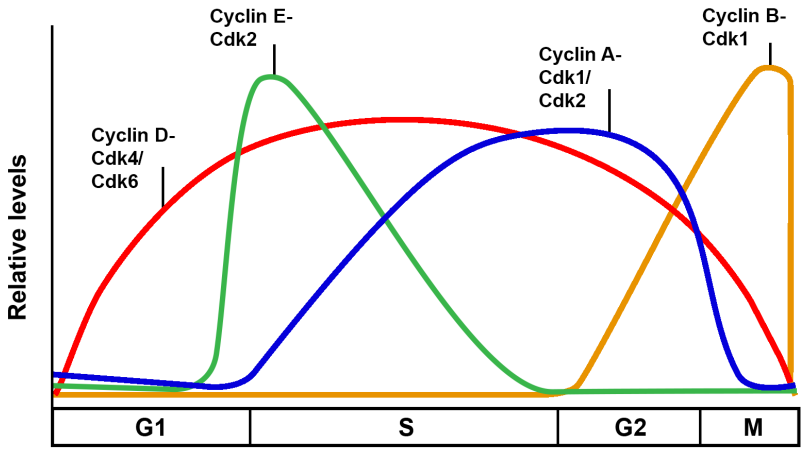

Figure 1.2: Cyclin expression levels during the cell cycle. Progression through the cell cycle is driven by the activity of cyclin/CDK complexes. The cell cycle expression profiles for the four main cyclins are shown with their cognate CDKs. The expression of cyclins oscillates throughout the cell cycle. When the expression of a particular cyclin surpasses a threshold level it is able to bind to and activate its cognate kinase. Cyclin D/CDK4 promotes progression through G1. Cyclin E/CDK2 drives the transition from G1 to S phase. Cyclin A/CDK1/2 drives the progression through S phase and the transition from S phase to G2. Cyclin B/CDK1 activity commits the cell to mitosis. Adapted from Gordon et al. (2018).

1.2 DNA damage

Nearly all of our genetic material is stored in the DNA in the nucleus of an individual cell. As DNA contains the instructions for life, maintaining the integrity of the genome is critical for survival. However, the genome is under a near-constant barrage from endogenous and exogenous factors that can cause structural changes to the DNA molecule. Such factors include ultraviolet (UV) radiation from the sun, chemical agents in the environment or byproducts from normal metabolic processes elsewhere in the cell (Aguilera and García-Muse, 2013; Tubbs and Nussenzweig, 2017) (Figure 1.3).

If left unrepaired, DNA damage can negatively affect DNA replication and gene transcription, which ultimately could prove detrimental to the survival of the cell (Hakem, 2008). Conversely, damage that occurs within a proto-oncogene has the potential to activate oncogenic properties in the transcribed protein, which can lead to cellular transformation and the development of disease (Anderson et al., 1992). Crucially, cells have evolved mechanisms that enable the detection and repair of damaged DNA to ensure normal cellular survival.

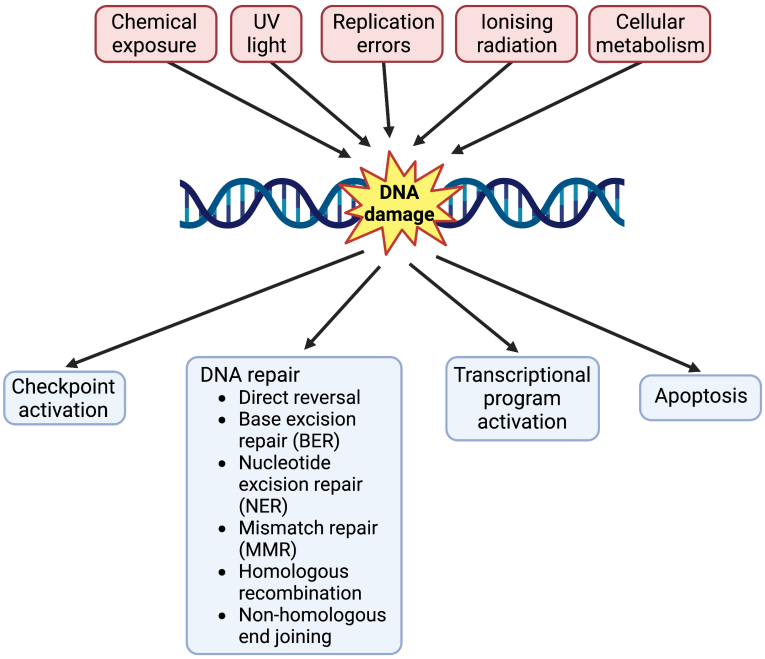

Figure 1.3: Causes and consequences of DNA damage in mammalian cells. DNA damage is caused by a number of endogenous and exogenous sources. DNA damage elicits a DNA damage response (DDR) which involves activation of cell cycle checkpoints, activation of transcriptional programs, DNA repair and, when necessary, the initiation of apoptosis.

1.2.1 Replication stress

Replication stress is defined as the slowing or stalling of DNA replication fork progression and/or protein synthesis (Zeman and Cimprich, 2014). A low level of replication stress can occur with each cell cycle though is overcome during the course of S phase (Wilhelm et al., 2014; Arora et al., 2017). Prolonged replication stress can result in a loss of genetic integrity due to a failure to accurately replicate DNA, as well as DNA damage that arises from replication fork collapse and abandonment (Cortez, 2015; Alexander and Orr-Weaver, 2016).

Replication stress is caused by a number of different endogenous and exogenous sources that continually pose a threat to chromosomal stability and result in the slowing or stalling of replication forks (Mazouzi et al., 2014). Experimentally, replication stress can be induced by chemical reagents such as hydroxyurea (HU). HU inhibits ribonucleotide reductase, an enzyme responsible for catalysing the formation of deoxyribonucleotides from ribonucleotides, resulting in cell cycle arrest due to a depletion of the nucleotide pool that is required for continued DNA synthesis (Elledge et al., 1992).

1.3 Cell cycle checkpoints

Cell cycle checkpoints are cellular surveillance mechanisms that monitor the integrity and fidelity of cellular processes and ensure that relevant processes occur only once before the cell proceeds to the next phase in the cell cycle (Barnum and O'Connell, 2014).

DNA damage arising from endogenous, environmental or chemical sources activates cell cycle checkpoints in G1, S phase and G2/M phases of the cell cycle (Kastan and Bartek, 2004) (Figure 1.4). The signalling pathways activated by cell cycle checkpoint signalling depends on the nature of the DNA damage and the point in the cell cycle in which the checkpoint is activated (Segurado and Tercero, 2009). Defects in cell cycle checkpoint activation can lead to uncontrolled cell proliferation that can result in the development of cancer, which highlights the importance of cell cycle checkpoint signalling pathways and the maintenance of genomic integrity (Molinari, 2000; Kastan and Bartek, 2004).

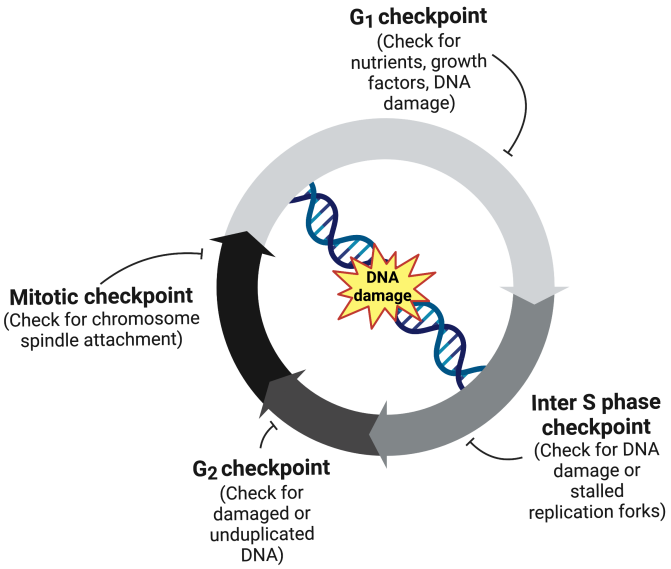

Figure 1.4: Cell cycle checkpoints. Distinct cell cycle checkpoints are activated throughout the cell cycle in response to DNA damage. Activated cell cycle checkpoint signalling results in cell cycle arrest allowing the cell sufficient time to repair DNA before cell cycle progression resumes.

1.3.1 G1/S phase checkpoint

In eukaryotic cells, cell cycle progression from G1 to S phase requires passage through the restriction point, after which the cell is committed to complete the remainder of the cycle, unless later checkpoints are activated, in which case, the cell can undergo apoptosis (Hume et al., 2020). In normal, favourable circumstances, the activity of cyclin E/CDK2 promotes the transition from G1 to S phase. Cyclin E/CDK2 phosphorylates retinoblastoma protein (Rb) and other S phase transition proteins, such as NPAT. Phosphorylation of Rb promotes the dissociation of the Rb-bound S phase transcription factor E2F, which is then able to activate transcription of S phase-specific genes that are required for progression through S phase (Bartek et al., 2004).

If conditions are unfavourable at the time the cell reaches the restriction point, the cell decides not to proceed with S phase and activates PIKK family proteins (ATM, ATR, CHK1, CHK2) leading to the phosphorylation and stabilisation of P53 (Appella and Anderson, 2001). Stabilised P53 then regulates the transcription of the CDK inhibitor $p21^{Cip1}$. Once synthesised, $p21^{Cip1}$ binds to cyclin D/CDK4 and promotes the degradation of cyclin D (Agami and Bernards, 2000). $p21^{Cip1}$ then binds to and inhibits the activity of cyclin E/CDK2, thereby preventing the phosphorylation of Rb, the release of E2F, the phosphorylation of NPAT and the expression of S phase-specific genes (Poon et al., 1996).

1.3.2 Intra-S phase checkpoint

The intra-S phase checkpoint ensures faithful DNA replication during S phase. The checkpoint is activated as a result of replication stress or from DNA double-strand breaks (DSBs) that may arise during the course of DNA replication and serves to arrest the cell cycle so the cell can rectify the source of replication stress and repair damaged DNA as necessary (Ciardo et al., 2019). Important components of the intra-S phase checkpoint are the sensors ATM and ATR, the ATR-interacting protein (ATRIP) complex, the ssDNA-binding protein RPA, mediators CLSPN, RAD17 and the RAD9-RAD1-HUS1 (9-1-1) complex (Bartek et al., 2004).

Targets of the intra-S phase checkpoint are stalled or collapsed replication forks and unfired

replication origins in order to prevent additional replication stress (Iyer and Rhind, 2017). Cells that are defective for intra-S phase checkpoint signalling fail to inhibit late-origin firing, leading to increased replication stress and genomic instability (Molinari, 2000; Kastan and Bartek, 2004).

1.3.3 G2/M phase checkpoint

The G2/M phase checkpoint ensures that DNA replication has been completed and is error-free before the cell enters mitosis (M phase) (Stark and Taylor, 2006). The G2/M phase checkpoint is activated in response to incomplete DNA replication or DNA damage in G2 and arrests the cell cycle in order to provide the cell with an opportunity to repair DNA damage before committing to mitosis. Failure of the G2/M checkpoint results in mitotic catastrophe, a form of programmed cell death that serves as a mechanism to prevent the formation of genetically abnormal daughter cells after cell division (Castedo et al., 2004; Löbrich and Jeggo, 2007). The primary target of the G2/M phase checkpoint is the inhibition of the cyclin B-CDK1 complex whose normal activity is to promote entry into mitosis (Nurse, 1990).

1.4 DNA damage response (DDR)

The cell cycle checkpoints are activated in response to various forms of DNA damage and are therefore an integral part of the DNA damage response (DDR) (Zhou and Elledge, 2000; Harper and Elledge, 2007). There are principally three components or levels within the theoretical framework describing the DDR: sensors, transducers (or mediators), and effectors, that function at different levels in the checkpoint signalling cascade, however, it is increasingly clear that there is significant overlap within these categories and a particular component can have multiple roles (Shaltiel et al., 2015) (Figure 1.5).

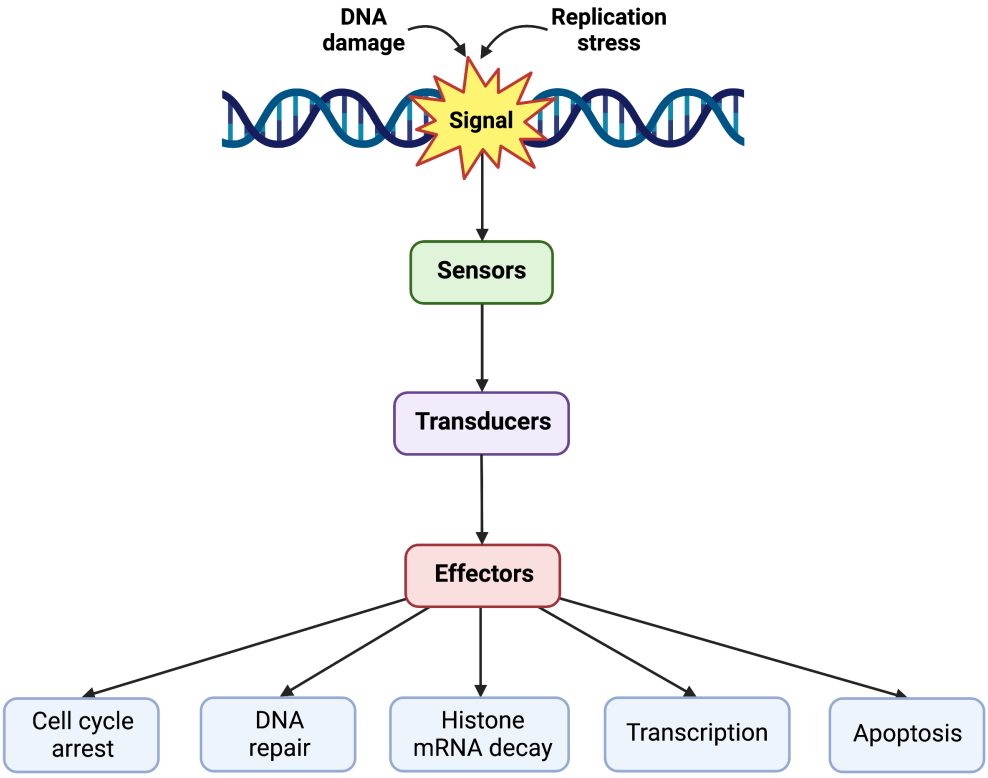

Figure 1.5: DNA damage response. DNA damage and replication stress activate DNA damage response (DDR) signal transduction pathways consisting of sensors (such as MDC1, 53BP1, BRCA1), transducers (such as ATM/ATR) and effectors (such as Chk1 and Chk2), to arrest the cell cycle and repair damaged DNA or resolve replication stress in order to maintain genomic integrity. In instances where DNA damage cannot be repaired and replication stress is persistent, prolonged DDR signalling can induce cell death by apoptosis.

1.4.1 DNA damage sensors

DNA damage sensors are proteins that detect the presence of DNA damage and initiate the DNA damage response. The DNA damage sensors ATM (ataxia-telangiectasia mutated) and ATR (ATM- and Rad3-related) are protein kinases that are activated in response to DSBs and stalled replication forks, respectively. ATM and ATR activate downstream checkpoint kinases CHK1 and CHK2 to arrest the cell cycle and provide time for the cell to rectify the source of DNA damage (Zhou and Elledge, 2000; Harper and Elledge, 2007).

1.4.1.1 Sensing and signalling by ATM

The DNA damage sensor ATM regulates the cellular response to DSBs that are caused by collapsed replication forks or DNA damaging agents, such as ultraviolet radiation (UV) or ionising radiation (IR) (Zhou and Elledge, 2000; Harper and Elledge, 2007). DSBs are first recognised by the MRN complex (comprised of MRE11, RAD50, and NBS1), which binds to DNA at the DSB and recruits ATM, resulting in its autophosphorylation and activation (Lee and Paull, 2005; Berkovich et al., 2007). Activated ATM then phosphorylates the histone variant H2A.X on S139 to form γ-H2A.X, which promotes the recruitment of DNA damage mediators, such as BRCA1, 53BP1 or MDC1, in order to transmit the DNA damage signal and initiate cell cycle arrest, DNA repair, or cell death pathways, depending on the severity of the DNA damage (Lee and Paull, 2005).

1.4.1.2 Sensing and signalling by ATR

While ATM is activated by DSBs, the sensor ATR is primarily activated by stalled replication forks that arise as a result of chemical inhibition of DNA replication, such as by hydroxyurea, or an endogenous depletion of the nucleotide pool required for the synthesis of new DNA (Zhou and Elledge, 2000; Harper and Elledge, 2007; Maréchal and Zou, 2013). ATR activates the DDR in conjunction with ATRIP and signals to downstream mediators and effectors such as CLSPN, RAD17 and the 9-1-1 complex to stabilise stalled replication forks and repair any damage before DNA replication resumes (Harper and Elledge, 2007; Maréchal and Zou, 2013).

1.4.2 Transducers and mediators

Transducers are proteins that act directly downstream of the DNA damage sensors ATM and ATR that recruit additional substrates to the site of DNA damage in order to assemble protein complexes that transmit the DNA damage signal to other proteins and pathways that are involved in DNA repair (Zhou and Elledge, 2000; Harper and Elledge, 2007).

To date, multiple transducers have been identified, including BRCA1, CLSPN, 53BP1 and MDC1 (Harper and Elledge, 2007). 53BP1 and MDC1 are recruited to sites of double-strand breaks (DSBs) by ATM, ATR or DNA-PK-mediated phosphorylation of H2A.X at the DSB and are activated in order to relay the DNA damage signal to downstream mediators and effectors (Harper and Elledge, 2007). Similarly, ATM, ATR or DNA-PK-dependent formation of γ-H2A.X in response to ionising radiation recruits MDC1 to sites of DNA damage, which promotes the recruitment of additional DNA damage mediators and effectors that lead to the formation of ionising radiation-induced foci (IRIF) (Rogakou et al., 1998).

1.4.3 Effectors

Effectors are the downstream targets of DNA damage mediators and transducers that interact with a host of intracellular protein targets to repair or mitigate the effects of DNA damage (Zhou and Elledge, 2000; Maréchal and Zou, 2013). Activated effectors signal to arrest the cell cycle and either repair the source of DNA damage or induce apoptosis in order to maintain genomic integrity. Effectors that promote DNA repair include FEN1, which recognises and helps repair single-strand DNA (Guo et al., 2008). Additionally, CHK1//2 are effectors that arrest the cell cycle and activate proteins such as RAD51, which is important for DNA repair by homologous recombination (HR) (Bartek and Lukas, 2003). Other effectors, such as P53, can either arrest the cell cycle or induce programmed cell death, depending on the severity of the DNA damage (Aubrey et al., 2018).

1.5 Histones

Histones are basic (positively charged) proteins that are necessary for negatively charged DNA in the nucleus of eukaryotic cells to be packaged and condensed into chromatin (Mariño-Ramírez et al., 2005). DNA that is not able to be condensed into chromatin is highly susceptible to DNA damage (Celona et al., 2011). Therefore, given their important role, it is unsurprising that histones are essential for cell and organism viability.

During S phase, newly replicated DNA associates with and condenses around a protein octamer made of two copies of each of the four core histones: H2A, H2B, H3 and H4, with each octamer connected by a fifth linker histone, H1 (Krude, 1995). The condensed DNA and histone octamer form the nucleosome, the basic structural unit of chromatin (Figure 1.6) in a complex process termed replication-dependent nucleosome assembly (Krude, 1995; Serra-Cardona and Zhang, 2018). Replication-dependent nucleosome assembly is a tightly regulated stepwise process in which nucleosomes ahead of the replication fork disassemble to allow progression of the replication fork machinery, followed by the reformation of new nucleosomes behind the fork on the daughter DNA strands with recycled parental histones and newly synthesised histones that are de-

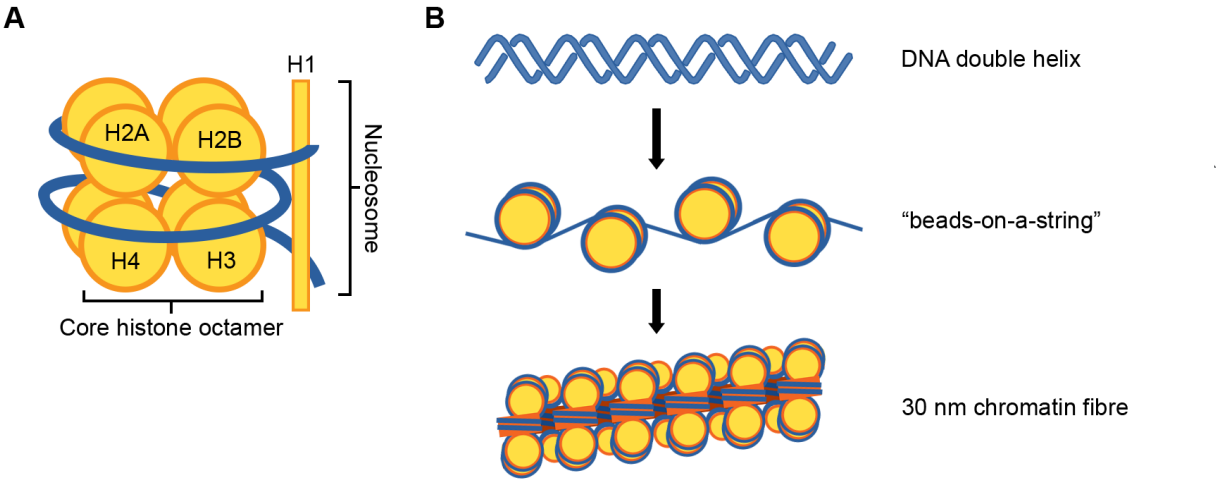

Figure 1.6: The structure of the nucleosome and its role in the formation of chromatin. (A) The nucleosome is the basic structural unit of chromatin. An octamer made from two copies of each of the four core histones forms a positively charged protein complex to which negatively charged DNA wraps around twice to form the nucleosome. **(B)** The DNA double helix (top) associates with histones to form the nucleosome and to condense into chromatin. The nucleosome is a dynamic structure that can 'open' or 'close' regions of the genome thereby regulating access to different genes.

livered to the nucleus by specialised histone chaperone proteins, such as CAF-1, Asf1, Rtt106 and FACT (Krude, 1995; Gunjan et al., 2005; Serra-Cardona and Zhang, 2018).

There are multiple different histone genes in metazoans, which can be divided into two categories: replication-dependent histone genes and replication-independent genes (Marzluff et al., 2002; Talbert and Henikoff, 2021). The replication-dependent histone genes are expressed only in S phase and provide the supply of histones that are necessary for newly synthesised DNA to condense into chromatin (Marzluff et al., 2002). The replication-independent genes encode variants of the canonical replication-dependent histones that can be expressed and deposited into chromatin outside of S phase, when required, with important roles in chromosome segregation, transcriptional regulation, DNA repair and epigenetics (Biterge and Schneider, 2014; Henikoff and Smith, 2015).

In S phase, the rate of DNA replication and histone biosynthesis are tightly coordinated, under normal conditions and under conditions of replication stress (Gunjan et al., 2005; Koseoglu et al., 2010). This is to ensure that enough histones are produced to correctly package the newly replicated DNA and to limit the accumulation of free histones when DNA replication is inhibited, as free histones themselves are a source of DNA damage and genomic instability (Gunjan and Verreault, 2003; Gunjan et al., 2005; Maya Miles et al., 2018). The coordination of decreased histone supply with the reduced rate of DNA replication under conditions of replication stress is achieved by a cellular surveillance mechanism that, when activated, results in the rapid degradation of histone mRNA and the inhibition of histone protein synthesis (Kaygun and Marzluff, 2005; Müller et al., 2007). The initiation of histone mRNA decay requires activated intra-S phase checkpoint signalling, however, the precise molecular mechanisms linking intra-S phase signalling to active histone mRNA decay are unknown.

1.5.1 Replication-dependent histones

Replication-dependent histone genes are a subgroup of histone genes that are transcribed specifically during S phase when DNA replication occurs (Marzluff et al., 2002, 2008). The five families of canonical replication-dependent histones (core histones H2A, H2B, H3, H4, and the linker histone H1) are encoded by $\sim$75 genes in mammals that are organised into three clusters within the genome: *HIST1*, which is the largest histone gene cluster located on chromosome 6 across 6p22.1-6p22.2, *HIST2* on chromosome 1 at 1q21.2, and *HIST3* on chromosome 1 at 1q42.13 (Marzluff et al., 2002) (Table 1.1). Each histone gene cluster is located in a region of the chromosome near the origin of replication, where DNA replication starts, allowing for their coordinated and efficient transcription during S phase (Marzluff et al., 2008).

Superfamily	Family	Subfamily	Gene	Chromosome
Linker	H1	H1H1	HIST1H1A, HIST1H1C, HIST1H1D, HIST1H1E, HIST1H1T	6p22.2
			HIST1H1B	6p22.1
Core	H2A	H2A1	HIST1H2AA, HIST1H2AB, HIST1H2AC, HIST1H2AD, HIST1H2AE	6p22.2
			HIST1H2AG, HIST1H2AH, HIST1H2AI, HIST1H2AJ, HIST1H2AK, HIST1H2AL, HIST1H2AM	6p22.1
		H2A2	HIST2H2AA, HIST2H2AB, HIST2H2AC	1q21.2
		H2A3	HIST3H2A	1q42.13
	H2B	H2B1	HIST1H2BA, HIST1H2BB, HIST1H2BC, HIST1H2BD, HIST1H2BE, HIST1H2BF, HIST1H2BG, HIST1H2BH, HIST1H2BI	6p22.2
			HIST1H2BJ, HIST1H2BK, HIST1H2BL, HIST1H2BM, HIST1H2BN, HIST1H2BO	6p22.1
		H2B2	HIST2H2BA, HIST2H2BB, HIST2H2BC, HIST2H2BD, HIST2H2BE	1q21.2
		H2B3	HIST3H2BA, HIST3H2BB	1q42.13
	H3	H3A1	HIST1H3A, HIST1H3B, HIST1H3C, HIST1H3D, HIST1H3E, HIST1H3F, HIST1H3G	6p22.2
			HIST1H3H, HIST1H3I, HIST1H3J	6p22.1
		H3A2	HIST2H3A, HIST2H3B, HIST2H3C	1q21.2
		H3A3	HIST3H3	1q42.13
	H4	H41	HIST1H4A, HIST1H4B, HIST1H4C, HIST1H4D, HIST1H4E, HIST1H4F, HIST1H4G, HIST1H4H	6p22.2
			HIST1H4I, HIST1H4J, HIST1H4K, HIST1H4L	6p22.1
		H42	HIST2H4A, HIST2H4B	1q21.2

Table 1.1: Replication-dependent histone genes. List of the genes encoding replication-dependent histone proteins along with the chromosomal location of each gene.

1.5.1.1 Replication-dependent histone gene regulation during the cell cycle

The expression of canonical histone genes is dependent on active DNA replication and as such is restricted to S phase of the cell cycle (Marzluff et al., 2002; Marzluff and Duronio, 2002). Transcription of replication-dependent histone genes is induced at the G1/S phase boundary by the activity of the transcription factor NPAT, which is phosphorylated and activated by cyclin E/CDK2 (Zhao et al., 2000). The activity of cyclin E/CDK2 decreases as cells progress through S phase due to the degradation of cyclin E, which prevents further activation of NPAT until the next cell cycle.

Histone gene transcription increases 3-to-5-fold in S phase and remains elevated as DNA replication progresses (Marzluff and Duronio, 2002; Marzluff et al., 2002) (Figure 1.7). During S phase, the half-life of histone mRNA is estimated to be 40-60 minutes, however, at the end of S phase, or when DNA replication is arrested, the half-life is reduced to ~10 minutes and histone mRNA is rapidly degraded to inhibit further histone protein synthesis in the absence of active DNA replication (Marzluff et al., 2008).

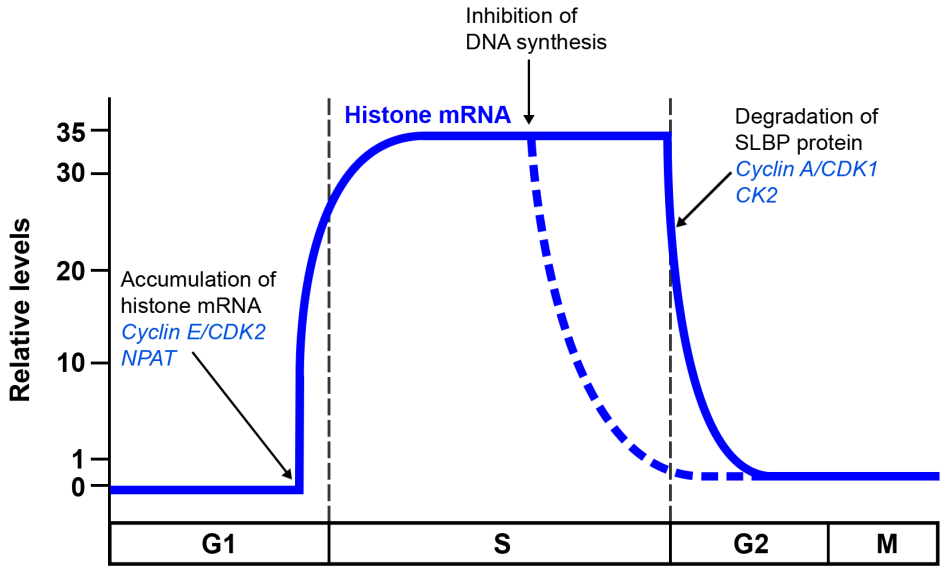

Figure 1.7: Cell cycle regulation of histone gene transcription. Histone mRNA transcription is induced at the G1/S phase boundary by the activity of cyclin E/CDK2 and NPAT. During S phase, histone mRNA transcript levels increase ~35-fold and remain elevated throughout S phase. At the end of S phase, or when DNA replication is inhibited, histone mRNA is rapidly degraded by the histone mRNA decay pathway to prevent an accumulation of histone proteins in the absence of active DNA replication. Adapted from Marzluff et al. (2008).

1.5.1.2 Replication-dependent histone mRNA

Replication-dependent histone mRNAs are unique in that, unlike all other mRNA transcripts in metazoan cells, they lack introns and have a conserved 16-nucleotide stem-loop structure in the 3'UTR instead of a poly(A) tail (Marzluff et al., 2008) (Figure 1.8). Histone pre-mRNA contains a histone downstream element located 3' to the stem-loop and endonucleolytic cleavage of this sequence is the only step required in order to form mature histone mRNA (Marzluff et al., 2008; Marzluff and Koreski, 2017). The remaining stem-loop acts as a functional homologue of poly(A) tails for the regulation of histone mRNA nuclear export, translation and stability (Marzluff et al., 2008).

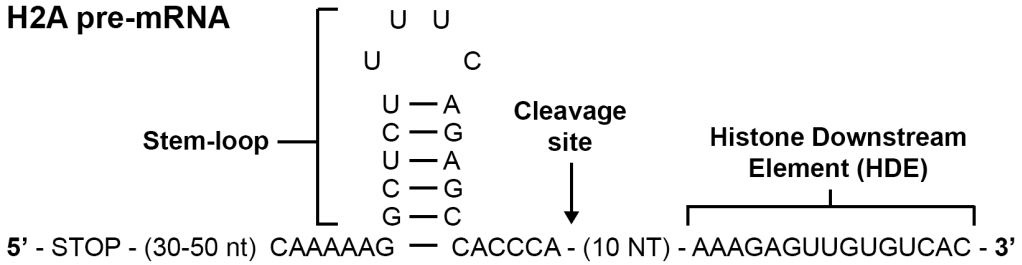

Figure 1.8: Histone pre-mRNA structure. Histone mRNAs are unique in that they lack a poly(A) tail and instead have a conserved stem-loop structure in the 3'UTR. The histone downstream element (HDE) is the site to which the U7 snRNP binds through complementary base-pairing, which facilitates the recruitment of cleavage factors that generate mature histone mRNA by cleaving the 3'UTR at the cleavage site downstream of the stem-loop.

1.5.2 Replication-independent histones

Replication-independent genes are those whose expression is not limited to S phase and can be incorporated into chromatin throughout the cell cycle (Martire and Banaszynski, 2020) (Table 1.2). These histones are typically histone variants with specialised epigenetic or tissue-specific functions (Sarma and Reinberg, 2005). The replication-independent genes can be divided into two broad categories, depending on the degree of divergence of their amino acid sequences compared to their related canonical histone: homomorphous histone variants have relatively few amino acid changes (e.g. H1.0), whereas heteromorphous variants display much greater divergence in histone structure (e.g. H2A.X, H2A.Z) (Ausió, 2006).

Transcription of replication-independent histone genes generally results in the production of mRNA transcripts with a poly(A) tail, unlike replication-dependent histone mRNA, and as such are regulated by canonical mRNA-processing complexes (Marzluff et al., 2008; Danckwardt et al., 2008). An interesting exception to this general rule is the histone variant gene *H2AFX*, encoding the H2A.X histone variant required for activation and resolution of the DDR in response to DSBs, which is a hybrid histone gene that can give rise to both stem-loop and poly(A)+ mRNA depending on when in the cell cycle the gene is expressed (Dankert et al., 2016; Griesbach et al., 2021). The replication-independent histone variants, genes and their respective chromosomal locations are listed in Table 1.2.

Superfamily	Family	Histone variant	Gene	Chromosome
Linker	H1	H1.0	H1F0	22q13.1
		H1.7	H1FNT	12q13.11
		H1.8	H1FOO	3q22.1
		H1.9	HILS1	17q21.33
		H1.10	H1FX	3q21.3
Core	H2A	H2A.B.1	H2AB1	Xq28
		H2A.B.2	H2AB2	Xq28
		H2A.B.3	H2AB3	Xq28
		H2A.J	H2AJ	12p12.3
		H2A.L.1	H2AL1	Xp21.1
		H2A.L.2	H2AL2	Xp21.1
		H2A.L.3	H2AL3	Xp11.4
		H2A.P	H2AP	Xp11.4
		H2A.Q	H2AQ1P	Xq26.3
		H2A.X	H2AFX	11q23.3
		H2A.Z.1	H2AZ1	4q23
		H2A.Z.2	H2AZ2	7p13
		macroH2A.1	H2AFY	5q31.1
		macroH2A.2	H2AFY2	10q22.1
	H2B	H2B.K	H2BK1	7q36.1
		H2B.L	H2BL1P	5q13.2
		H2B.N	H2BN1	17q11.2
		H2B.W.1	H2BW1	Xq22.2
		H2B.W.2	H2BW2	Xq22.2
		H2B.W.3	H2BW3P	Xq22.2
		H2B.W.4	H2BW4P	Xq22.2
	H3	H3.Y.1	H3Y1	5p15.1
		H3.Y.2	H3Y2	5p15.1
		CENP-A	CENPA	2p23.3
		H3.3A	H3-3A	1q42.12
		H3.3B	H3-3B	17q25.1
		H3.3C	H3-5	12p11.21
	H4	H4-16	H4C16	12p12.3

Table 1.2: Replication-independent histone variant genes. List of the genes encoding replication-independent histone proteins along with the chromosomal location of each gene.

1.6 Stem-loop binding protein (SLBP)

Stem-loop binding protein (SLBP; Q14493) is the only eukaryotic protein known to bind directly to the stem-loop of replication-dependent histone mRNA and is the master regulator of all aspects of histone mRNA metabolism (Martin et al., 1997; Wang et al., 1996; Zheng et al., 2003). SLBP is a 270 amino acid protein with a predicted molecular weight of 31 kDa that is encoded in humans by the *hSLBP* gene (NM006527), which is comprised of eight exons spanning ~19.5 kb on the short arm of chromosome 4 (4p16.3) (Martin et al., 1997).

Like histone mRNA, the expression of SLBP mRNA is also cell cycle regulated (Figure 1.9) and is restricted to S phase by both translational and post-translational mechanisms (Whitfield et al., 2000; Koseoglu et al., 2008). SLBP gene transcription is induced at the G1/S phase boundary after which the synthesised protein is trafficked into the nucleus by Imp-α/Imp-β transport factors (Whitfield et al., 2000; Erkmann et al., 2005b). Once inside the nucleus, SLBP binds to histone pre-mRNA and promotes processing of the 3'UTR to form mature histone mRNA (Wang et al.,

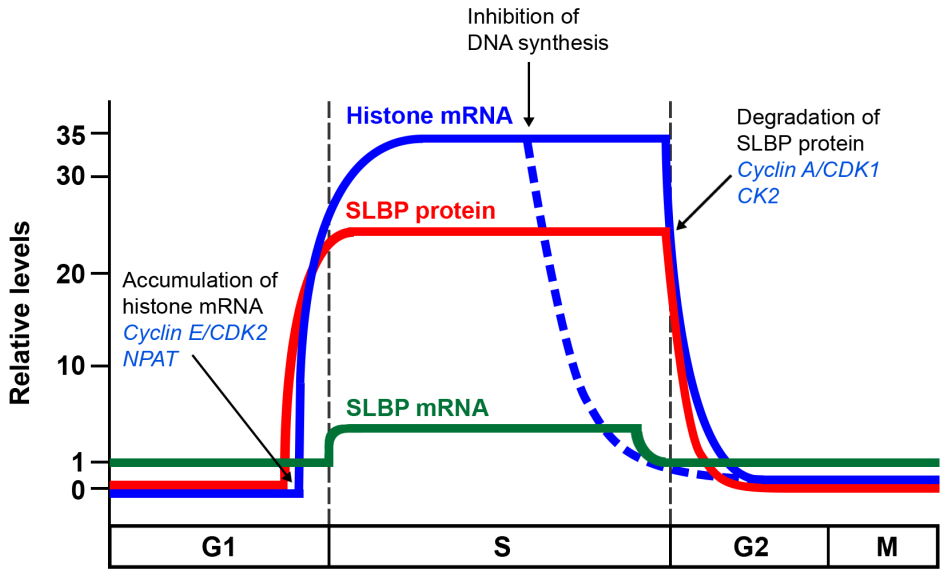

Figure 1.9: Cell cycle regulation of SLBP expression. SLBP protein synthesis, like replication-dependent histone gene expression, is cell cycle regulated and is restricted to S phase. SLBP protein levels increase ~25-fold in S phase and remain elevated until S phase is complete. At the end of S phase, CKII and cyclin A/CDK1 phosphorylate T61 and T62, respectively, which is required in order for cyclin F to bind to SLBP and mediate its polyubiquitination and degradation. Importantly, unlike histone mRNA, SLBP protein remains stable when DNA replication is inhibited. Adapted from Marzluff et al. (2008).

1996). SLBP, bound to histone mRNA, is then trafficked out of the nucleus and histone protein synthesis begins once SLBP and histone mRNA associate with ribosomes in the cytoplasm (Erkmann et al., 2005a; Marzluff et al., 2008).

Regions of the SLBP protein that have been identified as important for its function include a bi-partite RNA-binding domain (RBD), which facilitates SLBP/histone mRNA binding and is the only region in SLBP that is evolutionarily conserved across all metazoans; the C-terminal domain that binds to factors required for histone mRNA 3'UTR processing; an N-terminal translation activation domain (TAD) that is responsible for promoting the initiation of histone mRNA translation; the TPNK motif located between the two RNA-binding interfaces of the RBD, which regulates SLBP/histone mRNA binding through threonine phosphorylation and proline isomerisation; and a central cyclin-binding motif (Cy motif) to which cyclins A and F bind to promote SLBP degradation at the end of S phase and in G2, respectively (Figure 1.10). Importantly, previous structural studies have shown that SLBP is unfolded and intrinsically disordered in the free state and undergoes a disordered-to-ordered transition upon binding to histone mRNA, forming a highly stable mRNA-protein complex that functions as an integral unit.

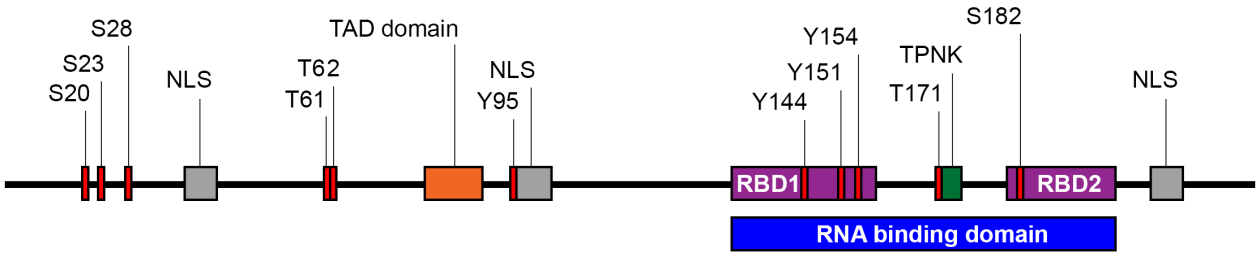

Figure 1.10: Linear domain structure of human SLBP. SLBP contains a C-terminal RNA binding domain (RBD) with a conserved TPNK motif that regulates the affinity of SLBP for histone mRNAs. A central translation activation domain (TAD) is required for efficient histone mRNA translation. Dephosphorylation of T171 in TPNK promotes dissociation of SLBP and histone mRNA. T61 and T62 are phosphorylated by CKII and CDK1, respectively, to facilitate cyclin F-mediated SLBP degradation at the end of S phase. S20 and S23, which are hypothesised to regulate the initiation of histone mRNA decay, are located in the N-terminus of SLBP.

Mutations introduced experimentally within the histone mRNA stem-loop have been shown to disrupt the interaction between SLBP and histone mRNA, resulting in nuclear retention of histone mRNA and a decrease in histone mRNA 3'UTR processing efficiency both *in vitro* and *in vivo*. It is therefore clear that the formation of the highly stable SLBP/histone mRNA complex is crucially important for maintaining the cell cycle regulation of histone protein levels in eukaryotic cells.

Taken together, data obtained from structural and functional analyses have shown that SLBP is a key protein that regulates all aspects of histone mRNA metabolism, including histone pre-mRNA processing, nucleo-cytoplasmic transport, histone mRNA translation and histone mRNA decay, which are discussed in further detail below.

1.6.1 SLBP and histone gene transcription

Cell cycle-dependent regulation of histone gene transcription is driven by the activity of cyclin E/CDK2 as cells approach the G1/S phase boundary (Zhao et al., 2000; Koseoglu et al., 2010). Active cyclin E/CDK2 phosphorylates and activates numerous targets that are important for S phase progression, including CDC6 to initiate DNA replication, E2F1 to express S phase genes, and NPAT to initiate histone gene transcription (Zhao et al., 2000). However, NPAT is not the only factor that promotes histone gene transcription and it appears to preferentially promote the expression of histone H4 family genes (Zhao et al., 2000). Interestingly, knockdown of SLBP itself has been shown to decrease global histone mRNA transcript levels, suggesting a role for SLBP in the regulation of histone gene transcription in addition to NPAT (Zhao et al., 2004). Transcription of histone genes occurs in specialised regions of the nucleus known as the histone locus body, which is associated with the *HIST1*, *HIST2* and *HIST3* gene clusters and is concentrated with the necessary factors, including SLBP, that are required for histone gene transcription and histone mRNA processing (Nizami et al., 2010; Morimoto and Boerkoel, 2013).

1.6.2 SLBP-dependent histone pre-mRNA processing

Regulation of histone mRNA 3' untranslated region (UTR) processing significantly influences histone protein synthesis rate, histone stoichiometry, and the timing of histone synthesis throughout the cell cycle. During late G1, the efficiency of histone mRNA processing increases tenfold (Harris et al., 1991). Alterations in the 3'-UTR affect various aspects of histone mRNA metabolism, such as mRNA processing, localisation, and translation, leading to changes in histone protein abundance (Marzluff and Duronio, 2002; Marzluff et al., 2008).

The formation of the histone mRNA 3' end requires two cis-acting elements in the histone pre-mRNA. The first element is a 26-nucleotide stem-loop sequence in the 3'-UTR of histone mRNA, which remains in the mature mRNA after pre-mRNA processing (Marzluff et al., 2008). The second element is a purine-rich downstream element (HDE) located 3' to the cleavage site, which undergoes cleavage during processing (Marzluff et al., 2008). These sequences recruit specific factors responsible for a single endonucleolytic cleavage event between the stem-loop and HDE, necessary for generating mature histone mRNAs.

The trans-acting factors involved in this process include SLBP, the small ribonucleoprotein particle (U7 snRNP), and a heat-labile processing factor (HLF) (Wang et al., 1996; Martin et al., 1997). The small ribonucleoprotein particle (U7 snRNP) contains U7 snRNA and a heptameric ring of Sm, Lsm10, and Lsm11 proteins, which interact with the histone pre-mRNA through base pairing between the HDE and the 5' end of U7 snRNA (Dominski and Marzluff, 1999; Pillai et al., 2001, 2003; Azzouz et al., 2005). HLF and a novel zinc finger protein (hZFP100) interact with the U7 snRNP, while SLBP binds to stem-loop histone mRNAs (Dominski et al., 2002; Azzouz et al., 2005)

The processing of histone pre-mRNA requires only endonucleolytic cleavage, occurring at the end of a conserved ACCCA sequence following the stem-loop (Gick et al., 1986), following which the downstream cleavage product undergoes degradation through 5'-3' exonuclease activity (Walther et al., 1998). The N-terminal region of Lsm11 interacts with the N-terminal region of FLICE-associated huge protein (FLASH), which recruits the histone pre-mRNA cleavage complex

(HCC), including CPSF73 (and its homologue CPSF100), and the scaffolding protein symplekin (a key component of HLF) to form the cleavage complex that mediates histone mRNA 3' end processing (Dominski et al., 2005; Sullivan et al., 2009; Yang et al., 2009). After processing, only SLBP remains bound to the stem-loop of the mature histone mRNA.

1.6.3 SLBP-dependent histone mRNA export

Following 3'-UTR processing, the mature histone mRNA with SLBP bound is then modified by the addition of the nuclear cap-binding complex (CBC) to the 5'-UTR (comprised of proteins CBC20 and CBC80), which promotes the recruitment of the canonical mRNA transport factor TAP (Erkmann et al., 2005a). Once bound, TAP then promotes the export of the mRNP through the nuclear pore (Erkmann et al., 2005a). Following export, the CBC is removed and is replaced by the cytoplasmic cap-binding protein eIF4E in order to prepare for the pioneer round of histone mRNA translation (Ishigaki et al., 2001).

1.6.4 SLBP-dependent histone mRNA translation

The accumulation of histone mRNA is influenced by two main factors: an increase in the rate of histone gene transcription and the efficiency of histone pre-mRNA processing. A key regulator of this process is SLBP, which also plays a crucial role in regulating histone mRNA translation (Marzluff and Duronio, 2002).

The stem-loop structure of histone mRNA is essential for both translation efficiency and mRNA stability (Marzluff and Koreski, 2017). Recently, SLIP1 (SLBP Interacting Protein 1) has been identified as a histone mRNA-specific translation initiation factor that interacts with SLBP bound to the stem-loop of mature histone mRNA. The SLBP-SLIP1 complex assembles on the 3'-UTR region of histone mRNA, bridging the 5' and 3' ends of the mRNA bound by eIF4E/eIF4G and SLBP (Bansal et al., 2013; von Moeller et al., 2013). This closed-loop configuration leads to the formation of a multicomponent complex that includes the SLBP-SLIP1-histone mRNA ternary complex, which promotes the recruitment of the small ribosomal subunit (40S) and the initiation

of histone mRNA translation (Bansal et al., 2013; von Moeller et al., 2013).

At the end of S phase, SLBP transitions to an inactive form and histone mRNA translation stops, in a process that involves the removal of SLBP from the histone mRNA 3'-UTR. This process is achieved by dephosphorylating T171 in the highly conserved TPNK sequence by the phosphatase PP2A and the prolyl isomerase Pin1 (Krishnan et al., 2012; Bansal et al., 2013). This dephosphorylation leads to the dissociation of the SLBP-SLIP1 heterotetramer and, subsequently, SLBP dissociates from the histone mRNA, marking it for exosome-mediated degradation in the cytoplasm (Krishnan et al., 2012; Bansal et al., 2013).

1.6.5 Connection between cell cycle checkpoints, SLBP and histone mRNA decay

Histone mRNA decay is a critical regulatory step that controls the accumulation of histone proteins during the cell cycle, specifically at the end of S phase. This process acts as a surveillance mechanism to ensure appropriate histone levels during cell division.

In most cellular mRNA decay, a multi-protein complex called the exosome plays a crucial role in 3'-5' exonucleolytic degradation. However, histone mRNA decay is a translation-dependent process that involves specific steps, including 3' oligouridylation, mRNA decapping, and the activity of both 5'-3' and 3'-5' nucleases (Kaygun and Marzluff, 2005; Mullen and Marzluff, 2008; Choe et al., 2013).

Additionally, histone mRNA decay is triggered by activated checkpoint signalling when DNA synthesis is inhibited, leading to the rapid repression of histone gene expression and S phase arrest (Kaygun and Marzluff, 2005; Marzluff et al., 2008; Mullen and Marzluff, 2008). This indicates that histone gene expression is targeted by the intra-S phase checkpoint. Replication stress-induced histone mRNA decay is blocked by inhibitors of checkpoint signalling, supporting the notion that it is part of the activated checkpoint response (Müller et al., 2007). Interestingly, the decay of histone mRNA during replication stress does not involve destabilisation and proteolytic destruction of

SLBP, as the SLBP protein remains detectable even after prolonged replication stress (Mullen and Marzluff, 2008; Krishnan et al., 2012; Choe et al., 2013).

The molecular details and signalling pathways that initiate histone mRNA decay are currently unknown, though Müller et al. (2007) reported that the kinase activity of ATR and DNA-PK, but not ATM, is required for histone mRNA decay in response to replication stress. Recently, stable-isotope labelling of amino acids in cell culture (SILAC) mass spectrometry data acquired by the Smythe group has provided evidence suggesting that S20 and S23 residues in the N-terminus of SLBP are targeted for phosphorylation in response to hydroxyurea-induced replication stress (Panomwan, 2017). Therefore, phosphorylation of S20 and/or S23 may be part of the intra-S phase checkpoint and may promote the dissociation of SLBP from histone mRNA to facilitate histone mRNA decay in response to replication stress.

1.7 Aim

When cells are exposed to replication stress, an immediate response is the rapid inhibition of histone protein synthesis via activation of the histone mRNA decay pathway to ensure the co-ordination of histone protein supply with the reduced rate of DNA replication. The precise mechanism by which replication stress induced signalling triggers histone mRNA decay remains to be accurately defined, however recent SILAC mass spectrometry evidence from the Smythe group suggests that phosphorylation of S20 and/or S23 may be involved. Therefore, the aim of the proposed project is to determine whether the phosphorylation status of S20 and/or S23 affects histone mRNA decay and, if so, to identify the kinase(s) responsible for phosphorylation in order to further understand the molecular mechanisms by which histone mRNA is degraded in response to replication stress.

Chapter 2

Materials and methods

2.1 Materials

2.1.1 Reagents

General laboratory chemicals were sourced from Sigma-Aldrich Ltd. (Gillingham, England, UK) unless otherwise stated. Tissue culture plasticware was obtained from Greiner Bio-one (Stonehouse, England, UK). Bio-Rad protein (Bradford) assay reagent and Mini-PROTEAN II protein gel electrophoresis equipment were from Bio-Rad Laboratories Inc. (Hemel Hempsted, England, UK). Amersham Protran 0.45 μm nitrocellulose blotting membrane and Whatmann 3 mm filter paper was from Fisher Scientific UK Ltd. (Loughborough, England, UK). Complete Mini EDTA-free protease inhibitor cocktail tablets were from Roche Diagnostics Ltd. (Lewes, England, UK). Dulbecco's modified Eagle's medium (DMEM), Dulbecco's phosphate buffered saline (PBS), trypsin, blasticidin, Hygromycin B and Doxycycline were obtained from Invitrogen Ltd. (Paisley, Scotland, UK). Plasmid DNA purification kits, the QIAquick gel extraction kit and Polyfect transfection reagent were from QIAGEN (Crawley, England, UK). Restriction endonucleases and associated buffers were from New England Biolabs Ltd. (Hitchin, England, UK) or Promega UK Ltd. (Southampton, England, UK). QuickChange site-directed mutagenesis kit, XL-10 Gold ultra-competent *E. coli* cells and Pfu Ultra DNA polymerase were from Agilent Technologies UK Ltd. (Cheadle, England, UK).

2.1.2 Antibodies

2.1.2.1 Primary antibodies

Antibody	Species	Raised against	Supplier (Catalogue #)	Dilution
Anti-FLAG M2	Mouse	FLAG tag	Sigma Aldrich (F1804)	WB: 1:5000
Anti-SLBP	Mouse	Human SLBP	Santa Cruz (sc-101140)	WB: 1:500
Anti-Nucleolin	Mouse	Human Nucleolin	Santa Cruz (sc-8031)	WB: 1:5000
Anti-BrdU	Rat	BrdU	Abcam (ab6326)	FC: 1:200

Table 2.1: Primary antibodies used in this study. Table detailing the species, target antigen, suppliers and working concentrations of the primary antibodies used in this study. WB = Western blot. FC = flow cytometry.

2.1.2.2 Secondary antibodies

Antibody	Species	Raised against	Supplier (Catalogue #)	Dilution
DyLight 800CW	Goat	Mouse IgG [H+L]	Invitrogen (SA535521)	WB: 1:5000
α-Rat IgG Alexa Fluor 568	Donkey	Rat IgG [H+L]	Invitrogen (A78946)	FC: 1:1000

Table 2.2: Secondary antibodies used in this study. Table detailing the species, target antigen, suppliers and working concentrations of secondary antibodies used in this study. WB = Western blot. FC = flow cytometry.

2.1.3 Primers

All primers were designed in-house and supplied by Invitrogen.

2.1.3.1 Site-directed mutagenesis primers

Mutagenesis	Sequence
FLAG-SLBP^{S20A}	Forward: 5'-GACGGTGACGCCGCCCCGCCGTCCCC-3' Reverse: 5'-GGGGACGGCGGGGCGGCGTCACCGTC-3'
FLAG-SLBP^{S23A}	Forward: 5'-CAGCCCGCCGGCCCCCGCGCG-3' Reverse: 5'-CGCGCGGGGGCCGGCGGGCTG-3'
FLAG-SLBP$^{s20a/S23A}$	Forward: 5'-GCCCCGCCGGCCCCCGCGC-3' Reverse: 5'-GCGCGGGGGCCGGCGGGGC-3'
FLAG-SLBP^{S20E}	Forward: 5'-CGACGGTGACGCCGAACCGCCGTCCCCCG-3' Reverse: 5'-CGGGGGACGGCGGTTCGGCGTCACCGTCG-3'
FLAG-SLBP^{S23E}	Forward: 5'-GCCAGCCCGCCGGAGCCCGCGCGATGG-3' Reverse: 5'-CCATCGCGCGGGCTCCGGCGGGCTGGC-3'
FLAG-SLBP$^{s20e/S23E}$	Forward: 5'-ACGCCGAACCGCCGGAACCCGCGCGATGGAG-3' Reverse: 5'-CTCCATCGCGCGGGTTCCGGCGGTTCGGCGTC-3'
FLAG-SLBP^{E20D}	Forward: 5'-CGACGGTGACGCCGATCCGCCGTC-3' Reverse: 5'-GACGGCGGATCGGCGTCACCGTCG-3'
FLAG-SLBP^{E23D}	Forward: 5'-CCAGCCCGCCGGATCCCGCGC-3' Reverse: 5'-GCGCGGGATCCGGCGGGCTGG-3'

Mutagenesis	Sequence
FLAG-SLBP$^{E20D/E23D}$	Forward: 5'-CGCGGGATCCGGCGGATCGGCGTCACC-3' Reverse: 5'-GGTGACGCCGATCCGCCGGATCCCGCG-3'
E23D D23 BamHI removal	Forward: 5'-CGCGCGGGATCGGGCGGTTCGGC-3' Reverse: 5'-GCCGAACCGCCCGATCCCGCGCG-3'
EE20/23DD D23 BamHI removal	Forward: 5'-GCCGATCCGCCCGATCCCGCGCG-3' Reverse: 5'-CGCGCGGGATCGGGCGGATCGGC-3'
FLAG-SLBP^{Y95F}	Forward: 5'-AGTTAACAAAGAAATGGCAAGATTTAAAAGGAAACTCCTCATCAATG-3' Reverse: 5'-CATTGATGAGGAGTTTCCTTTTAAATCTTGCCATTTCTTTGTTAACT-3'
FLAG-SLBP^{RYAAAA_K96A}	Forward: 5'-GGACCAGAGTTAACAAAGAAATGGCAAGATATGCAAGGAAACTCCTCATCA-3' Reverse: 5'-TGATGAGGAGTTTCCTTGCATATCTTGCCATTTCTTTGTTAACTCTGGTCC-3'
FLAG-SLBP^{RYAAAA_k96a_R97A}	Forward: 5'-CAAAGTCATTGATGAGGAGTTTCGCTGCATATCTTGCCATTTCTTTGT-3' Reverse: 5'-ACAAAGAAATGGCAAGATATGCAGCGAAACTCCTCATCAATGACTTTG-3'
FLAG-SLBP^{RYAAAA_k96a_r97a_K98A}	Forward: 5'-CCAAAGTCATTGATGAGGAGTGCCGCTGCATATCTTGCCATTTC-3' Reverse: 5'-GAAATGGCAAGATATGCAGCGGCACTCCTCATCAATGACTTTGG-3'
FLAG-SLBP^{RYAAAA_k96a_r97a_k98a_L99A}	Forward: 5'-CAAAGTCATTGATGAGGGCTGCCGCTGCATATCTTGCC-3' Reverse: 5'-GGCAAGATATGCAGCGGCAGCCCTCATCAATGACTTTG-3'

Table 2.3: Site-directed mutagenesis primers used in this study.

2.1.3.2 qPCR primers

Target	Sequence
HIST1H3B	Forward: 5'-GGTAAAGCGCCACGCAAGCA-3' Reverse: 5'-GGCGGTAACGGTGAGGCTTT-3'
H2AFX	Forward: 5'-CTGCTGCCCAAGAAGACC-3' Reverse: 5'-CGGGCCCTCTTAGTACTCCT-3'
GAPDH	Forward: 5'-TCGCTCTCTGCTCCTCCTGTTC-3' Reverse: 5'-CGACCAAATCCGTTGACTCCGACC-3'

Table 2.4: qPCR primers used in this study.

2.1.3.3 Sequencing primers

Name	Sequence
Forward CMV	5'-CGCAAATGGGCGGTAGGCGTG-3'
Reverse BGH	5'-TAGAAGGCACAGTCGAGG-3'

Table 2.5: Sequencing primers used in this study.

2.1.4 Plasmids

Plasmid	Origin	Antibiotic
pOG44	Invitrogen	Ampicillin
pcDNA5/FRT/TO/FLAG-SLBP^{WT}	Dr Pornpen Panomwan (Smythe Lab)	Ampicillin
pcDNA5/FRT/TO/FLAG-SLBP^{siRes}	Dr Pornpen Panomwan (Smythe Lab)	Ampicillin
pcDNA5/FRT/TO/FLAG-SLBP$^{siRes_S20A/S23A}$	This study	Ampicillin
pcDNA5/FRT/TO/FLAG-SLBP^{siRes_S20A}	This study	Ampicillin
pcDNA5/FRT/TO/FLAG-SLBP^{siRes_S23A}	This study	Ampicillin
pcDNA5/FRT/TO/FLAG-SLBP$^{siRes_S20E/S23E}$	This study	Ampicillin
pcDNA5/FRT/TO/FLAG-SLBP^{siRes_S20E}	This study	Ampicillin
pcDNA5/FRT/TO/FLAG-SLBP^{siRes_S23E}	This study	Ampicillin
pcDNA5/FRT/TO/FLAG-SLBP$^{siRes_S20D/S23D}$	This study	Ampicillin
pcDNA5/FRT/TO/FLAG-SLBP^{siRes_S20D}	This study	Ampicillin
pcDNA5/FRT/TO/FLAG-SLBP^{siRes_S23D}	This study	Ampicillin
pcDNA5/FRT/TO/FLAG-SLBP^{siRes_Y95F}	This study	Ampicillin
pcDNA5/FRT/TO/FLAG-SLBP^{siRes_4A}	This study	Ampicillin
pcDNA5/FRT/TO/FLAG-SLBP$^{siRes_S20A/4A}$	This study	Ampicillin
pcDNA5/FRT/TO/FLAG-SLBP$^{siRes_S23A/4A}$	This study	Ampicillin
pcDNA5/FRT/TO/FLAG-SLBP$^{siRes_Y95F/4A}$	This study	Ampicillin

Table 2.6: Plasmids used in this study. Table detailing the plasmid, source and bacterial selection antibiotic of the plasmids used in this study. See Appendix B and Appendix C for FLAG-SLBP^{WT} and FLAG-SLBP^{siRes} cDNA sequences.

2.1.5 siRNA

Custom human SLBP siRNA:

5'-GAGAGAGAAAAUCAUCAUCUU-3'

(obtained from Horizon Discovery, Cambridge, England, UK)

A non-targeting siRNA (Thermo Scientific, D-001810-01) was used as a negative control.

2.2 Methods

2.2.1 Molecular biology techniques

2.2.1.1 Site-directed mutagenesis

Site-directed mutagenesis was performed using either the QuickChange II site-directed mutagenesis kit (Agilent Technologies UK Ltd.) or the Phusion High-Fidelity DNA polymerase and buffer (ThermoFisher). For mutagenesis with the QuickChange II site-directed mutagenesis kit, each 50µL reaction was prepared on ice and contained 10× Pfu Ultra HF buffer (5 µL), double-stranded plasmid DNA template (50 ng), forward primer (200 nM), reverse primer (200 nM), dNTPs (2.5 mM each of dATP, dTTP, dCTP, dGTP) and 1 µL (2.5 U) of Pfu Ultra HF DNA polymerase, diluted in ddH_2O. QuickChange II site-directed mutagenesis PCR thermal cycling parameters are detailed in (Table 2.7). When the PCR reaction was complete, the template plasmid DNA was digested by adding 1 µL of DpnI restriction enzyme and incubating at 37°C for 1 hour. The remaining mutated plasmid DNA was then used to transform XL-10 Gold Ultracompetent *E. coli* cells, as described in Section 2.2.2.1 below.

Segment	Cycles	Temperature	Time
1	1	95°C	2 min
2	35	95°C	30 sec
		55°C	30 sec
		72°C	7 min
3	1	72°C	10 min
4	1	4°C	∞

Table 2.7: QuickChange II site-directed mutagenesis PCR thermal cycling parameters.

PCR was performed using the Phusion High-Fidelity polymerase (ThermoFisher) for mutagenesis of GC-rich regions of SLBP. Each 50µL reaction was prepared on ice and contained 2× Phusion High-Fidelity GC buffer (25 µL), double-stranded plasmid DNA template (100 ng), forward primer (400 nM), reverse primer (400 nM), dNTPs (2.5 mM each of dATP, dTTP, dCTP, dGTP), DMSO (1.5 µL) and 1 µL (2 U) of Phusion HF DNA polymerase, diluted in ddH_2O. Phusion High-Fidelity site-directed mutagenesis PCR thermal cycling parameters are detailed in (Table 2.8). When the PCR reaction was complete, the template plasmid DNA was digested by adding 1 µL of DpnI restriction enzyme and incubating at 37°C for 1 hour. The remaining mutated plasmid DNA was then used to transform XL-10 Gold Ultracompetent *E. coli* cells, as described in Section 2.2.2.1 below.

Segment	Cycles	Temperature	Time
1	1	98°C	30 sec
2	35	98°C	10 sec
		55°C	20 sec
		72°C	3 min 30 sec
3	1	72°C	10 min
4	1	4°C	∞

Table 2.8: Phusion High-Fidelity site-directed mutagenesis PCR thermal cycling parameters.

2.2.1.2 DNA gel electrophoresis

Samples of plasmid DNA to be analysed by gel electrophoresis were prepared and stored on ice until use. Each 20 µL sample contained 100 ng of DNA and 4 µL of 5× DNA loading dye diluted in ddH_2O. A 1% agarose gel containing ethidium bromide (1 µg/mL) was prepared and placed into a DNA gel electrophoresis tank filled with 1× TAE buffer and an equal concentration of ethidium bromide. 5 µL of HyperLadder 1 kb (Bioline, London, England) and 20 µL samples were then loaded into appropriate wells and electrophoresed for 1 hour at 100 V. Gels were imaged using a Bio-Rad Gel Doc EZ Imaging System.

2.2.1.3 DNA sequencing

DNA sequencing was performed by the University of Sheffield Core Genomic Facility using an Applied Biosystems 3730 DNA Analyser. Returned DNA sequences were verified and analysed using SnapGene Viewer (v4.2.2) and BLAST online software.

2.2.2 Bacterial techniques

2.2.2.1 Bacterial transformation

50 µL of thawed XL-10 Gold Ultracompetent *E. coli* cells (Aligent Technologies UK Ltd.) were placed in a pre-chilled 14 mL BD Falcon polypropylene round bottom tube. 2 µL β-mercaptoethanol was added and the cells were incubated on ice for 10 min. 1 µL of DpnI-treated DNA then was added and incubated on ice for a further 30 min. Cells were heat shocked at 42°C for 30 seconds and then immediately placed back on ice for 2 min. 500 µL of pre-warmed NZY^+ media was added and incubated at 37°C in an orbital shaker at 225 rpm for 1 hour. 200 µL of the cell solution was then plated on LB agar plates with the appropriate antibiotic and incubated overnight at 37°C.

2.2.2.2 Miniprep purification of plasmid DNA from bacteria for routine cloning and sequencing

Plasmid DNA for use in routine cloning or sequencing was purified from transformed bacteria using a Miniprep kit (QIAGEN). Single colonies were picked from an agar plate and were incubated for 8-16 hours at 37°C in an orbital shaker at 225 rpm in 5 mL of LB media containing an appropriate antibiotic. Bacteria were then centrifuged at 4000 × g for 10 minutes at 4°C. The supernatant was discarded and the bacterial pellet was resuspended in 250 µL Buffer P1 (resuspension buffer) with 50 µg/mL RNase A freshly added. 250 µL Buffer P2 (lysis buffer) was added to the bacterial suspension and the tube was inverted 5 times to mix. Cells were incubated for 3 minutes at room temperature before adding 350 µL Buffer N3 (neutralisation buffer) and inverting 5 times. The bacterial lysate was then transferred to a QIAGEN Miniprep spin column and columns were centrifuged at 13,200 × g for 30 seconds at 4°C. The flow-through was discarded and the column

was washed twice by centrifugation with 500 µL Buffer PE (wash buffer). After the final wash, the column was centrifuged again for 1 minute at 13,200 × g to ensure removal of residual wash buffer. The column was then placed into a clean, labelled Eppendorf tube and 35 µL ddH_2O was added directly to the column membrane before centrifugation at 13,200 × g for 30 seconds at 4°C to elute the DNA. The concentration of purified plasmid DNA was measured with a NanoDrop ND-1000 spectrophotometer (Thermo Scientific) and samples stored at -20°C.

2.2.2.3 Purification of transfection-grade plasmid DNA from bacteria using a modified Miniprep protocol (Miraprep)

Transfection-grade plasmid DNA was isolated from transformed bacteria following the Miraprep protocol, a modified Miniprep protocol that uses a Miniprep kit (QIAGEN) and requires only 50 mL of bacterial culture to produce DNA yields comparable to Maxiprep purifications that are suitable for mammalian transfection (Pronobis et al., 2016). A single colony was picked from an agar plate and grown for 8-16 hours at 37°C in an orbital shaker at 225 rpm in 5 mL of LB media containing an appropriate antibiotic. 45 mL LB media was then added to the 5 mL starter culture and bacteria were further incubated overnight at 37°C at 225 rpm. The next day the culture was transferred to a 50 mL Falcon tube and centrifuged at 4000 × g for 10 minutes at 4°C. The supernatant was discarded and the bacterial pellet resuspended in 2 mL Buffer P1 (resuspension buffer) with 50 µg/mL RNase A freshly added. 2 mL Buffer P2 (lysis buffer) was added to the bacterial suspension and the tube was inverted 5 times to mix. Cells were incubated for 3 minutes at room temperature before adding 2 mL Buffer N3 (neutralisation buffer) and inverting 5 times. The bacterial lysate was then distributed into four 1.5 mL Eppendorf tubes and centrifuged at 13,200 × g for 10 minutes at 4°C. Supernatants were then collected in a 15 mL Falcon tube and the pellets discarded. 1× volume of 96% ethanol (∼ 5 mL) was added to the supernatants and mixed throughly. The solution was then loaded onto five QIAGEN Miniprep spin columns in three sequential 700 µL aliquots, and columns were centrifuged at 13,200 × g for 30 seconds at 4°C after the addition of each aliquot. After each spin the flow-through was discarded. Columns were washed with 750 µL Buffer PE (wash buffer) and centrifuged for 30 sec. The flow-through was discarded and columns were centrifuged again for 1 minute to remove residual wash buffer. The columns were then transferred to clean 1.5 mL Eppendorf tubes and plasmid DNA was eluted by

adding 35 µL ddH_2O to the column and centrifuging at 13,200 × g for 30 seconds at 4°C. Eluted plasmid DNA was then pooled (∼175 µL final volume) and the DNA concentration was measured with a NanoDrop ND-1000 spectrophotometer (Thermo Scientific) and samples stored at -20°C.

2.2.2.4 Glycerol stocks of transformed bacterial cells

Single colonies were picked from an agar plate and grown overnight at 37°C in an orbital shaker at 225 rpm in 5 mL of LB media containing an appropriate antibiotic. 700 µL of culture was mixed with 300 µL of 50% glycerol and cells were then stored at -80°C.

2.2.3 Mammalian cell culture techniques

2.2.3.1 Cell culture

SLBP T-REx HeLa cells were maintained in Dulbecco's minimum essential media (DMEM) supplemented with 10% FBS, 1× penicillin/streptomycin and 200µg/mL Hygromycin B at 37°C with 5% CO_2, unless stated otherwise. Cells were split every two days by washing with warm PBS and trypsinising for 5 minutes before resuspending in 10 mL media. 1 mL of cells were then transferred to a fresh tissue culture flask with an appropriate volume of complete media and the flask returned to the incubator.

2.2.3.2 Generation of mutant FLAG-SLBP T-REx HeLa cell lines

Stably transfected SLBP T-REx HeLa cell lines were created using the Flp-In T-REx system as per the manufacturer's guidelines (Invitrogen). The day before transfection, 1×10^6 isogenic Flp-In T-REx HeLa host cells, containing a single integrated genomic flippase recombination target (FRT) site, were seeded in 100 mm dishes in DMEM media containing 1× penicillin/streptomycin, 4 µg/mL Blasticidin and 50 µg/mL Zeocin (Invitrogen). The following day, pcDNA5/FRT/TO/CAT:FLAG-SLBP plasmids were co-transfected with pOG44 at a 9:1 ratio using Polyfect transfection reagent (QIAGEN). Transfected cells were then maintained in DMEM supplemented with

10% FBS, 1× penicillin/streptomycin and 4 μg/mL Blasticidin but without Zeocin for 24 hours. The next day, cells were washed with warm PBS and fresh DMEM media supplemented with 10% FBS, 1× penicillin/streptomycin and 200 μg/mL Hygromycin B added to select for transfected cells. The media was changed every 2-3 days until foci of transfected cells were visible. Foci were trypsinised and transferred to T25 flasks for further expansion to produce stable cell lines.

2.2.3.3 Doxycycline-induced gene expression in Flp-In T-REx HeLa cells

Exogenous expression of FLAG-SLBP in Flp-In T-REx HeLa cell lines was induced by adding Doxycycline at a concentration of 0.5 μg/mL in complete media and incubating at 37°C with 5% CO_2 for 5 - 24 hours.

2.2.3.4 siRNA transfection using Lipofectamine RNAiMAX transfection reagent

Cells were transfected with non-targeting or SLBP siRNA using Lipofectamine RNAiMAX transfection reagent (Thermo Fisher). 0.125×10^5 SLBP T-REx HeLa cells were seeded into 6-well cell culture plates and incubated overnight at 37°C with 5% CO_2. The following day, 9 μL of Lipofectamine RNAiMAX reagent was diluted into 150 μL Opti-MEM media in a clean Eppendorf tube. In another Eppendorf tube, 3 μL of 10 μM siRNA (30 pmol) was diluted in 150 μL Opti-MEM media and the contents of both tubes were combined and incubated at room temperature for 5 minutes. After siRNA-lipid complexes had formed, 250 μL of the siRNA-lipid complex solution (25 pmol siRNA) was added to a single well on the 6-well plate. Volumes were scaled up depending on the number and size of wells containing cells to be transfected. After the addition of the siRNA-lipid complex solution, cells were incubated for 24-72 hours with or without 0.5 μg/mL Doxycycline at 37°C with 5% CO_2.

2.2.3.5 Plasmid DNA transfection using Lipofectamine 3000 transfection reagent

Transient transfection of Flp-In T-Rex HeLa cells with plasmid DNA was performed using Lipofectamine 3000 transfection reagent (Thermo Fisher). The following are conditions for the trans-

fection of cells in a single 100 mm dish. Volumes were scaled up accordingly depending on the number of dishes containing cells to be transfected. 2.5 $\times$ 10^5 SLBP T-REx HeLa cells were seeded into a 100 mm cell culture dish and incubated overnight at 37°C with 5% CO2. The following day, 43.4 µL of Lipofectamine 3000 reagent was diluted into 500 µL Opti-MEM media in a clean Eppendorf tube. In another Eppendorf tube, 14 µg of transfection-grade plasmid DNA was diluted in 500 µL Opti-MEM media with 28 µL P3000 reagent and the contents of both tubes were combined and incubated at room temperature for 15 minutes. After DNA-lipid complexes had formed, 1000 µL of the DNA-lipid complex solution ($\sim$14 µg plasmid DNA) was added to cells and cells were incubated for 24 hours with or without 0.5 µg/mL Doxycycline at 37°C with 5% CO2.

2.2.3.6 Cryo-preservation of cells

Cells growing in culture were washed, trypsinised and resuspended at 1 $\times$ 10^6 cells/mL in 1$\times$ freezing medium (50% complete DMEM, 45% FBS, 5% DMSO). Cryovials containing 1 mL of cells were stored overnight at -80°C in a Mr Frosty cell freezing chamber (Invitrogen) before being transferred to liquid nitrogen (-196°C) for long-term storage.

2.2.4 Flow cytometry

For bivariate flow cytometry, 1 $\times$ 10^6 cells were first seeded into 100 mm cell culture dishes and incubated overnight before being transfected with 200 nM NT or SLBP siRNA using Lipofectamine RNAiMAX, as in Section 2.2.3.4. After transfection, doxycycline was added to a final concentration of 0.5 µg/mL and cells were incubated at 37°C with 5% CO_2 for 24 hours. The following day, cells were washed with warm PBS before media containing 25 µM BrdU was added and cells incubated for 30 min at 37°C. After incubation with BrdU, cells were washed again with warm PBS and trypsinised. Cells were resuspended in PBS without Ca/Mg, containing 5% dialysed FBS and 5 mM EDTA to reduce cell aggregation. Cells were then centrifuged at 500 x g for 5 mins and the cell pellet was resuspended in 0.5 mL PBS containing 5 mM EDTA before adding 4.5 mL of ice-cold 70% ethanol drop by drop while vortexing to fix cells. Fixed cells were stored at 4°C overnight before being washed in 1 mL ice-cold wash buffer (PBS + 0.5% BSA) and resuspended

in 1 mL 2M HCl to permeabilise the plasma membrane and denature DNA. Cells were then washed with 1 mL ice-cold wash buffer and residual HCl was neutralised by resuspending cells in 1 mL 0.1M sodium borate (pH 8.5) and incubating for 3 mins. After a further wash with ice-cold wash buffer, fixed and permeabilised cells were incubated with 0.1 mL of rat α-BrdU primary antibody in antibody dilution buffer (PBS + 0.5% BSA + 0.2% Tween-20) for 2 hours at 4°C with gentle agitation. Labelled cells were washed with 1 mL ice-cold wash buffer and cells were then incubated with 0.1 mL of AlexaFlour 568 goat α-Rat secondary antibody in dilution buffer for 1 hour at 4°C. After incubation, cells were washed a final time and then resuspended in 1 mL PBS + 5 mM EDTA containing 0.1 µg/mL DAPI and 200 µg/mL RNase A. Prepared samples were then analysed using an Attune NxT Flow Cytometer (ThermoFisher) in the School of Biosciences and data analysis was performed using Flowjo software (v10.5.3).

2.2.5 RNA techniques

2.2.5.1 RNA extraction using the Monarch RNA Miniprep kit

Total RNA was extracted and purified from eukaryotic cells using the Monarch RNA Miniprep kit (New England Biolabs). Cells seeded into 6-well tissue culture plates were washed twice with ice-cold PBS and then lysed by the addition of 300 µL RNA lysis buffer. The cell lysate was removed by pipetting and transferred to a labelled gDNA removal column in a collection tube and centrifuged at 16,000 × g for 30 seconds at 4°C. After centrifugation, the gDNA column was discarded and 1× volume of 96% ethanol was added to the flow-through in the collection tube. The contents of the collection tube was then transferred to a labelled RNA purification column in a fresh collection tube and centrifuged at 16,000 × g for 30 seconds at 4°C. The flow-through was discarded and the column was washed by centrifugation with 500 µL RNA wash buffer, with the flow-through discarded again. In a separate tube, 5 µL DNase I was combined with 75 µL DNase I reaction buffer and the solution was pipetted directly onto the column membrane before incubating at room temperature for 15 minutes to enzymatically remove residual gDNA. 500 µL RNA priming buffer was added and the column was centrifuged at 16,000 × g for 30 seconds at 4°C and the flow-through was discarded. The column was then washed twice with 500 µL RNA wash buffer and after the final wash, the column was centrifuged again for 1 minute 30 seconds to

ensure removal of residual RNA wash buffer. The RNA purification column was then transferred to a clean, labelled Eppendorf tube and 50 µL ddH_2O was added directly to the column membrane. RNA was then eluted by centrifugation at 16,000 × g for 30 seconds at 4°C. The concentration of purified RNA was measured with a NanoDrop ND-1000 spectrophotometer (Thermo Scientific) and samples were stored at -20°C.

2.2.5.2 Reverse transcription

Extracted RNA was converted to cDNA using the High Capacity RNA-to-cDNA kit (Applied Biosystems). 20 µL reactions were set up as per the manufacturer's instructions, with a -RT reaction omitting the reverse transcriptase enzyme set up alongside as a control. Samples were then incubated at 37°C for 1 hour followed by 95°C for 5 minutes. Samples were stored at -20°C.

2.2.5.3 Quantitative real-time PCR (qPCR)

qPCR was performed in a 96-well plate using a Bio-Rad C1000 Touch thermal cycler with a Bio-Rad CFX96 RT-PCR optical reaction module. 50 µL reactions were tested in triplicate with each reaction well containing 25 µL of 2× SYBR Green JumpStart Taq ReadyMix (Sigma), 100-250 ng cDNA, 400-800 nM forward primer and 400-800 nM reverse primer, diluted in ddH_2O. No template control wells were included to check for contamination and the formation of primer dimers. Plates were sealed with adhesive PCR film (ThermoFisher) and the target was amplified using a program consisting of 35 cycles as detailed in Table 2.9. Results were quantified using the $2^{-\Delta\Delta C_T}$ method and were normalised to *GAPDH* (Livak and Schmittgen, 2001).

Segment	Cycles	Temperature	Time
1	1	98°C	10 sec
2	35	98°C	1 sec
		55°C	5 sec
		72°C	1 min
3	1	72°C	5 min
4	1	55°C - 98°C (Melt curve)	5 sec
5	1	4°C	∞

Table 2.9: qPCR thermal cycling parameters.

2.2.6 Protein techniques

2.2.6.1 Whole cell lysate preparation

Whole-cell lysates were prepared by first placing cells grown in appropriate-sized culture dishes on ice and washing three times with ice-cold PBS. After the final wash, the dish was tilted and residual PBS allowed to drain before aspirating. 1× RIPA lysis buffer was then pipetted onto cells (75 µL for a 100 mm dish) and incubated on ice for 5 minutes before cells were scraped and transferred to 1.5 mL Eppendorf tubes. Unclarified lysates were incubated for a further 10 minutes on ice and then centrifuged at 13,200 rpm for 15 minutes at 4°C. The supernatants were then transferred to fresh Eppendorf tubes and stored at -80°C.

2.2.6.2 Bradford assay

The protein concentration of cellular lysates was determined using a Bio-Rad protein assay reagent based on the protein-dye binding method of Bradford (1976). 5 µL of cell lysate was diluted in 1 mL of 1× protein assay reagent and absorbance measured at 595 nm using a spectrophotometer. The protein concentration was calculated using a standard curve constructed with known concentrations of BSA.

2.2.6.3 SDS-polyacrylamide gel electrophoresis

SDS-polyacrylamide gel electrophoresis was performed under denaturing conditions using 1.5 mm thick 10% polyacrylamide mini-gels (100 mm × 80 mm) according to the method of Laemmli (1970). Polymerised gels were assembled into a Bio-Rad Mini-PROTEAN II apparatus and the inner and outer reservoirs were filled with 1× SDS-PAGE running buffer. Typically, 20 μg protein sample was diluted in 25 μL of 1× SDS-PAGE loading buffer with 100 μM dithiothreitol (DTT), boiled for 5 minutes at 100°C, and then loaded into a 1.5 mm well. 3 μL of Bio-Rad Colour Pre-stained Protein Standard Broad Range ladder was used as a molecular weight marker. Electrophoresis was routinely performed at 160 V (constant) for 80 minutes.

2.2.6.4 Immunoblotting

Immunoblotting was performed essentially as described by Burnette (1981). Immediately after electrophoresis, polyacrylamide gels were removed from their retaining plates and placed on nitrocellulose paper, which was then sandwiched between four sheets of Whatmann chromatography paper and two pieces of sponge in a transfer cassette. The transfer cassettes were then loaded into a Bio-Rad Mini-PROTEAN II apparatus filled with 1× gel transfer buffer and containing one ice pack to dissipate heat generated during transfer. Electric current was applied at 100 V (constant) for 1 hour to allow the transfer of proteins from the SDS-PAGE gel to the nitrocellulose membrane. After transfer, the membrane was blocked in 1× WB blocking buffer for 1 hour at room temperature with gentle agitation. Blocking buffer was then removed and replaced with primary antibody (see Table 2.1) diluted in 1× Western blot antibody buffer and incubated for 1 hour at room temperature or overnight at 4°C with gentle agitation. The membrane was then washed three times with 1× TBST for 5 minutes each before adding the secondary antibody, diluted in 1× Western blot antibody buffer, and incubating for a further hour at room temperature. The membrane was then washed again three times with 1× TBST for 5 minutes each and the membrane was then allowed to dry between two pieces of chromatography paper before being scanned using a LI-COR Odyssey SA Imaging System (LI-COR Biosciences UK Ltd., Cambridge, England, UK).

2.2.6.5 Immunoprecipitation using α-FLAG M2 agarose beads

Immunoprecipitation of FLAG-SLBP was performed with α-FLAG M2 affinity agarose beads (Sigma). Cells grown in culture were washed twice with ice-cold PBS and lysed in A2220 immunoprecipitation buffer containing protease and phosphatase inhibitors (Appendix A). 40 µL (∼20 µL packed gel volume) of α-FLAG M2 affinity agarose bead gel suspension was added to a clean 1.5 mL Eppendorf per reaction and tubes were centrifuged at 7,000 × g for 30 seconds. The supernatant was removed and beads were resuspended and washed twice with 500 µL of TBS. 1 mg of protein was added and the final volume was brought to 1 mL with A2220 lysis buffer containing protease and phosphatase inhibitors. Samples were then incubated on a roller shaker for 2 hours at room temperature or overnight at 4°C. After capture, samples were centrifuged at 7,000 × g for 30 seconds to pellet the resin with bound protein and the supernatant was removed. The resin with bound protein was then washed three times with 330 µL of TBS. Elution of FLAG-SLBP and interacting proteins was performed by incubating beads for 30 minutes at room temperature with 100 µL of 3X FLAG peptide at 300 ng/µL (Sigma). Eluted protein was stored at -80°C.

2.2.7 Proteomic techniques

2.2.7.1 Reduction and alkylation of proteins

Proteins eluted from α-FLAG immunoprecipitates were prepared for LC-MS/MS analysis using Protifi S-Trap micro spin columns (Profiti, Fairport, NY, USA). Reduction and alkylation of proteins was achieved by first combining 11.5 µL of 2X A2220 buffer + 10% SDS with 11.5 µL of the immunoprecipitation eluate, after which the diluted sample was briefly vortexed to mix. 1 µL of 120 mM TCEP (5 mM final concentration) was then added and samples were incubated at 55°C for 15 mins to reduce cysteine residues. Disulphides were then alkylated by adding 1 µL of 500 mM MMTS (20 mM final concentration) and incubating for 10 mins at room temperature. Reduced and alkylated samples were then acidified by adding ∼2.5 µL of 25% phosphoric acid to achieve a pH ≤ 1.

2.2.7.2 Enzymatic digestion

Reduced and alkylated proteins were diluted in 165 µL binding/wash buffer (100 mM TEAB in 90% MeOH) and loaded onto an S-Trap column placed inside a clean 1.5 mL Eppendorf tube in order to trap proteins prior to on-column enzymatic digestions. After centrifugation at 4,000 x g for 30 seconds to trap proteins, the flow through was discarded and trapped proteins were washed three times with 150 µL binding/wash buffer. The S-trap column was then transferred to a new 1.5 µL Eppendorf tube and 20 µL of 1X GluC digestion buffer containing 100 ng GluC protease was added (New England Biolabs). The S-Trap column was then wrapped loosely with parafilm and incubated for 4 hours at 37°C in a water bath. After incubation, peptides were eluted into the Eppendorf collection tube by sequential centrifugation with elution buffers 1 (50 mM TEAB), 2 (0.2% formic acid) and 3 (50% acetonitrile). Eluates were pooled, dried down and resuspended in 2% acetonitrile, 0.1% formic acid.

2.2.7.3 Liquid chromatography-mass spectrometry

Mass spectrometry samples were analysed by staff in the University of Sheffield Biological Mass Spectrometry Facility. Briefly, resuspended peptides were injected into a ThermoFisher Scientific OrbiTrap Elite mass spectrometer equipped with a Nanospray Flex Ion ESI source using a Dionex Ultimate 3000 uHPLC connected to an Acclaim PepMap100 C18 column (2 µm particle size, 100 Å pore size, 75 µm internal diameter). Peptides were separated over a 60-minute gradient of increasing acetonitrile from 2.4% to 72%, in 0.1% formic acid at 300 nL/min at 45°C. Nanospray ionisation was conducted at 2.3 kV, with the ion transfer capillary at 250°C, and S-lens setting of 60%. MS1 spectra were acquired at a resolving power of 60,000 with an AGC (automatic gain control) target value of 1×10^6 ions by the Orbitrap detector, with a range of 350-1850 *m/z*. Following MS1 analysis, the most abundant precursors were selected for data-dependent activation (MS2 analysis) using CID (collision-induced dissociation), with a 10 ms activation time and an AGC setting of 10,000 ions in the dual cell linear ion trap on normal scan rate resolution. Precursor ions of a single charge were rejected and a 30-second dynamic exclusion window setting was used after a single occurrence of an ion.

Chapter 3

Validation of FLAG-SLBP Flp-In T-REx HeLa cell lines and experimental methods

3.1 Introduction

SLBP is an essential protein required for histone mRNA biosynthesis and is indispensable for long-term cell and organism viability (Marzluff and Koreski, 2017; Turner et al., 2019; Potter-Birriel et al., 2021). As such, to investigate the function of SLBP in mammalian cells and address the specific aims of this project, it was necessary to utilise a genetically tractable model system to conditionally express mutant versions of SLBP alongside or in place of endogenous SLBP. The Flp-In T-REx HeLa cell expression system (Invitrogen) allows for the generation of stably transfected isogenic cell lines that conditionally express a gene of interest (GOI) when cells are cultured in the presence of a small molecule inducer (described in Section 3.1.1). The Flp-In TRex system provides several benefits compared to the transient transfection of an expression vector containing a GOI, in particular, eliminating the need to perform cationic lipid-mediated transfection, which exhibits variable transfection efficiency and a degree of cytotoxicity (Ward et al., 2011; Szczesny et al., 2018; Stepanenko and Heng, 2017). There are, however, potential limitations that may arise when using a conditional expression system that must be considered, such as "leaky" background expression in the absence of an inducer and the possibility of inducing an artificially high level of protein expression when the inducer is present (Senkel et al., 2009).

Biochemical analysis of protein function in mammalian cells is routinely facilitated by the ex-

pression and characterisation of fusion-tagged wild-type or mutant versions of a GOI gene product. Fusion proteins can be expressed in Flp-In T-REx cells by engineering the GOI cDNA such that the coding sequence for the desired tag is in frame with the 5' or 3' end of the GOI coding sequence (Thomas et al., 2004; Torres et al., 2009). Often only a particular amino acid or a short sequence of amino acids are of interest within a protein. Specific amino acids can be altered or deleted by site-directed mutagenesis of the GOI prior to transfection to generate mutant Flp-In T-REx cell lines for comparative analysis against wild-type cells. Site-directed mutagenesis that incorporates silent mutations in a known RNAi target sequence enables the additional capability of performing RNAi rescue experiments with mutant cell lines after knockdown of the endogenous GOI (Cullen, 2006).

N-terminal FLAG-tagged SLBP^{WT} and FLAG-SLBP^{siRes} (siRNA resistant) Flp-In T-REx HeLa cells were inherited from Dr Pornpen Panomwan (Smythe Lab, The University of Sheffield) for use in this project. The FLAG tag is an eight amino acid (DYKDDDDK) epitope tag to which there are high-quality, commercially available antibodies and reagents that can be used for the identification and purification of FLAG-tagged proteins. Key elements of the present study require the routine identification and relative quantification of mutant SLBP expression by Western blotting, and the isolation of SLBP and associated proteins by immunoprecipitation from complex cell lysates. As the α-FLAG antibody for Western blotting and α-FLAG agarose beads for immunoprecipitation were available in-house and had been used successfully by our group in the past, utilising the FLAG tag remained a central aspect of the experimental strategy in the present study.

Previous reports in the literature provide evidence that RNAi-mediated SLBP knockdown reduces replication-dependent histone mRNA levels by 40-60% in HeLa and U2OS cell lines, leading to nuclear retention of unprocessed histone pre-mRNA, an accumulation of cells in S phase and a reduced rate of cell proliferation (Zhao et al., 2004; Sullivan et al., 2009). In the experiments presented in the current chapter, I have validated FLAG-SLBP^{WT} and FLAG-SLBP^{siRes} Flp-In T-REx HeLa cell lines and have optimised and validated qPCR and flow cytometry RNAi rescue experiments to confirm that the expression of FLAG-SLBP^{siRes} following siRNA-mediated knockdown of endogenous SLBP is sufficient to restore SLBP function and rescue the cellular phenotypes associated with SLBP knockdown that have been reported previously. In addition, I have validated

an immunoprecipitation protocol to isolate and purify FLAG-SLBP and interacting proteins from complex cell lysates that, together with the qPCR and flow cytometry RNAi rescue experiments, will be used throughout the project to interrogate the function of SLBP.

3.1.1 Overview of the Flp-In T-REx HeLa cell system

The Flp-In T-REx HeLa cell system is a Tet-On inducible expression system that allows for the conditional expression of a stably transfected GOI in mammalian cells (Ward et al., 2011; Szczesny et al., 2018). The system utilises a *Saccharomyces cerevisiae*-derived flippase recombinase (Flp) enzyme and site-specific recombination (Cox, 1983; Craig, 1988) to integrate a GOI into a single chromosomal site in a pre-engineered Flp-In T-REx HeLa host cell line. After stably transfected cells have been selected with the appropriate selection antibiotic, the expression of the GOI in the established cell line is induced and maintained by the addition of a small molecule inducer to cell culture growth media (see Figure 3.1).

Our Flp-In T-REx HeLa host cells were kindly provided some time ago by Professor Patrick Eyers (The University of Liverpool). Flp-In T-REx host cells are generated by transfecting HeLa cells with pFRT/*lac*Zeo and pcDNA6/TR plasmids, which both randomly and independently insert into the HeLa cell genome. The pFRT/*lac*Zeo plasmid contains a flippase-recombination target (FRT) sequence flanked by a transcription initiation codon and the coding sequence for a *lac*Z-Zeocin fusion protein. The pcDNA6/TR plasmid contains the coding sequence for a Tet repressor (TetR) under the control of the human CMV promoter. Successfully transfected Flp-In T-REx host cells are then selected by culturing cells in media containing Zeocin and individual clones are screened for single pFRT/*lac*Zeo integrants. Expression-competent cells can then be generated by co-transfecting Flp-In T-REx host cells with a pcDNA5/FRT/TO vector containing a GOI and a pOG44 plasmid that constitutively expresses Flp. Flp-mediated recombination inserts the pcDNA5/FRT/TO plasmid containing the GOI into the genome using the integrated FRT site in the Flp-In T-REx host cells and the FRT site in the pcDNA5/FRT/TO plasmid. The *lac*Zeo gene is inactivated due to it being separated from the SV40 promotor following recombination. As a result of recombination, cells become resistant to hygromycin allowing for the selection of stably trans-

fected cells by culturing cells in media containing hygromycin. Expression of the integrated GOI is repressed by TetR binding to two TetO2 sites, which blocks the progression of RNA polymerase II. TetR is sensitive to tetracycline and its more stable derivative, doxycycline, which when added to culture media, binds to TetR and induces a conformational change resulting in the dissociation of TetR from the TetO2 sites. Dissociation of TetR allows RNA polymerase II to progress unimpeded leading to transcription of the GOI.

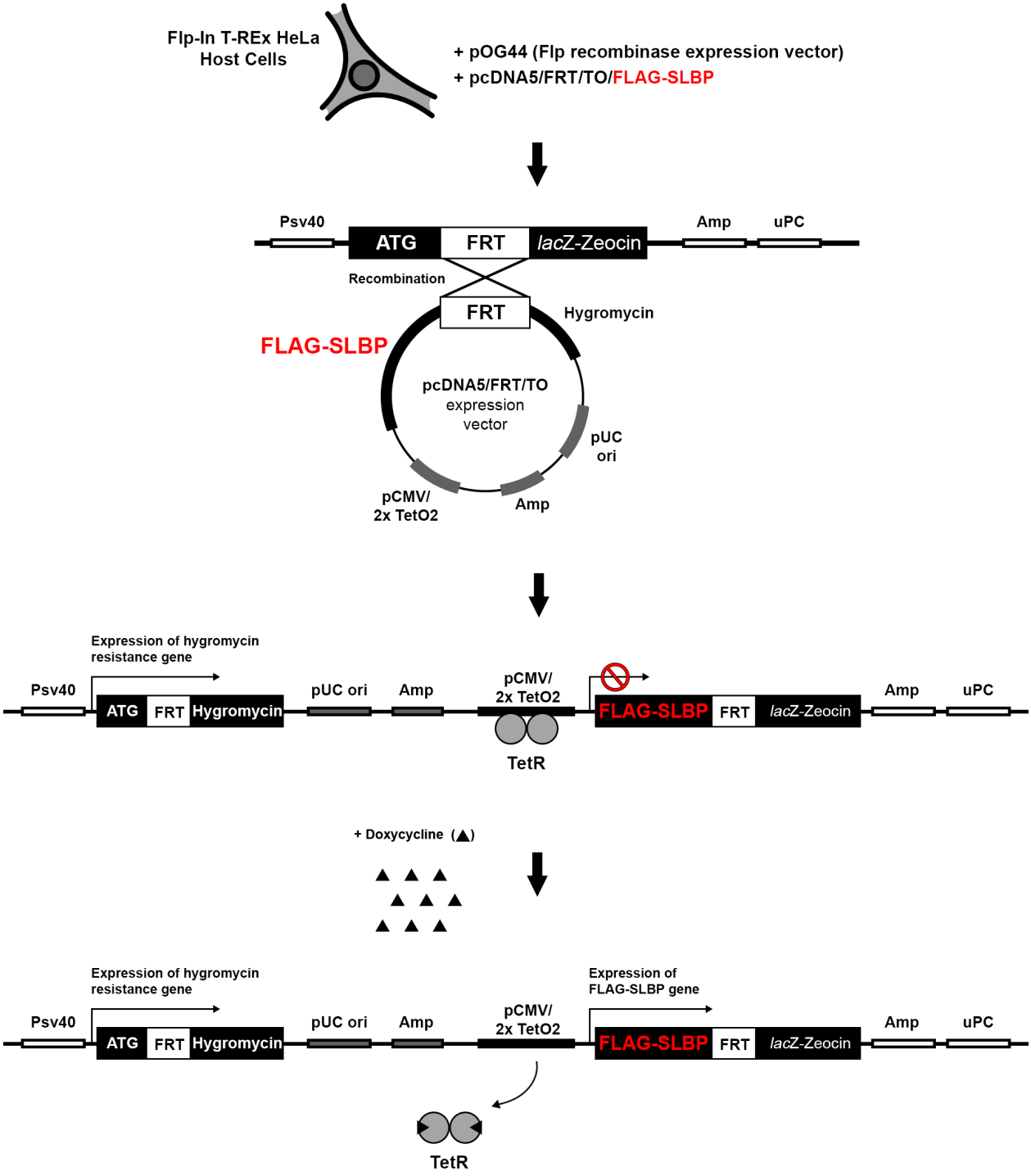

Figure 3.1: Schematic diagram providing an overview of the Flp-In T-Rex HeLa cell system. Flp-In T-REx host cells containing a single flippase recombinase target (FRT) sequence are co-transfected with pOG44 and a pcDNA5/FRT/TO plasmid containing a GOI. The Flp recombinase expressed from pOG44 mediates recombination between the genomic FRT site and the FRT site in the pcDNA5/FRT/TO plasmid, resulting in the integration of the pcDNA5/FRT/TO plasmid and its contents into the genome of the Flp-In T-Rex host cells. Stable integrants are selected by propagating cells in growth media containing hygromycin. Expression of the GOI is conditional on the presence of tetracycline, or its derivative, doxycycline, in growth media. Tetracycline/doxycycline binds to the TetR repressor and induces a conformational change in TetR, leading to the dissociation of TetR and expression of the GOI.

3.2 Results

3.2.1 Validation of FLAG-SLBP^{WT} and FLAG-SLBP^{siRes} Flp-In T-REx HeLa cell lines

3.2.1.1 Doxycycline induces expression of FLAG-tagged SLBP at levels equal to endogenous SLBP in asynchronous cells

The expression of an exogenous GOI in Flp-In T-REx cells is repressed by default due to TetR binding to two TetO2 sites located between the CMV promoter and the GOI, thereby blocking the progression of RNA polymerase II (Figure 3.1). Expression is achieved through the addition of tetracycline, or its more stable derivative, doxycycline, to cell culture media, which induces a conformational change in TetR and dissociation of TetR from the TetO2 sites. I confirmed doxycycline-induced expression of FLAG-SLBP^{WT} in Flp-In T-REx HeLa cells by growing 1×10^6 asynchronous FLAG-SLBP^{WT} cells in 100 mm cell culture dishes for 24 hours before adding 0.1, 0.5 or 1.0 μg/mL doxycycline in DMEM media and incubating for a further 5 hours. Cell lysates were then harvested and analysed by Western blot (Figure 3.2). Doxycycline treatment induced the expression of FLAG-SLBP^{WT} as evidenced by the clear signal in lanes 2, 3 and 4 of the FLAG immunoblot and by the presence of a second slightly heavier band in lanes 2, 3 and 4 of the SLBP immunoblot (Figure 3.2A). FLAG-tagged SLBP migrates at a slightly slower rate than endogenous SLBP on the SDS polyacrylamide gel due to the increased molecular weight of FLAG-SLBP compared to wild-type and the strong negative charge of the aspartate-rich FLAG tag. FLAG-SLBP^{WT} protein levels were identical at each doxycycline concentration tested and were expressed at a level equal to endogenous SLBP (Figure 3.2B). The absence of an increase in FLAG-SLBP^{WT} protein levels with increasing concentrations of doxycycline demonstrates that the expression of exogenous FLAG-SLBP^{WT} is maximal after 5 hours of exposure to doxycycline at concentrations as low as 0.1 μg/mL and that submaximal expression of FLAG-SLBP in this system, if needed, would require lower doxycycline concentrations and/or shorter doxycycline exposure times. Previous experiments conducted in the Smythe Lab with FLAG-SLBP Flp-In T-REx HeLa cells routinely used a doxycycline concentration of 0.5 μg/mL (Panomwan, 2017) and, as there is no observed overexpression of FLAG-SLBP^{WT} at this concentration, 0.5 μg/mL doxycycline was used to induce the expression of exogenous FLAG-tagged SLBP in all subsequent experiments.

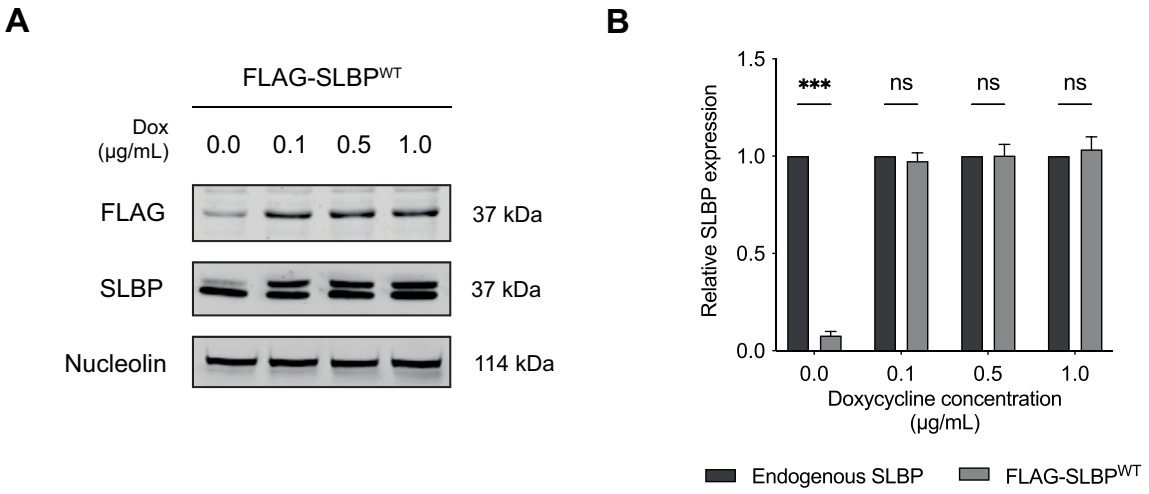

Figure 3.2: Doxycycline-induced expression of FLAG-SLBP^{WT} in Flp-In T-REx HeLa cells. **(A)** Asynchronous FLAG-SLBP^{WT} Flp-In T-REx HeLa cells were cultured in media supplemented with 0.1, 0.5 and 1.0 µg/mL doxycycline for 5 hours and cell lysates were analysed by Western blot using α-FLAG, α-SLBP and α-nucleolin antibodies. Nucleolin is used as a loading control. Note that SLBP (predicted MW: 31 kDa) has an observed MW of 37 kDa and that a heavier band is visible in the SLBP immunoblot when cells are grown in media containing doxycycline due to the presence of the FLAG tag. **(B)** Relative quantification of FLAG-SLBP^{WT} (upper band) and endogenous SLBP (lower band) band intensities in SLBP immunoblot in (A). *** = $p < .001$, ns = non-significant. Student's unpaired t-test. Data are mean $\pm$ S.E.M. n = 3 experiments.

Having determined a concentration of doxycycline that induces the expression of FLAG-SLBP^{WT} at the same level as endogenous SLBP in Flp-In T-REx HeLa cells, I next sought to ascertain the duration of doxycycline-induced gene expression when cells are exposed to 0.5 μg/mL doxycycline. To achieve this, 1×10^6 asynchronous FLAG-SLBP^{WT} cells were seeded into 100 mm or 150 mm cell culture dishes and were incubated with 0.5 μg/mL doxycycline for 5-96 hours before analysing by Western blot (Figure 3.3). Cells for the 72-hour and 96-hour time-points were seeded into 150 mm dishes to provide sufficient area for growth such that cell cycle arrest due to contact inhibition would not result in decreased expression of SLBP (Gérard and Goldbeter, 2014). As in Figure 3.2, exposure to 0.5 μg/mL doxycycline for 5 hours was sufficient to induce the expression of FLAG-SLBP^{WT} at levels equal to endogenous SLBP, and levels remained comparable for up to 48 hours before the intensity of the FLAG-SLBP^{WT} band (upper band in SLBP immunoblot) began to decrease (Figure 3.3A and B). At 72 hours the intensity of the FLAG-SLBP^{WT} band had reduced to 63% relative to endogenous SLBP and by 96 hours it was reduced to 33% (Figure 3.3B). The intensity of the endogenous SLBP band (lower band in SLBP immunoblot) remained relatively stable over time, with only a slight reduction being evident at 96 hours (Figure 3.3A), indicating that the reduction in the FLAG-SLBP^{WT} signal intensity at later timepoints was not a result of cell cycle arrest due to contact inhibition and was instead likely due to the decreased availability of soluble doxycycline. This result is consistent with doxycycline exhibiting a half-life of 24 hours in cell culture media. Thus, it was concluded that a concentration of 0.5 μg/mL doxycycline is effective at inducing maximal FLAG-SLBP^{WT} gene expression in Flp-In T-REx HeLa cells for up to 48 hours and that it is necessary to replenish cell culture media containing doxycycline after 48 hours in any experiments where expression of FLAG-SLBP is required over longer time periods.

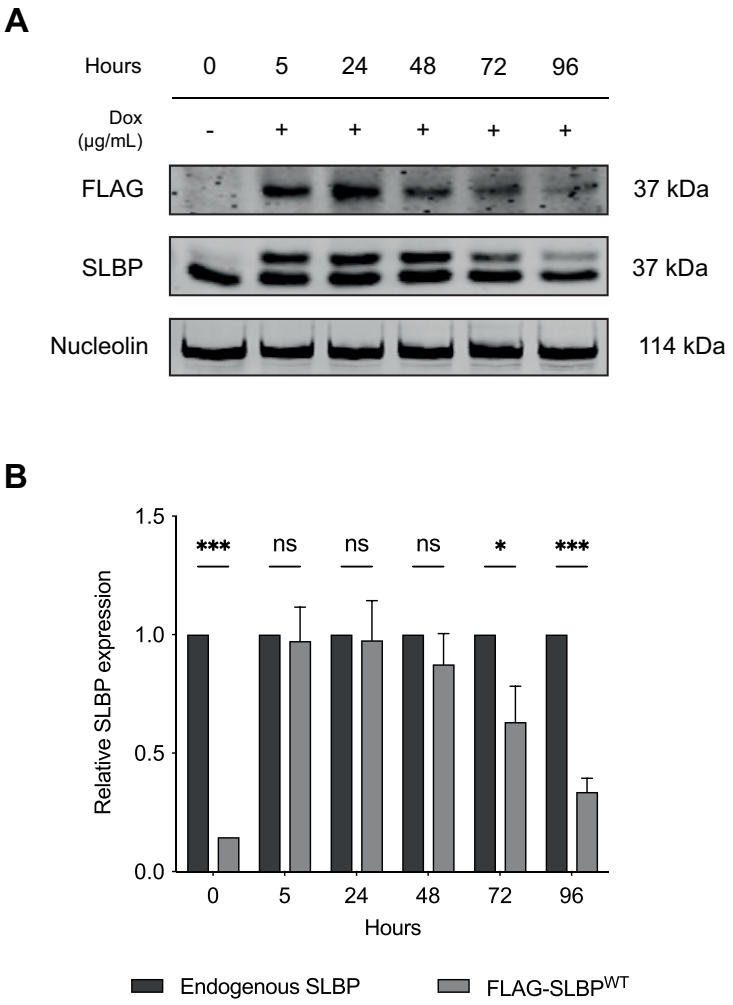

Figure 3.3: Doxycycline-dependent FLAG-SLBP^{WT} protein levels compared to endogenous SLBP over time. (A) Asynchronous FLAG-SLBP^{WT} cells were cultured in 100 mm (0, 5, 24 and 48 hours) and 150 mm (72 and 96 hours) dishes in media supplemented with 0.5 µg/mL doxycycline for up to 96 hours and cell lysates were analysed by Western blot using α-FLAG, α-SLBP and α-nucleolin antibodies. Nucleolin is used as a loading control. **(B)** Relative quantification of FLAG-SLBP^{WT} (upper band) and endogenous SLBP (lower band) band intensities in SLBP immunoblot in (A). * = $p < .05$, *** = $p < .001$, ns = non-significant. Student's unpaired t-test. Data are mean $\pm$ S.E.M. n = 3 experiments.

3.2.1.2 FLAG-SLBP^{siRes} cells are resistant to siRNA-mediated knockdown of SLBP

Post-transcriptional gene silencing using RNAi technology is an invaluable tool for determining the function of genes in mammalian cells (Fire et al., 1998; Shi, 2003). Transient or inducible RNAi with short interfering RNA (siRNA) or short hairpin RNA (shRNA) is particularly useful when attempting to elucidate the function of an essential gene, such as that for SLBP, as the generation of knockout cell lines for essential genes is unfeasible. Here, using FLAG-SLBP^{WT} and FLAG-SLBP^{siRes} Flp-In T-REx HeLa cells inherited from Dr Pornpen Panomwan, I demonstrate siRNA-mediated knockdown of endogenous SLBP and FLAG-SLBP^{WT}, and the subsequent expression of siRNA-resistant FLAG-SLBP^{siRes}, which forms the basic experimental procedure underlying the RNAi rescue experiments conducted throughout this study.

ON-TARGETplus siRNA targeting a region in exon 4 of SLBP was obtained from Horizon Discovery (Cambridge, England, UK) and 200 nM siRNA was transfected using 45 μL Lipofectamine RNAiMAX transfection reagent into 1×10^6 asynchronous FLAG-SLBP^{WT} and FLAG-SLBP^{siRes} Flp-In T-REx HeLa cells grown in 100 mm cell culture dishes. A non-targeting siRNA was transfected into FLAG-SLBP^{WT} cells as a control. 0.5 μg/mL doxycycline was added to cells 19 hours post-transfection and cells were incubated for a further 5 hours before analysis by Western blot and qPCR (Figure 3.4). Using this protocol, SLBP siRNA, but not non-targeting siRNA, resulted in $\sim$80% knockdown of endogenous SLBP and FLAG-SLBP^{WT} protein (Figure 3.4A, compare lanes 1 and 2 with lanes 3 and 4), confirming that the SLBP siRNA and the transfection protocol used are effective at silencing SLBP in Flp-In T-REx HeLa cells. Knockdown of endogenous SLBP occurred in FLAG-SLBP^{siRes} cells (Figure 3.4A, lanes 5 and 6), though the FLAG-SLBP^{siRes} protein that was induced after the addition of doxycycline remained stable in the presence of SLBP siRNA and was expressed at levels similar to FLAG-SLBP^{WT} in control cells (Figure 3.4A, compare lanes 2 and 6). This result confirms that the two silent nucleotide substitutions in the FLAG-SLBP^{siRes} cDNA coding sequence are sufficient to confer resistance to siRNA-mediated knockdown of SLBP.

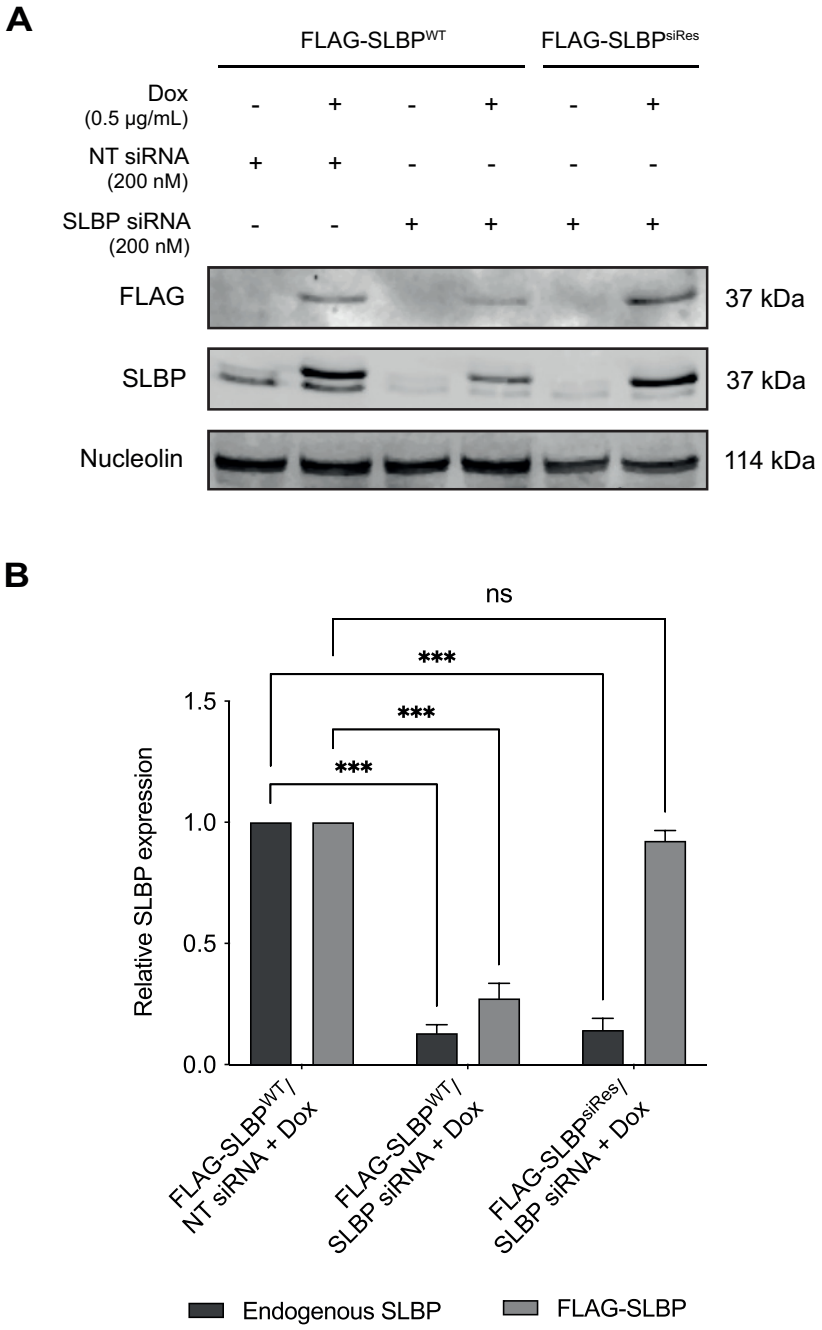

Figure 3.4: FLAG-SLBP^{siRes} is resistant to siRNA-mediated SLBP knockdown. **(A)** Asynchronous FLAG-SLBP^{WT} and FLAG-SLBP^{siRes} cells were transfected with 200 nM non-targeting (NT) or SLBP siRNA for 24 hours and incubated with or without 0.5 µg/mL doxycycline for the final 5 hours, and cell lysates were analysed by Western blot using α-FLAG, α-SLBP and α-nucleolin antibodies. Nucleolin is used as a loading control. **(B)** Relative quantification of FLAG-SLBP (upper band) and endogenous SLBP (lower band) band intensities in lanes 2, 4 and 6 (+0.5 µg/mL doxycycline) of SLBP immunoblot in (A). *** = $p < .001$, ns = non-significant. Dunnett's two-way ANOVA. Data are mean $\pm$ S.E.M. n = 3 experiments.

In addition, I determined the duration of transient siRNA-mediated SLBP knockdown by transfecting 200 nM NT or SLBP siRNA into 1×10^6 asynchronous FLAG-SLBP^{WT} Flp-In T-REx HeLa cells seeded in 100 mm or 150 mm cell culture dishes. Cells were incubated for up to 96 hours post-transfection before analysing by Western blot and qPCR (Figure 3.5). As in Figure 3.3, cells for the 72-hour and 96-hour time-points were seeded into 150 mm dishes to provide sufficient area for growth such that cell cycle arrest due to contact inhibition would not result in decreased expression of SLBP (Gérard and Goldbeter, 2014). Significant knockdown of SLBP was only evident at the 24-hour time-point. By 48 hours the intensity of the SLBP signal had returned to a level similar to that of cells transfected with NT siRNA and remained at this level for the remainder of the experiment, suggesting that siRNA-mediated gene silencing of SLBP under these conditions is only effective for 24 hours.

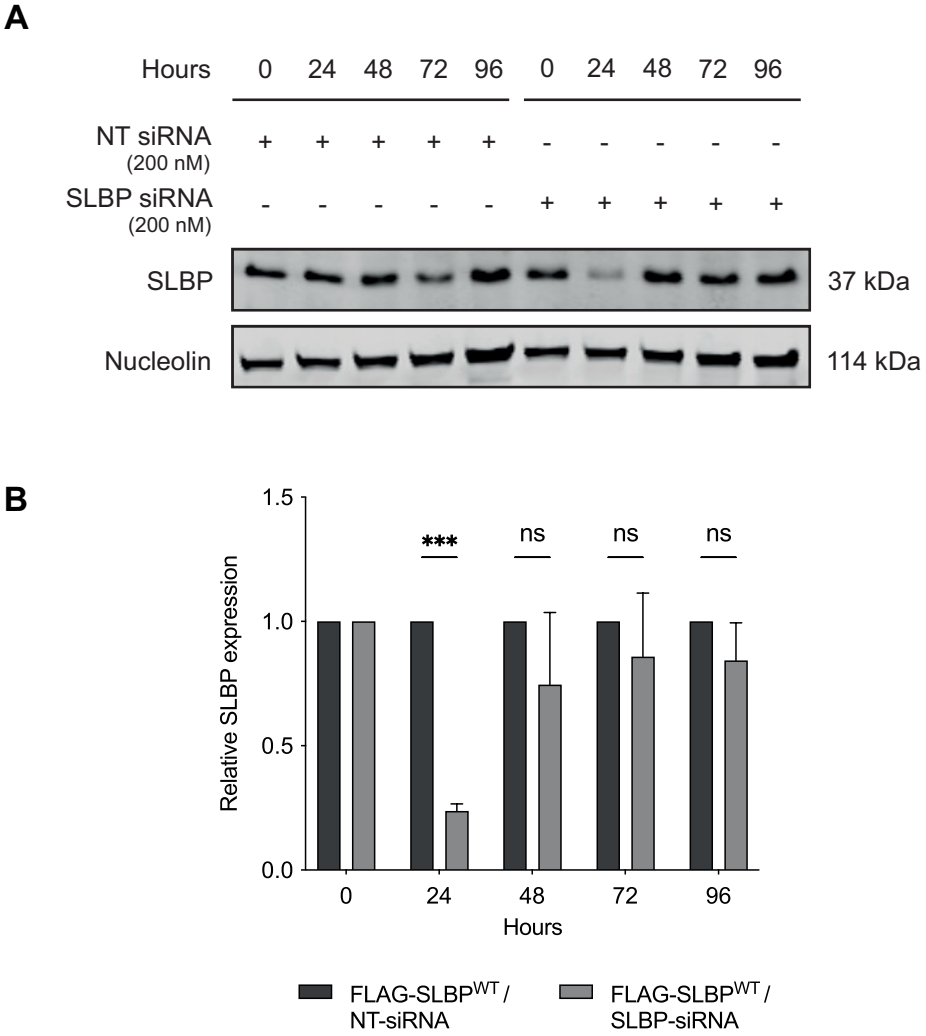

Figure 3.5: Duration of siRNA-mediated SLBP knockdown. **(A)** Asynchronous FLAG-SLBP^{WT} cells were transfected with 200 nM non-targeting (NT) or SLBP siRNA and cultured in 100 mm (0, 24 and 48 hours) and 150 mm (72 and 96 hours) dishes for up to 96 hours and cell lysates were analysed by Western blot using α-SLBP and α-nucleolin antibodies. Nucleolin is used as a loading control. **(B)** Relative quantification of SLBP band intensities in (A). *** = $p <$ .001, ns = non-significant. Student's unpaired t-test. Data are mean $\pm$ S.E.M. n = 3 experiments.

3.2.1.3 Expression of FLAG-SLBP^{siRes} is sufficient to rescue SLBP siRNA-induced defects in cell cycle progression

RNAi-mediated knockdown of SLBP results in an increase of cells in S phase due to a delay in the progression of cells from S phase to G2/M (Zhao et al., 2004; Wagner et al., 2005; Sullivan et al., 2009; Kerzendorfer et al., 2012). Expression of RNAi-resistant SLBP in cells exposed to siRNA targeting SLBP has previously been shown to rescue the cell cycle defects associated with SLBP knockdown (Wagner et al., 2005). In order to replicate these observations and confirm that expression of FLAG-SLBP^{siRes} is sufficient to rescue the phenotype in Flp-In T-REx HeLa cells, I transfected asynchronous FLAG-SLBP^{WT} and FLAG-SLBP^{siRes} cells with either 200 nM NT or SLBP siRNA and incubated cells for 24 hours, with or without 0.5 μg/mL doxycycline, and analysed cell cycle distributions by flow cytometry (Figure 3.6). As shown previously, knockdown of SLBP with siRNA resulted in a significant increase in the number of cells in S phase (Figure 3.6A, compare left and middle panels). Quantification of data from three independent experiments showed that under these experimental conditions, the number of cells in S phase increased by $\sim$10% in SLBP knockdown cells whereas the number of cells in G1 and G2/M decreased by $\sim$10% and $\sim$25%, respectively (Figure 3.6B). This result is consistent with there being a defect in S phase progression in SLBP knockdown cells (Zhao et al., 2004; Wagner et al., 2005; Sullivan et al., 2009; Kerzendorfer et al., 2012). As expected, the subsequent expression of FLAG-SLBP^{siRes} in cells lacking endogenous SLBP was sufficient to reverse the observed phenotype (Figure 3.6A and B).

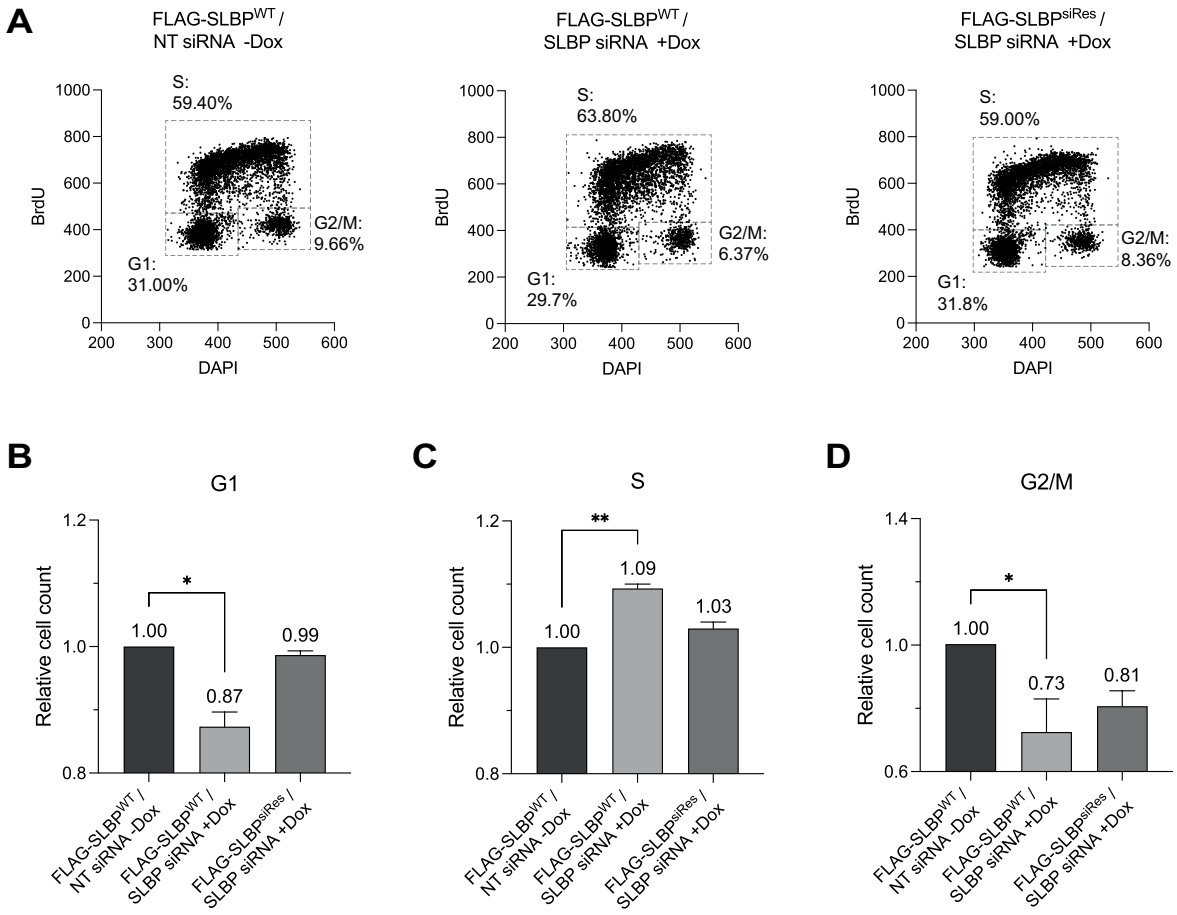

Figure 3.6: Expression of FLAG-SLBP^{siRes} rescues the SLBP RNAi-induced accumulation of cells in S phase. Bivariate flow cytometric analysis of FLAG-SLBP^{WT} & FLAG-SLBP^{siRes} cell cycle distributions. **(A)** 1×10^6 FLAG-SLBP^{WT} and FLAG-SLBP^{siRes} cells were transfected with 200 nM NT or SLBP siRNA using Lipofectamine RNAiMAX in 100 mm cell culture dishes and incubated with or without 0.5 μg/mL doxycycline for 24 hours. Cells were pulsed for 30 minutes with 25 μM bromodeoxyuridine (BrdU), fixed and incubated with an α-BrdU (Rat) antibody before further incubation with an α-Rat IgG Alexa Fluor 568 secondary antibody. The DNA content of BrdU-labelled cells was stained with DAPI and cells were analysed with an Attune NxT Flow Cytometer. Data are from a single representative experiment. **(B)** Quantification of G1 gate data from 3 independent experiments. **(C)** Quantification of S phase gate data from 3 independent experiments. **(D)** Quantification of G2 gate data from 3 independent experiments. * = $p < .05$, ** = $p < .01$. Dunnett's one-way ANOVA. Data are mean ± S.E.M. n = 3 experiments.

3.2.2 Development and validation of *HIST1H3B* and *H2AFX* qPCR assays for analysis of SLBP-dependent regulation of histone mRNA metabolism

Quantitative real-time PCR (qPCR) is a highly sensitive analytical technique used to detect and quantify nucleic acids in biological samples (Livak and Schmittgen, 2001; Wong and Medrano, 2005). Total RNA is extracted from cells and used to synthesise cDNA, which is used as a template for the amplification of specific cDNA targets through repeated rounds of PCR with gene-specific primers. Relative target cDNA levels in samples can be determined by comparative analysis of cycle threshold (C_T) values that have been normalised to a calibrator gene using the $2^{-\Delta\Delta C_T}$ method (Livak and Schmittgen, 2001). Using this method, the fold change in target gene expression ($2^{-\Delta\Delta C_T}$) is calculated from the change in target and calibrator C_T values between samples using the equation:

$$\Delta\Delta C_T = \Delta C_{T(\text{experiment})} - \Delta C_{T(\text{control})}$$

where:

$$\Delta C_{T(\text{experiment})} = C_{T(\text{target-experiment})} - C_{T(\text{calibrator-experiment})}$$

and:

$$\Delta C_{T(\text{control})} = C_{T(\text{target-control})} - C_{T(\text{calibrator-control})}$$

The $2^{-\Delta\Delta C_T}$ method assumes that the PCR amplification efficiencies for the target and calibrator genes are equal and are 100%, or in other words, that every target molecule in a sample is duplicated in each PCR cycle. As such, the optimisation of primers and PCR conditions for both the target and calibrator genes is of critical importance when developing a reliable and robust assay that is capable of producing reproducible results (Taylor et al., 2019).

For the present study, I used primers targeting *HIST1H3B* (a replication-dependent histone gene), *H2AFX* (a hybrid histone gene encoding the histone H2A variant, H2A.X) and *GAPDH*

(a "housekeeping" gene used for qPCR data normalisation) in qPCR RNAi rescue experiments to assay SLBP-dependent regulation of histone mRNA transcript levels in Flp-In T-REx HeLa cells.

The *HIST1H3B* gene encodes a histone H3 family member (see Table 1.1) that is downregulated when SLBP expression is inhibited by RNAi and is degraded in response to hydroxyurea-induced replication stress in cells expressing SLBP (Zhao et al., 2004; Panomwan, 2017). qPCR analysis of *HIST1H3B* mRNA transcript levels in cells expressing various FLAG-SLBP mutants will therefore likely act as a suitable readout for understanding SLBP-dependent regulation of replication-dependent histone mRNA metabolism.

Histone H2A.X is targeted and phosphorylated on serine 139 by checkpoint proteins ATM, ATR or DNA-PK, forming γ-H2A.X, in response to DNA double-strand breaks (DSBs) that arise as a result of DNA damage or prolonged replication stress (Rogakou et al., 1998; Ward and Chen, 2001; Furuta et al., 2003). The formation of γ-H2A.X is required for the recruitment of DNA repair proteins to sites of DNA damage and for the effective resolution of DSBs (Paull et al., 2000). Interestingly, *H2AFX* is a unique hybrid histone gene that produces stem-loop mRNA during S phase and poly(A)+ mRNA when expressed elsewhere in the cell cycle (Mannironi et al., 1989). Dankert et al. (2016) report that the expression of an SLBP mutant that fails to be degraded at the end of S phase results in increased translation of *H2AFX* mRNA in G2, leading to an increased deposition of H2A.X in chromatin, which sensitises cells to genotoxic stress. As SLBP regulates the expression of replication-dependent histone genes (Sullivan et al., 2009), it seemed likely that SLBP would also be implicated in the regulation of *H2AFX* gene transcription in S phase and when SLBP is mutated and stabilised in G2.

I began optimisation by first determining the RNA extraction method that would provide a high yield of RNA that was free of genomic DNA (gDNA), protein and salt contaminants that might interfere with cDNA synthesis and lead to low or non-specific amplification in qPCR. Total RNA was isolated using the phenol-chloroform extraction method described in Chomczynski and Sacchi (1987), the QIAGEN RNeasy total RNA extraction kit or the Monarch RNA miniprep total RNA extraction kit, according to the manufacturer's instructions. Extracted RNA yields and A_{260}/A_{280} ratios, an indicator of RNA purity, were measured using a Nanodrop spectrophotometer

and compared. The Monarch RNA miniprep kit yielded ∼50 µg of RNA, the highest yield of the extraction methods tested, and had an average A_{260}/A_{280} ratio of 2.04, indicating that the RNA extracted using this method was of high quality and free of contaminants (Figure 3.7). Phenol-chloroform extraction provided the second highest RNA yield but had the lowest A_{260}/A_{280} ratio (∼25 µg RNA; A_{260}/A_{280} = 1.99). The QIAGEN RNeasy total RNA extraction kit was the poorest performing RNA extraction method in terms of yield but produced relatively clean RNA (∼6 µg RNA; A_{260}/A_{280} = 2.04). The Monarch RNA miniprep kit was selected for use when extracting RNA upstream of qPCR due to the high yield and purity of the extracted RNA, the ease of use, and because it does not require the use of highly toxic reagents.

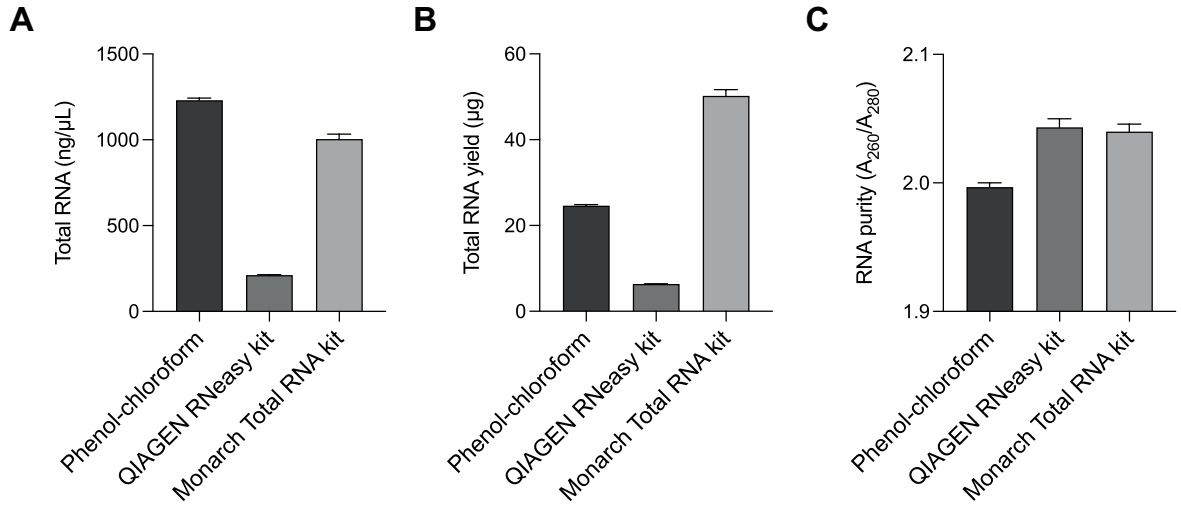

Figure 3.7: RNA extraction method comparison. (A) Extracted RNA concentration (ng/µL), **(B)** Total RNA yield (µg), and **(C)** RNA purity (A_{260}/A_{280}) comparison of RNA extracted from FLAG-SLBP^{WT} cells using phenol-chloroform, QIAGEN RNAeasy or Monarch Total RNA extraction methods detailed in Section 2.2.5. Data are mean ± S.E.M. n = 3 experiments.

I next synthesised cDNA using the High Capacity RNA-to-cDNA kit and 1 μg of RNA extracted from FLAG-SLBP^{WT} cells using the Monarch Total RNA extraction kit and confirmed the primer annealing temperature to be used in *HIST1H3B*, *H2AFX* and *GAPDH* qPCR by performing PCR with 100 ng cDNA and a gradient of annealing temperatures from 55 - 72°C (see Table 3.1). PCR reactions using material from cDNA reactions that omitted the reverse transcriptase enzyme were included as a control. PCR products were analysed by gel electrophoresis to assess annealing temperatures and verify amplicon lengths (Figure 3.8). Single bands of the expected sizes for *HIST1H3B* (91 bp), *H2AFX* (96 bp) and *GAPDH* (116 bp) were detected only in PCR samples that used material from cDNA reactions containing reverse transcriptase, confirming that cDNA synthesis was successful and that the *HIST1H3B*, *H2AFX* and *GAPDH* primer pairs are specific for their intended targets. The band intensities of *HIST1H3B*, *H2AFX* and *GAPDH* PCR products appeared to be strongest when using an annealing temperature of 55°C and all tapered off as the annealing temperature rose above 63.5°C. Thus, a primer annealing temperature of 55°C was used in qPCR experiments throughout this study.

Segment	Cycles	Temperature	Time
1	1	98°C	10 sec
2	35	98°C	1 sec
		55°C - 72°C	5 sec
		72°C	1 min
3	1	72°C	5 min
4	1	4°C	∞

Table 3.1: PCR thermal cycling parameters for qPCR primer annealing temperature optimisation.

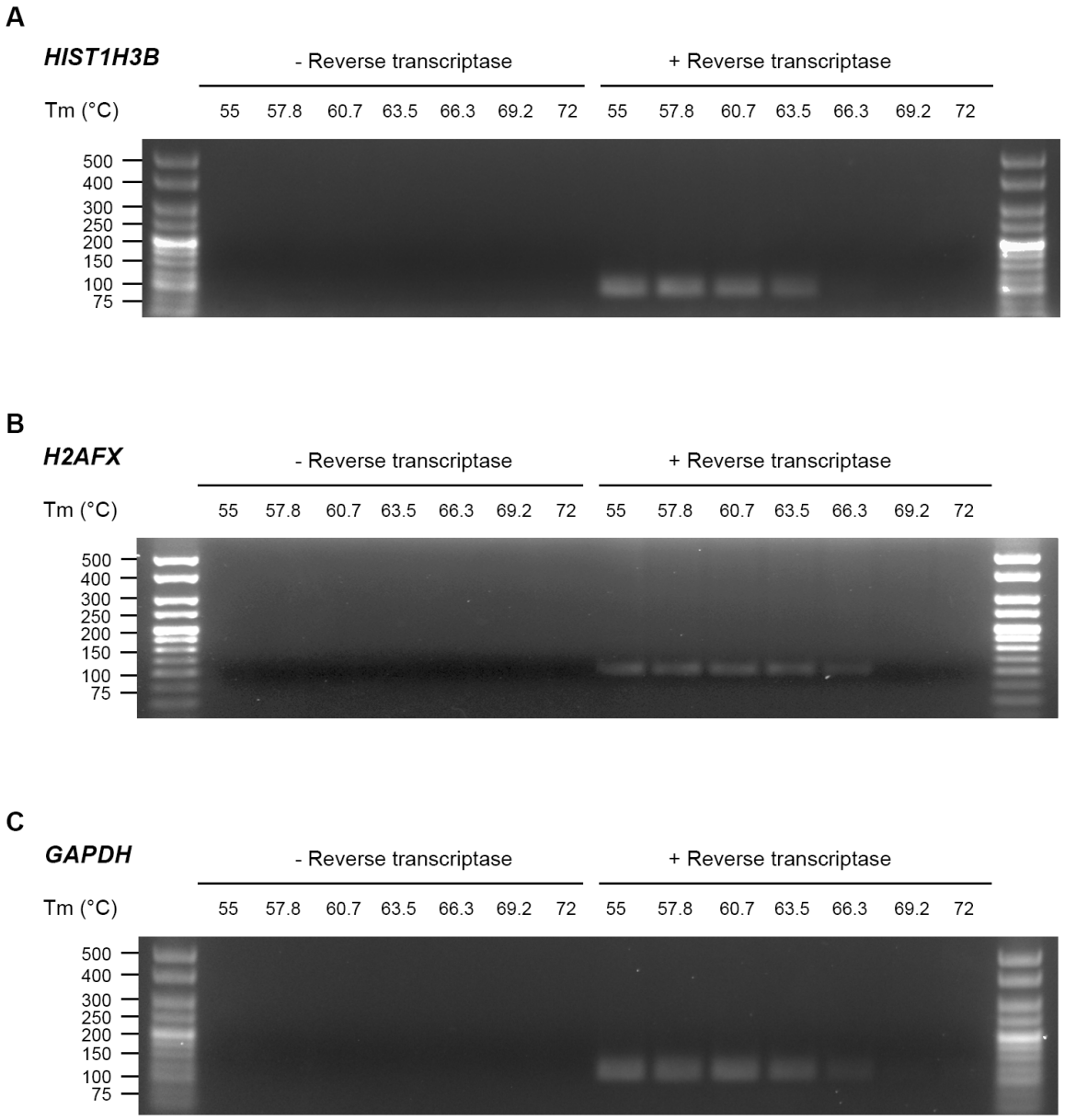

Figure 3.8: qPCR primer annealing temperature optimisation. Agarose gel electrophoresis of **(A)** *HIST1H3B* (91 bp), **(B)** *H2AFX* (96 bp), and **(C)** *GAPDH* (116 bp) PCR products following a gradient PCR reaction using cDNA generated using RNA extracted from FLAG-SLBP^{WT} cells. Annealing temperature (Tm) range: 55 - 72°C. PCR products were electrophoresed on a 1.5% agarose gel. Samples from RNA-cDNA reactions omitting reverse transcriptase are run alongside as a control. Lanes 1 and 16 contain HyperLadder 25 bp DNA molecular size ladder (Bioline, London, England).

I next validated the SYBR Green qPCR experimental protocol and determined the amplification efficiencies and overall performance of the *HIST1H3B*, *H2AFX* and *GAPDH* primer pairs. To achieve this, I performed qPCR, as outlined in Section 2.2.5.3 and Table 2.9, using a 7-point 1:10 serial dilution series of cDNA (starting concentration = 10 ng/µL) generated from RNA that was extracted from FLAG-SLBP^{WT} cells using the Monarch Total RNA miniprep kit (Figure 3.9A, Figure 3.10A and Figure 3.11A). The obtained C_T values were used to plot standard curves (Figure 3.9B, Figure 3.10B and Figure 3.11B) from which the PCR efficiency (*E*), as a percentage, was calculated using the equation:

$$E = \left[10^{\left(\frac{-1}{\text{slope}}\right)} - 1\right] \times 100$$

Melt curve analyses were conducted on end-point qPCR products to confirm the generation and presence of a single amplicon in each reaction.

Reliable amplification curves for *HIST1H3B* and *GAPDH* were generated in a limited number of qPCR reactions when using 1:10 cDNA dilutions and 400 nM of both forward and reverse primers (Figure 3.9A and Figure 3.11A). For *H2AFX*, 1:10 cDNA dilutions failed to produce more than one amplification curve with a C_T <30 (data not shown), therefore a 1:2 cDNA dilution series was used (starting concentration = 10 ng/µL) and the primer concentrations were increased to 800 nM (Figure 3.10A). Using C_T values from these amplification curves, the PCR efficiencies for *HIST1H3B*, *H2AFX* and *GAPDH* were calculated to be 112.62%, 111.72% and 116.47%, respectively, and the correlation coefficient (R^2) for all three standard curves was >0.99 (Figure 3.9B, Figure 3.10B and Figure 3.11B). Dissociation melt curves indicate that the melting temperatures (T_m) of *HIST1H3B*, *H2AFX* and *GAPDH* qPCR products were 87-89°C (Figure 3.9C, Figure 3.10C and Figure 3.11C). Plotting the first order derivative of these curves (-ΔRFU/ΔT) against temperature (°C) produced a single peak around the target T_m (Figure 3.9D, Figure 3.10D and Figure 3.11D). Taken together, these data provide an indication of the dynamic range of the *HIST1H3B*, *H2AFX* and *GAPDH* qPCR assays and confirm that the primer pairs used generate single *HIST1H3B*, *H2AFX* and *GAPDH* amplicons.

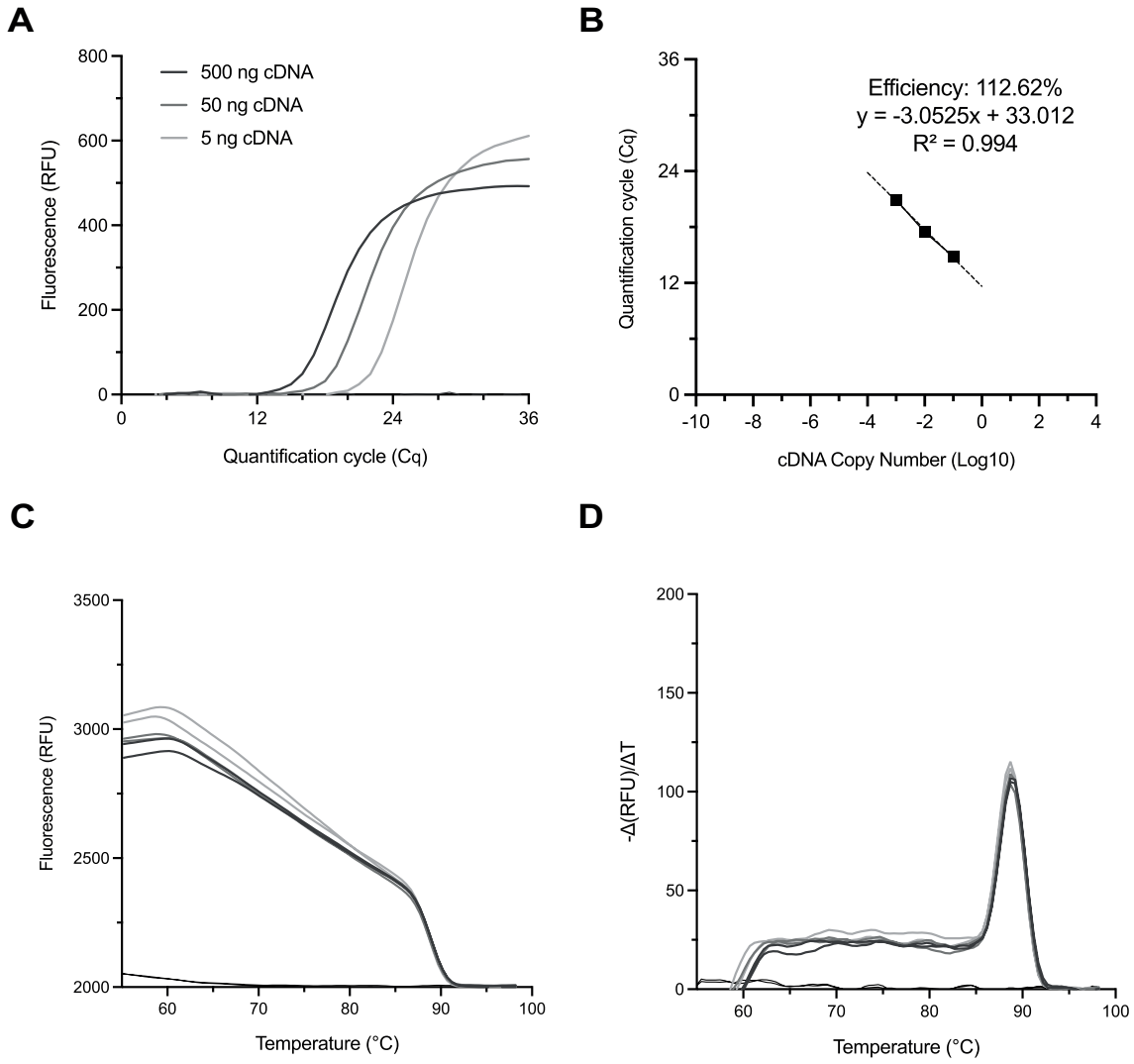

Figure 3.9: *HIST1H3B* qPCR validation. qPCR was performed with *HIST1H3B* primers (400 nM each) and 1:10 serial dilutions of cDNA generated with the High Capacity RNA-cDNA kit (Applied Biosystems) using total RNA extracted from asynchronous FLAG-SLBP^{WT} cells (starting cDNA concentration = 10 ng/μL) to determine the optimal cDNA concentration for *HIST1H3B* qPCR and to assess the performance of *HIST1H3B* qPCR primers. **(A)** *HIST1H3B* qPCR amplification curves. Relative fluorescence units (RFU; Y-axis) are plotted against the quantification cycle (C_q; X-axis). **(B)** *HIST1H3B* standard curve. Quantification cycle (C_q; Y-axis) is plotted against $\log_{10}$ cDNA input concentration (X-axis). Correlation coefficient (R^2 = 0.994; slope = -3.0525; efficiency = 112.62%). **(C)** *HIST1H3B* dissociation melt curve. Relative fluorescence units (RFU; Y-axis) are plotted against temperature (°C; X-axis). **(D)** *HIST1H3B* derivative melt curve. Change in relative fluorescence units with time (-Δ(RFU)/ΔT; Y-axis) is plotted against temperature (°C; X-axis).

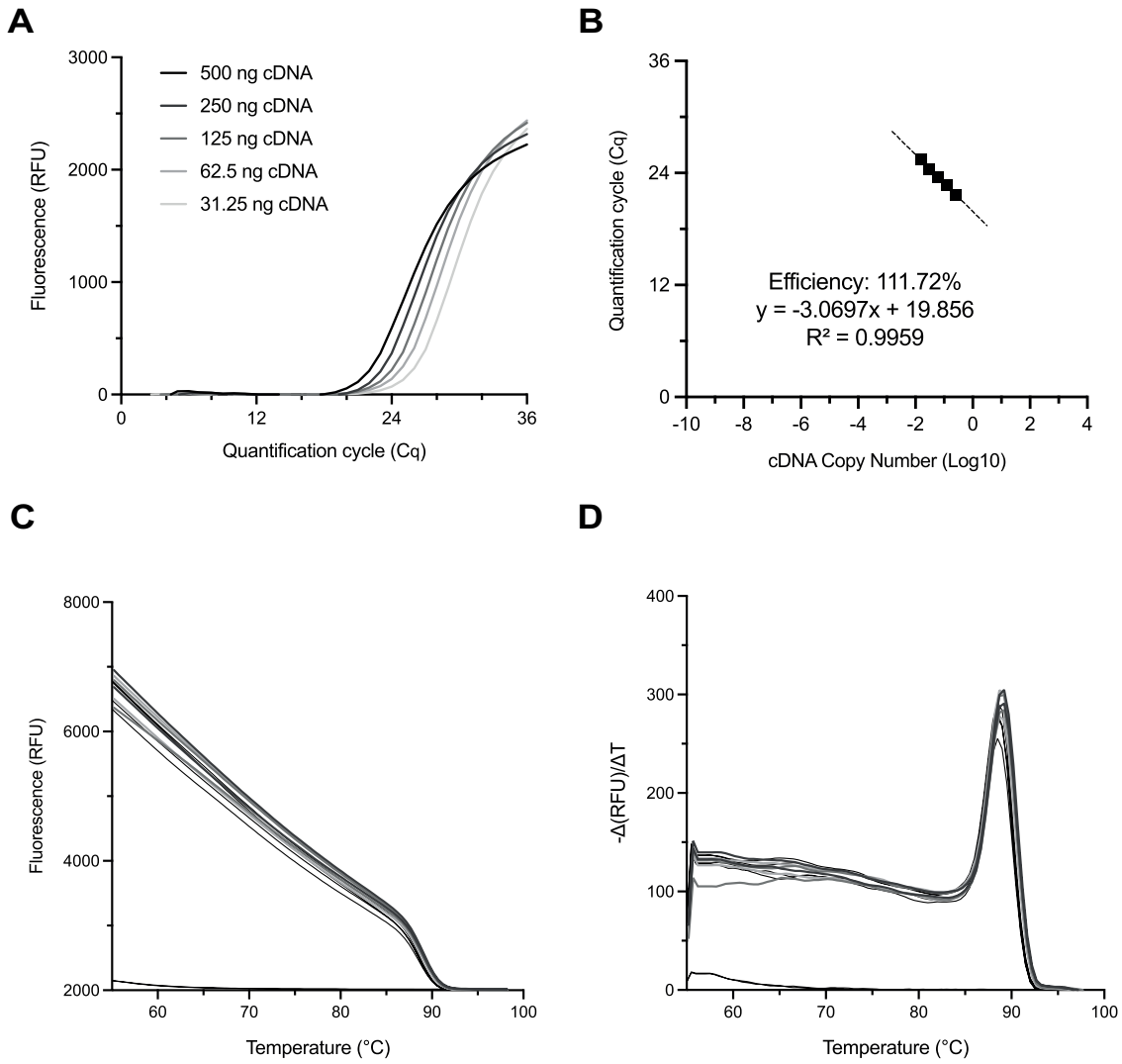

Figure 3.10: *H2AFX* qPCR validation. qPCR was performed with *H2AFX* primers (800 nM each) and 1:2 serial dilutions of cDNA generated with the High Capacity RNA-cDNA kit (Applied Biosystems) using total RNA extracted from asynchronous FLAG-SLBP^{WT} cells (starting cDNA concentration = 10 ng/μL) to determine the optimal cDNA concentration for *H2AFX* qPCR and to assess the performance of *H2AFX* qPCR primers. **(A)** *H2AFX* qPCR amplification curves. Relative fluorescence units (RFU; Y-axis) are plotted against the quantification cycle (C_q; X-axis). **(B)** *H2AFX* standard curve. Quantification cycle (C_q; Y-axis) is plotted against $\log_{10}$ cDNA input concentration (X-axis). Correlation coefficient (R^2 = 0.9959; slope = -3.0697; efficiency = 111.72%). **(C)** *H2AFX* dissociation melt curve. Relative fluorescence units (RFU; Y-axis) are plotted against temperature (°C; X-axis). **(D)** *H2AFX* derivative melt curve. Change in relative fluorescence units with time (-Δ(RFU)/ΔT; Y-axis) is plotted against temperature (°C; X-axis).

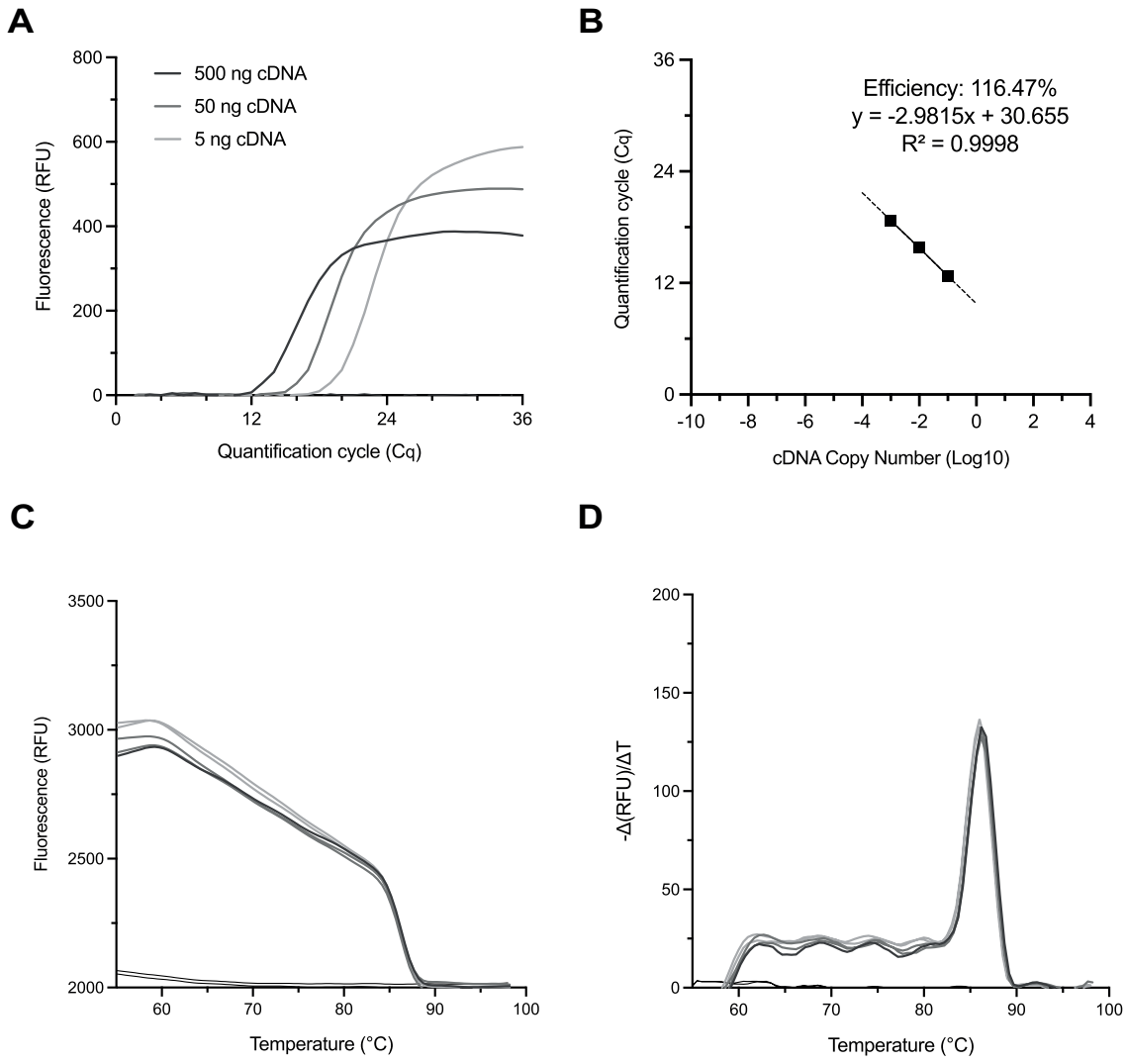

Figure 3.11: *GAPDH* qPCR validation. qPCR was performed with *GAPDH* primers (400 nM each) and 1:10 serial dilutions of cDNA generated with the High Capacity RNA-cDNA kit (Applied Biosystems) using total RNA extracted from asynchronous FLAG-SLBP^{WT} cells (starting cDNA concentration = 10 ng/μL) to determine the optimal cDNA concentration for *GAPDH* qPCR and to assess the performance of *GAPDH* qPCR primers. **(A)** *GAPDH* qPCR amplification curves. Relative fluorescence units (RFU; Y-axis) are plotted against the quantification cycle (C_q; X-axis). **(B)** *GAPDH* standard curve. Quantification cycle (C_q; Y-axis) is plotted against $\log_{10}$ cDNA input concentration (X-axis). Correlation coefficient (R^2 = 0.9998; slope = -2.9815; efficiency = 116.47%). **(C)** *GAPDH* dissociation melt curve. Relative fluorescence units (RFU; Y-axis) are plotted against temperature (°C; X-axis). **(D)** *GAPDH* derivative melt curve. Change in relative fluorescence units with time (-Δ(RFU)/ΔT; Y-axis) is plotted against temperature (°C; X-axis).

3.2.2.1 FLAG-SLBP^{siRes} expression rescues SLBP siRNA-induced *HIST1H3B* and *H2AFX* mRNA downregulation

Having successfully optimised qPCR experimental conditions, I then sought to confirm that expression of FLAG-SLBP^{siRes} protein following RNAi-mediated knockdown of endogenous SLBP restores replication-dependent histone mRNA transcript levels to that observed in wild-type cells. To achieve this, I measured the mRNA transcript levels of the replication-dependent histone *HIST1H3B* by qPCR in control, knockdown and FLAG-SLBP^{siRes} expressing cells (Figure 3.12A). Transfection of SLBP-specific siRNA, but not NT siRNA, resulted in a 40% reduction of *HIST1H3B* mRNA, as has been reported previously in the literature (Zhao et al., 2004; Sullivan et al., 2009). As expected, the expression of the siRNA-resistant FLAG-SLBP^{siRes} protein in cells transfected with SLBP siRNA was sufficient to restore *HIST1H3B* mRNA transcript levels to that of the control cell population (Figure 3.12A). For *H2AFX*, transfection of SLBP-specific siRNA, but not NT siRNA, resulted in a 30% reduction of *H2AFX* mRNA, and the subsequent expression of FLAG-SLBP^{siRes} restored *H2AFX* mRNA transcript levels to that of the control cell population (Figure 3.12B). This result suggests that SLBP regulates the expression of *H2AFX* mRNA transcripts in S phase in addition to replication-dependent histone mRNAs and that expression of siRNA-resistant SLBP is sufficient to rescue the observed *H2AFX* mRNA downregulation following SLBP RNAi. Taken together with the data reported in Section 3.2.1.3, these data are consistent with the notion that the expression of siRNA-resistant FLAG-SLBP restores the function of SLBP in cells where endogenous SLBP has been knocked-down by RNAi (Wagner et al., 2005).

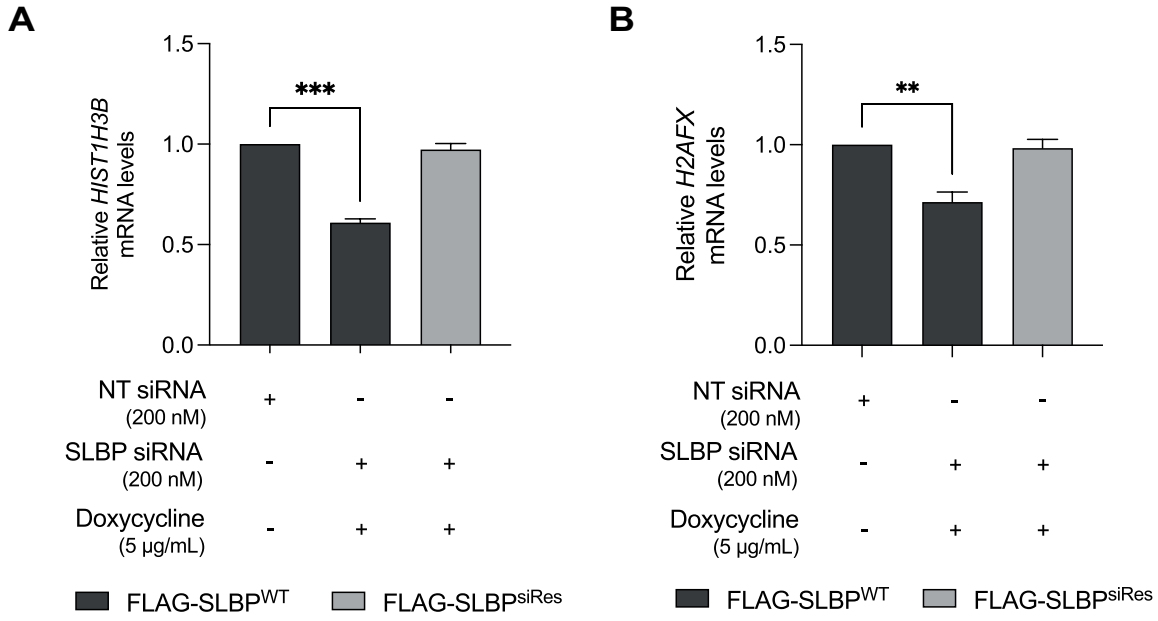

Figure 3.12: SLBP regulates *HIST1H3B* and *H2AFX* mRNA transcript levels. Total RNA was extracted from asynchronous FLAG-SLBP^{WT} and FLAG-SLBP^{siRes} cells transfected with 200 nM non-targeting (NT) or SLBP siRNA for 24 hours and incubated with or without 0.5 µg/mL doxycycline for the final 5 hours. cDNA was generated using the High Capacity RNA-cDNA kit (Applied Biosystems) and qPCR was performed using **(A)** *HIST1H3B* or **(B)** *H2AFX* primers. qPCR samples were tested in triplicate and were quantified and normalised to *GAPDH* using the $2^{-\Delta\Delta C_T}$ method. ** = $p < .01$, *** = $p < .001$. Dunnett's one-way ANOVA. Data are mean $\pm$ S.E.M. n = 3 experiments.

3.2.2.2 FLAG-SLBP^{siRes} facilitates replication-dependent histone *HIST1H3B* mRNA decay following hydroxyurea-induced DNA replication stress

Replication-dependent histone mRNAs are rapidly degraded at the end of S phase and in response to DNA replication stress (Kaygun and Marzluff, 2005). The degradation of replication-dependent histone mRNA is a multi-step process that requires the SLBP-dependent and SLBP-independent recruitment of decay factors, such as Lsm1-2, Upf1 and Dcp1/2, and the dissociation of SLBP from the stem-loop of histone mRNA (Kaygun and Marzluff, 2005; Mullen and Marzluff, 2008; Marzluff and Koreski, 2017). Recent data from our group suggest that specific residues in the N terminus of SLBP are phosphorylated in response to hydroxyurea-induced replication stress and it is hypothesised that phosphorylation of these residues may be implicated in the initiation of histone mRNA decay under such conditions (Panomwan, 2017). To test this hypothesis, I planned to use the developed qPCR assay to measure the rate of histone mRNA decay in Flp-In T-REx HeLa cells expressing RNAi-resistant FLAG-tagged SLBP mutants following RNAi-mediated knockdown of endogenous SLBP and subsequent exposure to hydroxyurea.

I began by validating the qPCR assay for use when measuring the rate of histone mRNA decay and confirmed that cells expressing FLAG-SLBP^{siRes} were able to perform histone mRNA decay at a comparable rate to control cells following exposure to hydroxyurea. Asynchronous FLAG-SLBP^{WT} and FLAG-SLBP^{siRes} cells were transfected with either 200 nM NT or SLBP siRNA for 24 hours and, after 19 hours, FLAG-SLBP^{siRes} cells were treated with 0.5 μg/mL doxycycline for a further 5 hours before both populations of cells were exposed to 5 mM hydroxyurea for up to 60 minutes. Total RNA was then extracted, converted to cDNA and used as a template for qPCR using *HIST1H3B* and *H2AFX* primers (Figure 3.13). Cells expressing FLAG-SLBP^{siRes} and lacking endogenous SLBP degraded *HIST1H3B* mRNA after exposure to hydroxyurea with similar decay kinetics to control cells expressing endogenous SLBP (Figure 3.13A), confirming that RNAi-resistant FLAG-SLBP^{siRes} is capable of facilitating replication-dependent histone mRNA decay following hydroxyurea-induced replication stress. There was no significant difference in *H2AFX* mRNA transcript levels after 30 or 60 minutes exposure to hydroxyurea in FLAG-SLBP^{WT} or FLAG-SLBP^{siRes} cells compared to control cells not exposed to hydroxyurea (Figure 3.13B). This result was expected as H2A.X is implicated in the DDR and translation of *H2AFX* mRNA is known to continue under conditions of replication stress (Liu et al., 2008).

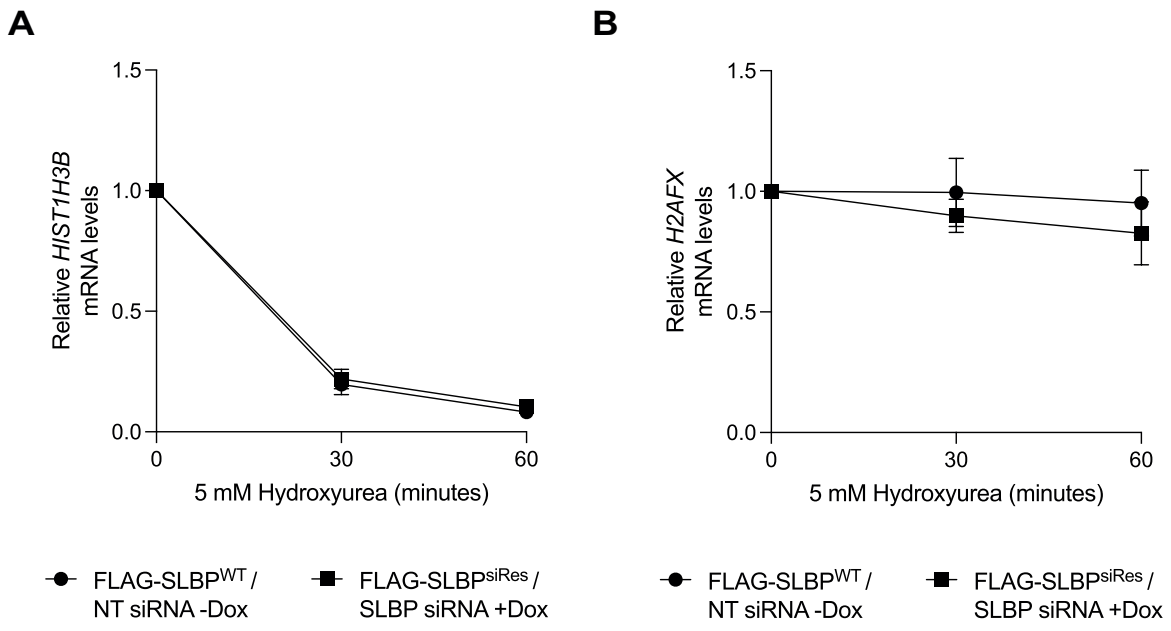

Figure 3.13: Hydroxyurea-induced DNA replication stress causes degradation of replication-dependent *HIST1H3B* mRNA. Total RNA was extracted from asynchronous FLAG-SLBP^{WT} and FLAG-SLBP^{siRes} cells transfected with 200 nM non-targeting (NT) or SLBP siRNA for 24 hours and incubated with or without 0.5 μg/mL doxycycline for the final 5 hours before being exposed to 5 mM hydroxyurea for 30 and 60 minutes. cDNA was generated using the High Capacity RNA-cDNA kit (Applied Biosystems) and qPCR was performed using **(A)** *HIST1H3B* or **(B)** *H2AFX* primers. qPCR samples were tested in triplicate and were quantified and normalised to *GAPDH* using the $2^{-\Delta\Delta C_T}$ method. Data are mean ± S.E.M. n = 3 experiments.

3.2.3 Immunoprecipitation of FLAG-SLBP^{siRes} using α-FLAG M2 affinity gel

Results presented in Section 3.2.1 and Section 3.2.2 provide evidence that the expression of FLAG-SLBP^{siRes} is sufficient to rescue SLBP function and support the notion that analysis of RNAi-resistant FLAG-SLBP mutants will act as a suitable proxy to understand SLBP activity *in vivo*. In order to study SLBP post-translational modifications and changes to the SLBP interactome as a function of SLBP mutation status and replication stress, I planned to perform immunoprecipitation experiments to isolate FLAG-SLBP^{siRes} mutants and bound interacting proteins from cells upstream of analysis by Western blot or mass spectrometry. FLAG-SLBP immunoprecipitation was optimised previously by Dr Pornpen Panomwan (Panomwan, 2017). Using 1 mg/mL 3X FLAG peptide and a modified TBS elution buffer (10 mM Tris-HCl pH 7.4, 30 mM NaCl), I was able to replicate successful isolation of the total fraction of FLAG-SLBP^{siRes} from 1 mg of cell lysate using 20 µL of α-FLAG-M2 affinity agarose gel beads (Figure 3.14).

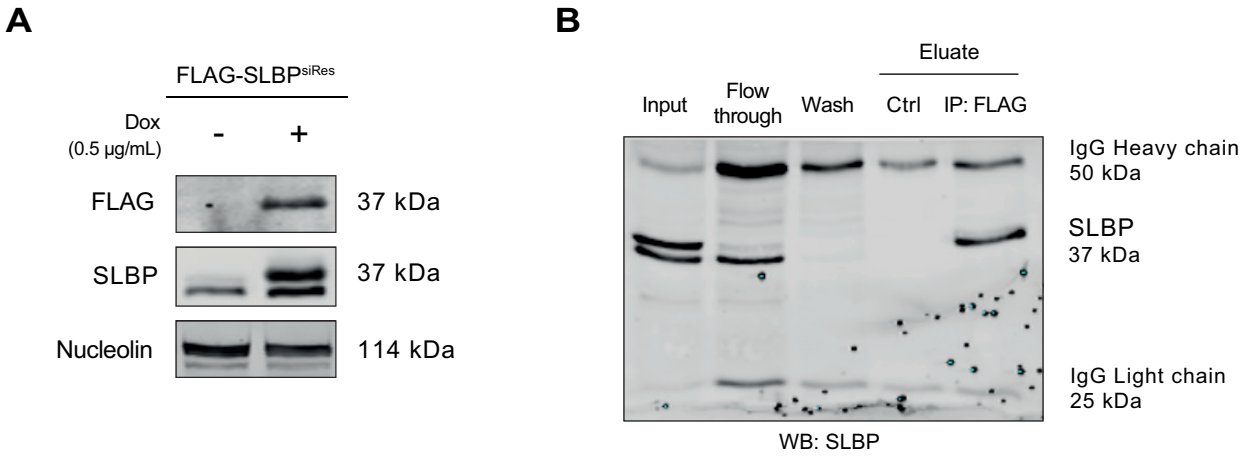

Figure 3.14: Immunoprecipitation of FLAG-SLBP^{siRes} using α-FLAG M2 affinity agarose gel beads. **(A)** Asynchronous FLAG-SLBP^{siRes} cells were cultured in media with or without 0.5 µg/mL doxycycline for 24 hours and analysed by Western blot using α-FLAG, α-SLBP and α-nucleolin antibodies to confirm the expression of FLAG-tagged SLBP protein in cell lysates used for immunoprecipitation in (B). Nucleolin is used as a loading control. **(B)** 1 mg of total protein isolated from cells exposed to 0.5 µg/mL doxycycline in (A) was incubated with 20 µL α-FLAG M2 agarose gel beads in a final volume of 1 mL A2220 lysis buffer for 2 hours. Beads were washed with TBS before competitive protein elution with 100 µL of 300 ng/µL 3X FLAG peptide in modified TBS elution buffer. 3.5% of input, flow-through, wash and eluate, including control eluate from cells not exposed to doxycycline (Ctrl), was analysed by Western blot using α-SLBP antibody to confirm successful elution of FLAG-SLBP^{siRes} protein.

3.2.4 Analysis of FLAG-SLBP^{siRes} immunoprecipitates by LC-MS/MS

Having confirmed the ability to isolate and purify FLAG-SLBP^{siRes} protein from crude cell lysates, I next analysed the eluates obtained from control (-dox) and FLAG-SLBP^{siRes} (+dox) cells in Figure 3.14 by mass spectrometry using an Orbitrap mass spectrometer (Biological Mass Spectrometry Facility, The University of Sheffield) to demonstrate the ability to isolate and identify SLBP-derived peptides that may be post-translationally modified in response to a stimulus such as replication stress, along with those from interacting proteins that co-immunoprecipitate with SLBP. 20 µL of each eluate was solubilised with 5% SDS and sonicated before proteins were reduced with 5 mM TCEP and alkylated with 20 mM MMS. After acidification with 2.5% phosphoric acid, samples were loaded into individual S-Trap spin columns (ProtiFi, Farmingdale, NY, USA) and washed several times before performing on-column enzymatic digestions by incubating bound proteins with 100 ng Glu-C in 20 µL 1X Glu-C digestion buffer (New England Biolabs) for 4 hours at 37°C and subsequent analysis by LC-MS/MS. Mass spectral data of identified peptides were matched to proteins in UniProtKB/Swiss-Prot databases using the SEQUEST search algorithm with a false discovery rate (FDR) threshold set at 0.01 (1%) by decoy database searching. Peptides derived from SLBP were present in the experimental eluate sample only, confirming the successful recovery and identification of FLAG-SLBP^{siRes} protein using the established immunoprecipitation and mass spectrometry protocols.

In addition to SLBP, there were 98 other proteins identified from one or more peptides with an ion intensity above 0 in the digested FLAG-SLBP^{siRes} eluate that were not present in the control sample (see Appendix D for full list). Of these, 68 proteins (69.39%) were considered contaminants due to their previous identification by LC-MS/MS in control samples from experiments using α-Flag antibody or α-Flag M2 affinity agarose gel to immunoprecipitate FLAG-tagged bait proteins from HeLa and U2OS cells (Mellacheruvu et al., 2013). The remaining 30 proteins (30.61%) are listed in Table 3.2. STRING analysis revealed a network of 22 proteins, including SLBP, supported by experimental evidence of physical interactions or predicted functional associations (Figure 3.15A) (Szklarczyk et al., 2020), and gene ontology (GO) enrichment analysis showed that there was a significant enrichment of proteins with mRNA binding functions that positively or negatively regulate translation and mRNA processing (Figure 3.15B) (Thomas et al., 2022).

Accession number	Protein	Gene ID	Rel. Intensity
P59044	NLR Family Pyrin Domain Containing 6	NLRP6	1.905
P63220	40S ribosomal protein S21	RPS21	1.283
F8W8D3	Histone RNA hairpin-binding protein	SLBP	1
G3V153	**Caprin-1**	**CAPRIN1**	0.652
Q13501	Sequestosome-1	SQSTM1	0.412
P19338	**Nucleolin**	**NCL**	0.326
Q580R0	Uncharacterized protein C2orf27	C2orf27A	0.294
A8MT87	Phenylethanolamine N-methyltransferase	PNMT	0.246
H7C3A1	**Serrate RNA effector molecule homolog**	**SRRT**	0.216
H0Y9X0	Protein furry homolog-like	FRYL	0.214
Q14152	Eukaryotic translation initiation factor 3 subunit A	EIF3A	0.204
X6RLN4	**La-related protein 4**	**LARP4**	0.198
E5RH50	La-related protein 1	LARP1	0.195
Q15459	Splicing factor 3A subunit 1	SF3A1	0.163
Q8NC51	**Plasminogen activator inhibitor 1 RNA-binding protein**	**SERBP1**	0.13
E7EWK3	**ATP-dependent RNA helicase DHX36**	**DHX36**	0.125
A0A0C4DGV5	Zinc finger Ran-binding domain-containing protein 2	ZRANB2	0.125
Q5VZU9	Tripeptidyl-peptidase 2	TPP2	0.121
P41567	Eukaryotic translation initiation factor 1	EIF1	0.12
H3BV01	Pre-mRNA-splicing factor ATP-dependent RNA helicase PRP16	DHX38	0.119
H3BQC6	Ubiquitin carboxyl-terminal hydrolase 10	USP10	0.108
O75643	U5 small nuclear ribonucleoprotein 200 kDa helicase	SNRNP200	0.101
H0Y8R1	**G-rich sequence factor 1**	**GRSF1**	0.076
G3V4Y7	Kinectin	KTN1	0.064
Q99459	**Cell division cycle 5-like protein**	**CDC5L**	0.063
P53618	Coatomer subunit beta	COPB1	0.063
Q5T4S7	E3 ubiquitin-protein ligase UBR4	UBR4	0.049
Q07065	**Cytoskeleton-associated protein 4**	**CKAP4**	0.044
C9JHK9	ATP-binding cassette sub-family F member 2	ABCF2	0.043
A0A0G2JQJ7	Microtubule-associated protein tau	MAPT	0.029
A0A087X0K8	Probable G-protein coupled receptor 179	GPR179	0.021

Table 3.2: FLAG-SLBP^{siRes} interacting proteins identified by LC-MS/MS. List of 31 proteins identified in LC-MS/MS analysis of a single FLAG-SLBP^{siRes} immunoprecipitation eluate ranked by ion intensity of the most abundant peptide from the identified protein relative to the ion intensity of the most abundant SLBP peptide. SLBP is highlighted in yellow. In bold text are proteins identified as FLAG-SLBP^{WT} interactors in Panomwan (2017).

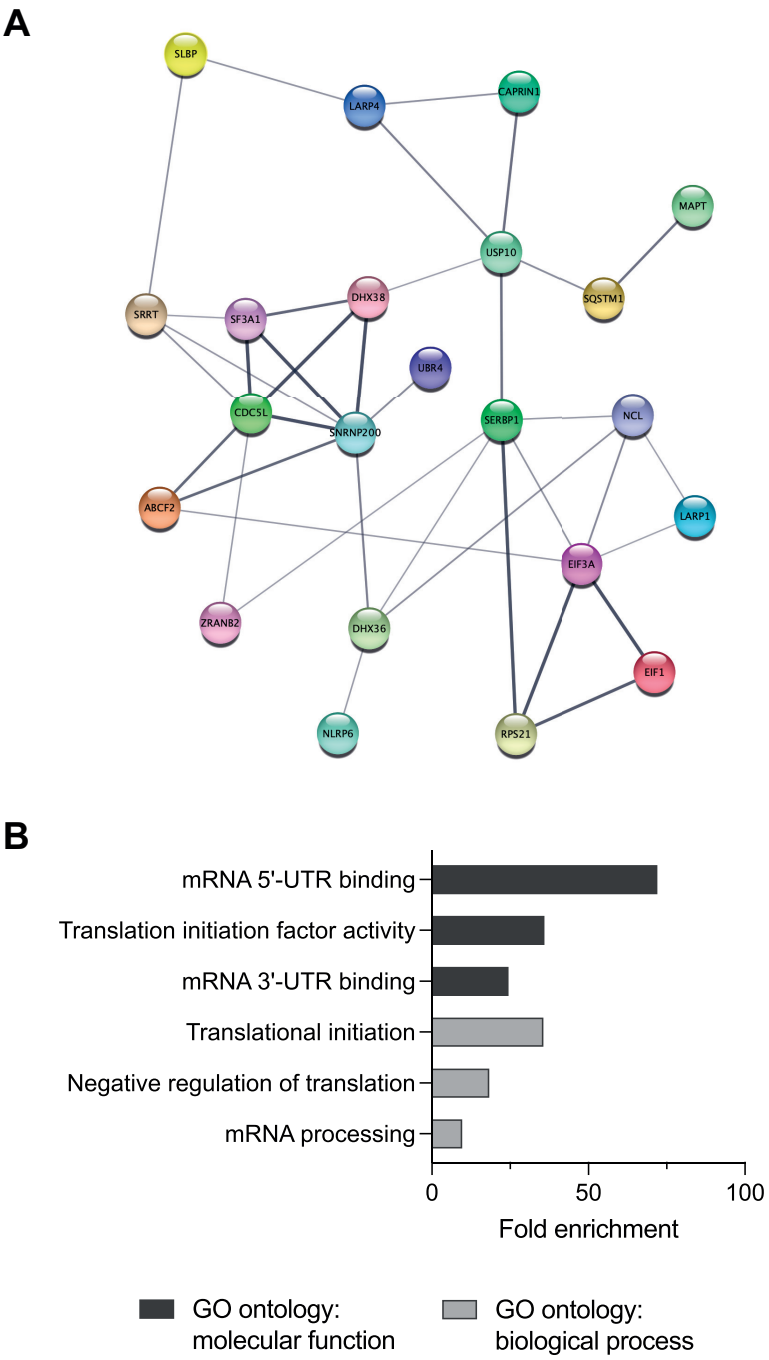

Figure 3.15: STRING network and gene ontology enrichment analysis of FLAG-SLBP^{siRes} interacting proteins identified by LC-MS/MS. (A) STRING network analysis was performed using accession numbers from 30 FLAG-SLBP^{siRes} interacting proteins identified by LC-MS/MS from immunoprecipitates performed using α-FLAG M2 affinity agarose gel. 22 out of the 30 proteins form a STRING network supported by experimental evidence and predicted functional associations. **(B)** Gene ontology (GO) enrichment analysis of the 30 FLAG-SLBP^{siRes} interacting proteins in FLAG-SLBP^{siRes} immunoprecipitates identified by LC-MS/MS. n = 1.

I was unable to identify key known SLBP interactors such as MIF4GD or SLIP1 (von Moeller et al., 2013), nuclear cap-binding protein subunits 1/2 (CBP80/20) (Choe et al., 2013), CBP80/20-dependent translation initiation factor (CTIF) (Choe et al., 2013) or zinc finger protein 473 (Dominski et al., 2002) in my analysis, however, 9 out of the 30 proteins (30%) considered here to be FLAG-SLBP^{siRes} interacting proteins were also identified as FLAG-SLBP^{WT} interactors in Panomwan (2017), including LARP4 and SRRT, which are the two nodes linking SLBP to the wider network illustrated in Figure 3.15A. LARP4 is an RNA-binding protein that interacts with the 5' cap and 3'UTR of poly(A)+ mRNAs and positively regulates translation by inhibiting deadenylation of the poly(A) tail and increasing poly(A)+ mRNA stability (Yang et al., 2011; Mattijssen et al., 2021). At the time of writing, there are no reports in the literature of LARP4 being implicated in the regulation of histone mRNA translation or histone mRNA decay. On the other hand, SRRT (also known as ARS2) binds to the 5' end of nuclear cap-binding complex-controlled mRNAs, including replication-dependent histone mRNAs, through its interaction with CBP80/20 and acts as a mediator between CBP80/20 and factors that promote proper mRNA 3' end formation (Gruber et al., 2012; O'Sullivan et al., 2015; Lykke-Andersen et al., 2021). Interestingly, Panomwan (2017) reported evidence of decreased LARP4 protein abundance in FLAG-SLBP^{WT} immunoprecipitates following hydroxyurea-induced replication stress, while SRRT levels remained unchanged, suggesting that LARP4 may be targeted in response to replication stress to negatively regulate *de novo* replication-dependent histone mRNA translation as SRRT remains associated with histone pre-mRNA in the nucleus, primed to facilitate histone pre-mRNA processing again when replication stress has been overcome and DNA replication resumes. Whether these are indeed aspects of activated intra-S phase checkpoint signalling remains an open question that warrants further investigation.

While the LC-MS/MS experiment described in this section lacks the necessary biological replicates required to perform a statistical analysis and state with confidence that proteins identified here are bona fide interactors of SLBP, it demonstrates the ability to detect peptides derived from SLBP in enzymatically-digested FLAG-SLBP^{siRes} Flp-In T-REx HeLa cell immunoprecipitation eluates and the potential to monitor SLBP post-translational modifications and the SLBP interactome in our model system using mass spectrometry.

3.3 Discussion

In this chapter, the aim was to validate the FLAG-SLBP^{WT} and FLAG-SLBP^{siRes} Flp-In T-REx HeLa cell lines that were inherited from Dr Pornpen Panomwan at the beginning of this project; to demonstrate the experimental capabilities and limitations of expressing FLAG-tagged SLBP using the Flp-In T-REx conditional expression cell system, and to develop and validate the analytical techniques that will be relied upon in order to study the function of SLBP and address the aims of this project.

3.3.1 Use of the Flp-In T-REx HeLa system for the conditional expression of stably transfected FLAG-tagged SLBP in mammalian cells

The *in vitro* biochemical analysis of SLBP function in mammalian cells has commonly been performed by expressing SLBP mutants from a transiently transfected mammalian expression vector or by generating and analysing stably transfected cell lines following the random integration of a plasmid construct containing SLBP cDNA into the genome of the transfected cell line (Zheng et al., 2003; Erkmann et al., 2005b; Koseoglu et al., 2008; Dankert et al., 2016). Despite the breadth of knowledge that has been acquired regarding the function of SLBP in mammalian cells *in vitro*, there are inherent limitations when using such approaches that may preclude further insights. A potentially significant drawback that may arise when performing chemically-induced transient transfections with an expression vector relates to the variation in transfection efficiency that may be observed between experiments due to batch-to-batch variability in the purity of the genetic material to be transfected (Ehlert et al., 1993). Such variations in transfection efficiency have the potential to result in inconsistent gene expression levels that could prove problematic when interpreting results. Additionally, foreign DNA and cationic lipid transfection reagents are cytotoxic and as such, even with optimised transfection conditions using the minimal effective dose of plasmid DNA and transfection reagent, the transfected cells will be under a degree of stress which may lead to changes in gene transcription and the activation of unintended cellular signalling pathways (Ishii and Akira, 2006; Fiszer-Kierzkowska et al., 2011). While the potential impact of these limitations can be mitigated through careful experimental design and the use of appropriate controls, the complexity of experiments would increase and could become a hindrance when factoring in

the additional need to perform siRNA transfections when conducting RNAi rescue experiments. Finally, gene expression from a transiently transfected expression plasmid is, by definition, short-lived and the level of expression will decrease over time as cells divide. The generation of stably transfected cell lines that contain a randomly integrated exogenous gene under the control of a constitutively active promoter eliminates the need to routinely transfect an expression vector, however, the position at which the expression cassette integrates into chromatin is random and will likely be different in each cell line generated, which may contribute to phenotypic differences between cell lines (Stepanenko and Heng, 2017). With this in mind, the Flp-In T-REx HeLa cell system (Invitrogen) was utilised previously by the Smythe lab to generate isogenic, stably transfected cell lines to study the function of SLBP in mammalian cells (Panomwan, 2017).

The Flp-In T-REx HeLa cell system is a Tet-On inducible expression system that allows for the conditional expression of a gene of interest (GOI) when cells are cultured in the presence of tetracycline or doxycycline (Ward et al., 2011; Szczesny et al., 2018). I began this project by validating FLAG-SLBP^{WT} and FLAG-SLBP^{siRes} Flp-In T-REx HeLa cells that were inherited from Dr Pornpen Panomwan. I started by testing a range of doxycycline concentrations (0.1 - 1 μg/mL doxycycline) to determine the optimal concentration required to induce expression of FLAG-SLBP^{WT}. The level of FLAG-SLBP^{WT} expression was equal across the range of doxycycline concentrations tested after 5 hours of exposure to doxycycline and, crucially, the levels of FLAG-SLBP^{WT} were equal to that of endogenous SLBP. As there was no evidence of a dose-dependent increase in FLAG-SLBP^{WT} expression, it was concluded that maximal FLAG-SLBP^{WT} expression can be achieved by exposing cells to a doxycycline concentration as low as 0.1 μg/mL for 5 hours. In keeping with previous efforts, a concentration of 0.5 μg/mL doxycycline was selected for use in later experiments (Panomwan, 2017). Importantly, the observation from an asynchronous population of cells that maximal FLAG-SLBP^{WT} protein levels were equal to endogenous SLBP, which is expressed only in S phase, provides evidence that FLAG-SLBP mRNA derived from a stably transfected exogenous gene is translationally regulated in a manner similar to endogenous SLBP mRNA to ensure that FLAG-SLBP protein synthesis is also restricted to S phase only (Whitfield et al., 2000; Djakbarova et al., 2014). Analysis of the duration of doxycycline-induced FLAG-SLBP^{WT} expression clearly demonstrated that 0.5 μg/mL doxycycline-induced maximal FLAG-SLBP^{WT} expression for up to 48 hours, after which the levels of FLAG-SLBP^{WT} began to decrease. The observed decrease

in FLAG-SLBP^{WT} expression at later time points was attributed to a reduced availability of doxycycline in the cell culture media and not a progressive reduction in the fraction of cells in S phase as cells reach confluency as (i) cells for later time points were seeded into larger tissue culture dishes to ensure that cells would not reach confluency by 96 hours, which is confirmed by the near equal levels of endogenous SLBP across all time points, and (ii) the intensity of the FLAG-SLBP^{WT} signal decreased by $\sim$50% every 24 hours after the 48-hour time point, which is consistent with doxycycline exhibiting a half-life of 24 hours in cell culture media. If necessary, the duration of FLAG-SLBP^{WT} expression could be increased by using a higher initial concentration of doxycycline or by replenishing cell culture media with 0.5 μg/mL doxycycline after 48 hours.

I next confirmed the siRNA-mediated knockdown of endogenous SLBP and the subsequent expression of siRNA-resistant FLAG-SLBP^{siRes}. Transfecting FLAG-SLBP^{WT} cells with 200 nM SLBP siRNA resulted in $\sim$80% knockdown of both endogenous SLBP and FLAG-SLBP^{WT} protein. An equivalent degree of endogenous SLBP knockdown was observed in FLAG-SLBP^{siRes} cells transfected with SLBP siRNA though, after 5 hours of culture in media containing 0.5 μg/mL doxycycline, FLAG-SLBP^{siRes} protein expression was evident and protein levels appeared comparable to endogenous SLBP and FLAG-SLBP^{WT} levels in control cells, confirming that the two silent nucleotide substitutions in the FLAG-SLBP^{siRes} transgene are sufficient to render FLAG-SLBP^{siRes} resistant to siRNA-mediated gene silencing. The duration of SLBP knockdown was assessed and, surprisingly, was deemed to only be effective for 24 hours after which FLAG-SLBP^{WT} protein levels returned to that of control cells. This result was surprising at first as Sullivan et al. (2009) reportedly achieved significant and sustained SLBP knockdown for up to 120 hours using siRNA, though theirs was a two-hit approach and a 2-fold higher siRNA concentration was used. Given the anticipated number of FLAG-SLBP mutant cell lines that may be required to be assayed simultaneously and routinely throughout this project, I opted to maintain a one-hit siRNA knockdown strategy and ensured that experiments to assay SLBP-dependent regulation of histone mRNA metabolism were conducted within 24 hours of transfecting cells with SLBP siRNA.

Knockdown of SLBP results in an overall decrease in histone mRNA transcript levels and the retention of unprocessed histone pre-mRNA in the nucleus, leading to the uncoupling of DNA replication and histone biosynthesis (Zhao et al., 2004; Wagner et al., 2005; Sullivan et al., 2009;

Kerzendorfer et al., 2012). Continued DNA replication in the absence of soluble histones results in underchromatinisation of newly synthesised DNA and a failure of cells to appropriately transition from S phase to G2 (Wagner et al., 2005; Kerzendorfer et al., 2012). Crucially, Wagner et al. (2005) showed that expression of an RNAi-resistant version of SLBP was able to restore proper S phase progression. To demonstrate the ability to reproduce and measure the effect of similar experimental conditions in our model system and to confirm that the expression of FLAG-SLBP^{siRes} is sufficient to restore SLBP function in cells exposed to SLBP siRNA, I performed bivariate flow cytometry to analyse the cell cycle distributions of FLAG-SLBP^{WT} control, knockdown and FLAG-SLBP^{siRes} cells. In experiments reported previously, analysis was performed on cells released after arrest at the G1/S transition by double thymidine block, with siRNA being transfected into cells at the time of the second thymidine block, or on an asynchronous population of cells that were cultured for 72 hours after two doses of siRNA (Zhao et al., 2004; Wagner et al., 2005; Sullivan et al., 2009; Kerzendorfer et al., 2012). I found that culturing asynchronous FLAG-SLBP^{WT} cells for 24 hours after transfection with one dose of SLBP siRNA was sufficient to induce a modest but statistically significant increase in S phase cells and a decrease in the number of cells in both G1 and G2/M. In FLAG-SLBP^{siRes} cells exposed to SLBP siRNA, expression of FLAG-SLBP^{siRes} for 5 hours reversed the observed changes in cell cycle distribution, confirming that expression of RNAi-resistant FLAG-SLBP is able to rapidly restore the function of SLBP in Flp-In T-REx HeLa cells lacking endogenous SLBP.

Taken together, these results demonstrate that the use of the Flp-In T-REx HeLa cell system coupled with RNAi and the expression of RNAi-resistant FLAG-SLBP provides a suitable working model system and experimental strategy that will aid the investigation of SLBP function in mammalian cells.

3.3.2 Development of a robust qPCR assay to measure histone mRNA transcript levels and the rate of histone mRNA decay in FLAG-SLBP Flp-In T-REx HeLa cells

After establishing that the Flp-In T-REx HeLa cell system and the RNAi rescue experimental strategy are suitable for use in this study, I then developed a qPCR assay that would be used throughout the project to measure histone mRNA transcript levels in cells expressing FLAG-SLBP^{siRes} mutants in the presence or absence of DNA replication stress. Using carefully optimised qPCR conditions, I validated the qPCR assay by demonstrating that (i) siRNA-mediated knockdown of SLBP led to a 40% reduction in *HIST1H3B* mRNA transcript levels, (ii) the observed reduction in *HIST1H3B* mRNA transcript levels in SLBP siRNA-treated cells was rescued by the expression of siRNA-resistant FLAG-SLBP^{siRes}, and (iii) addition of hydroxyurea to both FLAG-SLBP^{WT} and FLAG-SLBP^{siRes} cells to induce DNA replication stress resulted in the rapid destruction of *HIST1H3B* mRNA. These observations are in agreement with previous reports in the literature describing SLBP-dependent regulation of replication-dependent histone mRNAs and, importantly, confirm that siRNA-resistant FLAG-SLBP^{siRes} is capable of facilitating histone mRNA decay, suggesting that the analysis of FLAG-SLBP-dependent regulation of *HIST1H3B* mRNA in our model system using the qPCR assay developed in this chapter will be indicative of family-wide replication-dependent histone mRNA regulation by SLBP (Zhao et al., 2004; Wagner et al., 2005; Sullivan et al., 2009).

Shortly before starting this project, Dankert et al. (2016) reported an increase in *H2AFX* mRNA translation in G2 and increased sensitivity to genotoxic stress in cells expressing an SLBP mutant that is stabilised at the end of S phase and into G2 (SLBP^{4A}, $^{96\text{-}}$KRKL>AAAA$^{\text{-}99}$), however, it was not clear if the observed increase in *H2AFX* mRNA translation was due to an increase in *H2AFX* gene transcription or increased translational efficiency. Therefore, in addition to *HIST1H3B*, I optimised qPCR to investigate SLBP-dependent regulation of *H2AFX* mRNA transcript levels. The *H2AFX* gene encodes a histone H2A variant, H2A.X, that is phosphorylated on serine 139 by ATM/ATR to form γ-H2A.X in response to DNA double-strand breaks (DSBs) in order to initiate the DNA damage response (Rogakou et al., 1998; Ward and Chen, 2001; Furuta et al., 2003). Unlike replication-dependent histone genes, *H2AFX* is expressed throughout the cell cycle and *H2AFX* mRNA is not degraded in response to DNA replication stress (Bonner et al., 1993;

Griesbach et al., 2021). *H2AFX* is a unique hybrid histone gene that expresses bimorphic histone mRNA transcripts; during S phase, expression of *H2AFX* gives rise to *H2AFX* mRNA that ends with a stem-loop in the 3'UTR, similar to replication-dependent histone mRNAs, whereas *H2AFX* expressed elsewhere in the cell cycle, or under conditions of DNA replication stress, results in the synthesis of longer *H2AFX* mRNA transcripts that contain a stem-loop but end in a poly(A)+ tail, and SLBP is capable of binding both isoforms (Bonner et al., 1993; Townley-Tilson et al., 2006; Brooks et al., 2015; Griesbach et al., 2021). The requirement for *H2AFX* mRNA to be expressed as poly(A)- and poly(A)+ isoforms is not clearly understood though the observation that the poly(A)+ isoform is expressed under conditions of replication stress suggests that the presence of the poly(A)+ tail may be required for *H2AFX* mRNA stability and the *de novo* synthesis and deposition of H2A.X into DNA damage-associated chromatin (Griesbach et al., 2021). Interestingly, in studies of zebrafish development, the loss of SLBP function during early stages of embryogenesis was shown to result in differential regulation of replication-dependent and *H2AFX* histone gene expression. At the 256-cell stage of development ($\sim$2.5 hours post fertilisation) cells from *slbp2*$^{-/-}$ embryos displayed a reduction in replication-dependent histone mRNAs and a significant increase in *H2AFX* mRNA (Turner et al., 2019). Similarly, *slbp*$^{ty77e/ty77e}$ mutant embryos with a point mutation that introduces a premature stop codon (Y180Stop) in the RNA binding domain giving rise to a truncated form of SLBP unable to bind histone mRNA and defective for histone pre-mRNA 3'UTR processing, showed widespread transcriptional upregulation of *H2AFX* in the developing nervous system at 3 days post fertilisation and a 2-fold increase in the percentage of cells in S phase as *slbp*^{ty77e} cells fail to transition from proliferation to differentiation (He et al., 2018). Thus, while *H2AFX* mRNA transcript levels were expected to and did remain stable after the addition of hydroxyurea in our model system, the qPCR evidence presented in this chapter showing a link between SLBP knockdown and the downregulation of *H2AFX* mRNA transcript levels is novel and was unexpected. This finding suggests that in differentiated cells, SLBP positively regulates *H2AFX* gene expression in addition to replication-dependent histone genes and that inhibition of SLBP activity not only uncouples the rate of replication-dependent histone protein synthesis with the rate of DNA replication but may also impair the ability of cells to initiate the DNA damage response and effectively resolve DSBs that would arise as a result of this uncoupling or from other sources of replication stress and DNA damage.

In summary, the use of qPCR in this project to accurately quantify *HIST1H3B* and *H2AFX* mRNA transcript levels in Flp-In T-REx HeLa cell lines expressing different FLAG-SLBP^{siRes} mutants is likely to provide valuable insights into the regulation of SLBP function, the SLBP-dependent regulation of histone gene transcription and the SLBP-dependent regulation of histone mRNA metabolism in human cells.

3.3.3 Immunoprecipitation of FLAG-SLBP^{siRes} and analysis FLAG-SLBP^{siRes} and interacting proteins by LC-MS/MS

In the final part of this chapter, I demonstrated the ability to isolate and purify FLAG-tagged SLBP from crude Flp-In T-REx HeLa cell lysates using commercially available α-FLAG M2 affinity gel and 3X FLAG peptide (Invitrogen) followed by analysis of FLAG-SLBP^{siRes} immunoprecipitation eluates by LC-MS/MS. Although only one replicate was performed, I was able to successfully isolate and purify FLAG-SLBP^{siRes} using an established immunoprecipitation protocol (Panomwan, 2017). Subsequent analysis of the experimental immunoprecipitation eluate by LC-MS/MS identified 98 proteins that co-immunoprecipitated with FLAG-SLBP^{siRes}. Of these, 68 had previously been identified in control immunoprecipitation-mass spectrometry experiments using α-FLAG antibody or α-FLAG M2 affinity agarose gel and so were regarded as contaminants in this experiment (Mellacheruvu et al., 2013). 9 out of the 30 proteins considered to be FLAG-SLBP^{siRes} interactors in this experiment were also identified as FLAG-SLBP^{WT} interactors in Panomwan (2017) and 5 of these were previously shown to display a decreased association with FLAG-SLBP^{WT} following hydroxyurea-induced replication stress (Panomwan, 2017). GO enrichment analysis of the 30 FLAG-SLBP^{siRes} interacting proteins identified here suggested an enrichment of proteins that bind either the 5' or 3'-UTR of mRNA, or translation initiation factors, that function to positively or negatively regulate mRNA translation or pre-mRNA processing and STRING analysis revealed a potentially functional network consisting of 22 of the 30 proteins identified. Due to the lack of biological replicates, it is not possible to draw meaningful conclusions from this dataset, however, the experiment presented here demonstrates the potential of using our model system to monitor the post-translational modification status of SLBP and the SLBP interactome using mass spectrometry.

In summary, the experiments presented in this chapter validate the FLAG-SLBP^{WT} and FLAG-SLBP^{siRes} cell lines that were gifted by Dr Pornpen Panomwan at the start of this project and demonstrate the experimental capabilities and limitations when using the Flp-In T-REx HeLa cell conditional expression system to study the function of essential genes, such as SLBP, in mammalian cells. Using this system and the qPCR assay developed in this chapter, I demonstrated for the first time that SLBP regulates the expression of *H2AFX* in addition to replication-dependent histone genes, and I demonstrated the ability to measure replication-dependent histone mRNA decay kinetics in response to hydroxyurea-induced replication stress using qPCR. Finally, I used established immunoprecipitation and mass spectrometry protocols to isolate FLAG-SLBP and interacting proteins from crude cell lysates, which will enable the monitoring of SLBP post-translational modifications and changes to the SLBP interactome as a function of the mutation status of FLAG-SLBP and/or experimental stimuli. Together, the results from the experiments presented here confirm that the use of our chosen model system, coupled with RNAi and the expression of RNAi-resistant FLAG-SLBP, provides an appropriate strategy for investigating the function of SLBP and the regulation of histone mRNA metabolism in mammalian cells.

Chapter 4

Analysis of replication-dependent histone mRNA stability in cells expressing non-phosphorylatable and phosphomimetic SLBP serine 20 and serine 23 mutants

4.1 Introduction

The rationale for the current project was based on the observation in Panomwan (2017) that phosphopeptides containing phosphorylated serine 20 (S20) and serine 23 (S23) were significantly enriched in LC-MS/MS analyses of immunoprecipitation eluates from FLAG-SLBP^{WT} cells treated with hydroxyurea to induce replication stress. This result was intriguing as phosphorylation of SLBP S20/S23 has previously been described as a phosphodegron that regulates SLBP polyubiquitination and degradation at the end of S phase. Krishnan et al. (2012) suggested that phosphorylation of S20 and/or S23 is required for the efficient interaction of SLBP with the prolyl isomerase Pin1, which, at the end of S phase, binds to threonine 171 (T171) in SLBP and catalyses the *cis-trans* isomerisation of the peptide bond linking T171 and proline 172 (P172) in the TPNK motif located within the SLBP RNA binding domain. The isomerisation of T171 and the resulting conformational change leads to the dissociation of histone mRNA from SLBP thereby facilitating histone mRNA decay by the nuclear exosome complex and the polyubiquitination and degradation of SLBP via the ubiquitin-proteasome system. Crucially, the authors demonstrated that mutation of both S20 and S23 to alanines abolished SLBP polyubiquitination. Evidence in Panomwan (2017)

of the enrichment of S20/S23 phosphopeptides in response to replication stress, when SLBP protein levels remain stable, led to the hypothesis that phosphorylation of S20 and/or S23 might be a general mechanism of inducing Pin1-mediated dissociation of histone mRNA and SLBP in order to facilitate histone mRNA decay at the end of S phase and in response to replication stress and that SLBP polyubiquitination and degradation at the end of S phase occurred by other means but nevertheless required prior dissociation of histone mRNA and SLBP mediated by Pin1. It was anticipated that the characterisation of histone mRNA decay kinetics, SLBP protein levels and the SLBP-interactome in cell lines expressing phosphomimetic and non-phosphorylatable S20 and S23 mutants would provide insights into how phosphorylation of S20/S23 contributes to the regulation of histone mRNA decay under conditions of replication stress.

Surprisingly, Western blot and qPCR analysis presented in this chapter revealed that expression of S20/S23 mutants in our model system had no apparent impact on SLBP protein or histone mRNA stability under steady-state conditions or the rate of hydroxyurea-induced histone mRNA decay, suggesting not only that phosphorylation of S20 or S23 does not constitute a phosphodegron as previously described but also that phosphorylation of S20 or S23 under conditions of replication stress does not regulate the initiation of histone mRNA decay.

4.2 Results

4.2.1 *In silico* predictions of SLBP S20 and S23 kinases

Phosphorylation of SLBP S20 and S23 has been observed in cells grown in culture under various experimental conditions, however, the functional significance of phosphorylated S20 and S23 along with identification of the kinase(s) responsible for phosphorylation and the context under which phosphorylation occurs remains to be accurately elucidated (Olsen et al., 2006; Bansal et al., 2013; Zhou et al., 2013; Krishnan et al., 2012; Panomwan, 2017). As a first approach to identify the kinase responsible for S20 or S23 phosphorylation, I performed *in silico* analyses using the PhosphoNET online database to identify kinases that are predicted to phosphorylate SLBP S20 or S23 based on the amino acid sequence local to the phosphosite and the known substrate phosphosite amino acid sequence preferences for ∼500 human protein kinases (Safaei et al., 2011). The top 10 predicated kinases with the potential to phosphorylate SLBP S20 and S23 according to the PhosphoNET algorithm are shown in Table 4.1 and Table 4.2, respectively.

This analysis identified two families of kinases that are predicted to target SLBP S20 or S23 and are implicated in stress signalling or the control of cell cycle progression. ERKs, JNKs and p38MAPKs are three subfamilies of kinases that constitute the mitogen-activated protein kinase (MAPK) family, which regulate cellular responses to a range of stimuli, including growth factor signalling, heat shock, osmotic stress, UV irradiation and pro-inflammatory cytokines, and appear predominantly in the list of S20 predicted kinases. Of these, the p38MAPK complex and JNK1/2 have been shown to be activated in response to hydroxyurea-induced replication stress independently of and in parallel with ATR/Chk1 to activate and maintain intra-S phase checkpoint signalling (Reinhardt and Yaffe, 2009; Llopis et al., 2012; Köpper et al., 2013). The second kinase family that features exclusively on the list of S23 predicted kinases are cyclin-dependent kinases (CDKs), specifically CDK3, CDK2 and CDK1, which are CDKs that regulate the G1/S phase transition, S phase progression and the S/G2 transition.

Zheng et al. (2003) demonstrated that cyclin A/CDK1 binds to SLBP at the end of S phase and phosphorylates threonine 62 (T62) to trigger SLBP degradation. The evidence presented in

Zheng et al. (2003) together with the S20/S23 kinase predictions presented here, the observation reported in Krishnan et al. (2012) that SLBP polyubiquitination is abolished in S20/S23 double alanine mutants and the replication stress LC-MS/MS data reported in Panomwan (2017) appeared to suggest that S23 may be the initial target of cyclin A/CDK1 at the end of S phase to promote the recruitment of Pin1 and the dissociation of histone mRNA from SLBP, which may be followed by phosphorylation of T62 by cyclin A/CDK1 to induce SLBP polyubiquitination and degradation, and that activated p38MAPK and/or JNK1/2 might target S20/S23 under conditions of replication stress to recruit Pin1, promote the dissociation of histone mRNA from SLBP and facilitate histone mRNA decay.

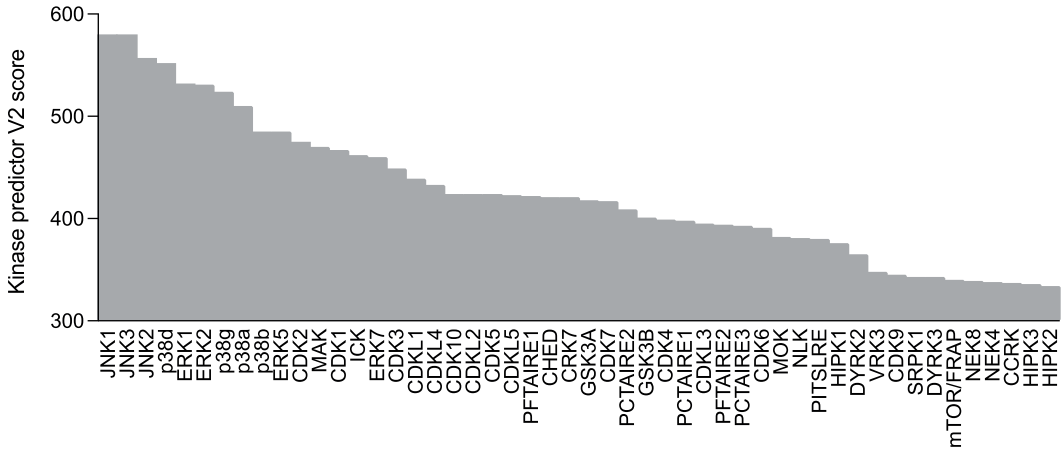

Figure 4.1: Ranked bar chart showing 50 kinases predicted to phosphorylate SLBP S20. Bar chart showing 50 kinases predicted to phosphorylate SLBP S20 identified using the PhosphoNET online database. Kinases are ranked by the PhosphoNET kinase predictor V2 score (`http://www.phosphonet.ca/`; Safaei et al., 2011).

#	Kinase	UniProt ID	Kinase predictor V2 score
1	JNK1	P45983	580
2	JNK3	P53779	580
3	JNK2	P45984	557
4	p38δ MAPK	O15264	552
5	ERK1	P27361	532
6	ERK2	P28482	531
7	p38γ MAPK	P53778	524
8	p38α MAPK	Q16539	510
9	p38β MAPK	Q15759	485
10	ERK5	Q13164	485

Table 4.1: Top 10 SLBP S20 predicted kinases. Top 10 predicted kinases for SLBP S20 identified using the PhosphoNET online database (`http://www.phosphonet.ca/`; Safaei et al., 2011).

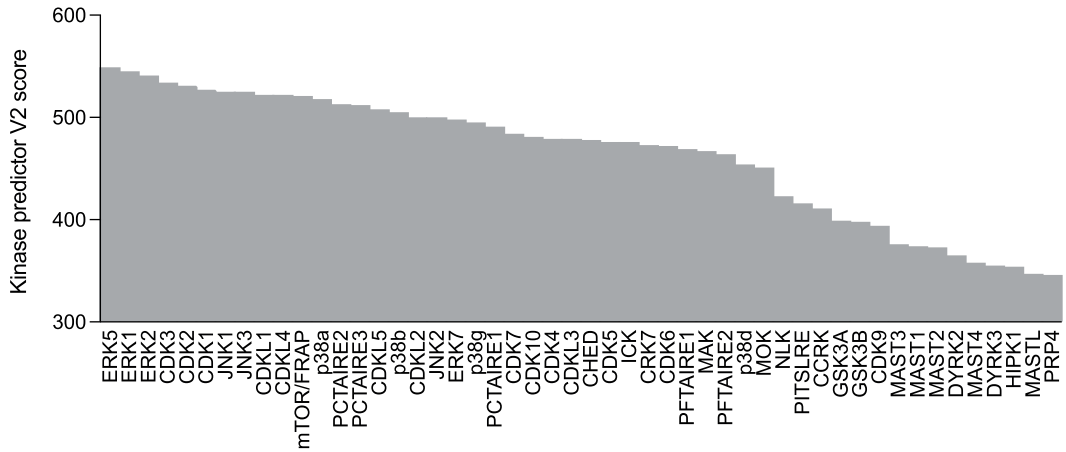

Figure 4.2: Ranked bar chart showing 50 kinases predicted to phosphorylate SLBP S23. Bar chart showing 50 kinases predicted to phosphorylate SLBP S23 identified using the PhosphoNET online database. Kinases are ranked by the PhosphoNET kinase predictor V2 score (`http://www.phosphonet.ca/`; Safaei et al., 2011).

#	Kinase	UniProt ID	Kinase predictor V2 score
1	ERK5	Q13164	549
2	ERK1	P27361	545
3	ERK2	P28482	541
4	CDK3	Q00526	534
5	CDK2	P24941	531
6	CDK1	P06493	527
7	JNK1	P45983	525
8	JNK3	P53779	525
9	CDKL1	Q00532	522
10	CDKL4	Q5MAI5	522

Table 4.2: SLBP S23 predicted kinases. Top 10 predicted kinases for SLBP S23 identified using the PhosphoNET online database (`http://www.phosphonet.ca/`; Safaei et al., 2011).

4.2.2 Generation and characterisation of FLAG-SLBP S20 and S23 non-phosphorylatable and phosphomimetic mutant cell lines

In order to investigate the significance of SLBP S20 and/or S23 phosphorylation in response to hydroxyurea-induced replication stress and address the aims of this project, I performed site-directed mutagenesis using the pcDNA5/FRT/TO/FLAG-SLBP^{siRes} plasmid listed in Table 2.6 as a template and primers outlined in Section 2.1.3.1 to produce novel plasmids with versions of RNAi-resistant SLBP that contain non-phosphorylatable (alanine, A) or phosphomimetic (aspartic acid, D, or glutamic acid, E) amino acid substitutions at positions 20 and 23. Mutant plasmids were co-transfected with pOG44 into Flp-In T-REx HeLa host cells as described in Section 2.2.3.2 to generate FLAG-SLBP^{AA}, FLAG-SLBP^{DD} and FLAG-SLBP^{EE} double mutant cell lines for functional analysis. Aspartic acid and glutamic acid mutants were generated as although both can be used to mimic phosphoserines or phosphothreonines due to their negative charge and chemical structure appearing similar to the negative charge and structure of phosphorylated serine and threonine, substitution does not always result in a successful phosphomimetic mutant and it is therefore prudent to evaluate and confirm the ability of either substitution to mimic phosphorylation before relying on one over the other (Persad et al., 2001; Paleologou et al., 2008; Chen and Cole, 2015).

Doxycycline-induced expression of RNAi-resistant FLAG-SLBP^{AA}, FLAG-SLBP^{DD} and FLAG-SLBP^{EE} was confirmed by Western blot (Figure 4.3). Protein levels for all three mutants appeared to be identical after 5 hours of exposure to doxycycline and were equal to endogenous SLBP and FLAG-SLBP^{WT} protein levels in control cells (Figure 4.3A). Assuming that aspartic acid and glutamic acid amino acid substitutions perform equally well as S20 and S23 phosphomimetics, the data presented here appear to suggest that phosphorylation of S20 and S23 does not induce proteasomal degradation of SLBP as reported in (Krishnan et al., 2012) and might therefore be involved with a separate aspect of SLBP function related to replication-dependent histone mRNA decay, though it remains possible that aspartic acid and glutamic acid amino acid substitutions in FLAG-SLBP^{DD} and FLAG-SLBP^{EE} cell lines fail to mimic S20 or S23 phosphorylation entirely. Expression of FLAG-SLBP^{AA}, FLAG-SLBP^{DD} and FLAG-SLBP^{EE} protein at levels equal to FLAG-SLBP^{WT} and FLAG-SLP^{siRes} in control cells after transfection with SLBP siRNA confirmed that the exogenous FLAG-SLBP^{AA}, FLAG-SLBP^{DD} and FLAG-SLBP^{EE} genes in mutant cell lines are resistant to SLBP siRNA-mediated gene silencing (Figure 4.3B).

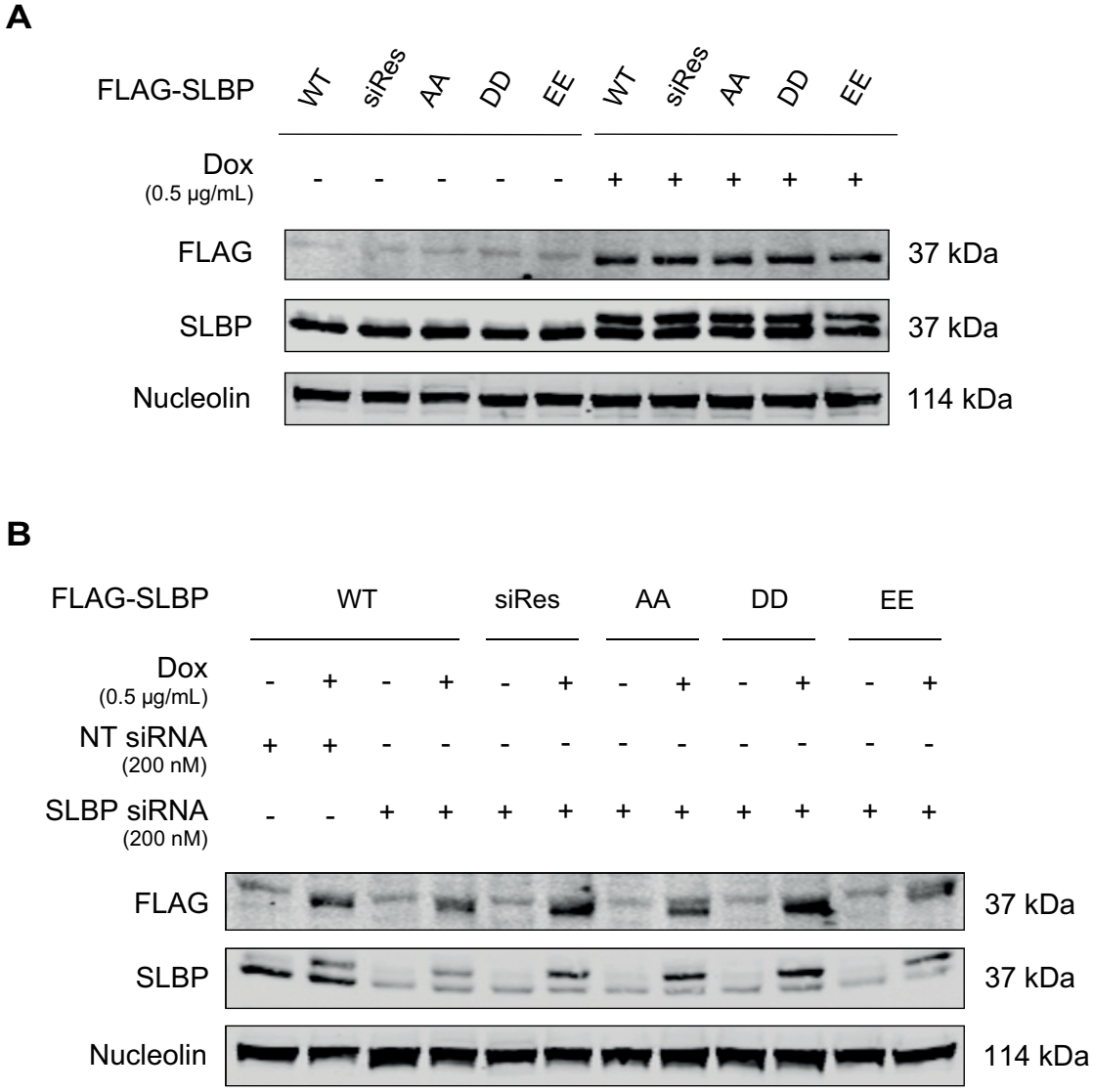

Figure 4.3: Validation of siRNA-resistant FLAG-SLBP S20 and S23 double mutant Flp-In T-REx HeLa cell lines. (A) Asynchronous FLAG-SLBP Flp-In T-REx HeLa cells were cultured in media with or without 0.5 µg/mL doxycycline for 5 hours and cell lysates were analysed by Western blot using α-FLAG, α-SLBP and α-nucleolin antibodies. Nucleolin is used as a loading control. **(B)** Asynchronous FLAG-SLBP Flp-In T-REx HeLa cells were transfected with 200 nM non-targeting (NT) or SLBP siRNA for 24 hours, with 0.5 µg/mL doxycycline added to indicated cell populations for the final 5 hours, and cell lysates were analysed by Western blot using α-FLAG, α-SLBP and α-nucleolin antibodies. Nucleolin is used as a loading control.

4.2.2.1 Steady-state histone mRNA levels and rate of hydroxyurea-induced histone mRNA decay in S20/S23 double mutant cell lines

Having successfully generated and validated RNAi-resistant S20 and S23 double mutant Flp-In T-REx HeLa cell lines, I then assayed replication-dependent histone mRNA transcript levels under steady-state conditions and under conditions of hydroxyurea-induced replication stress in FLAG-SLBP^{AA}, FLAG-SLBP^{DD} and FLAG-SLBP^{EE} cells using the qPCR assay developed in Chapter 3. If the hypothesis that phosphorylation of S20 and/or S23 is implicated in regulating replication-dependent histone mRNA decay is correct and the aspartic acid and/or glutamic acid amino acid substitutions in FLAG-SLBP^{DD} and FLAG-SLBP^{EE} cells are true phosphomimetics, then the ability of FLAG-SLBP^{DD} and FLAG-SLBP^{EE} cells to rescue *HIST1H3B* downregulation following RNAi-mediated knockdown of endogenous SLBP may be compromised and the rate of *HIST1H3B* mRNA decay after the addition of hydroxyurea to cells would be significantly reduced. qPCR analysis of *HIST1H3B* mRNA transcript levels after RNAi-mediated knockdown of endogenous SLBP showed that *HIST1H3B* mRNA levels were reduced by $\sim$40% in FLAG-SLBP^{WT} cells and that this effect of RNAi was rescued in FLAG-SLBP^{siRes} and FLAG-SLBP^{AA} cells after 5 hours of exposure to doxycycline, as expected, however, *HIST1H3B* mRNA downregulation was also completely rescued in FLAG-SLBP^{DD} and FLAG-SLBP^{EE} cells (Figure 4.4A). This result suggests that either (1) phosphorylation of S20 or S23 might regulate histone mRNA decay but the aspartic acid and glutamic acid amino acid substitutions in FLAG-SLBP^{DD} and FLAG-SLBP^{EE} cells do not mimic the phosphorylation of S20 or S23, in which case FLAG-SLBP^{DD} and FLAG-SLBP^{EE} cells would likely display a reduced rate of histone mRNA decay similar to FLAG-SLBP^{AA} cells when exposed to hydroxyurea, or (2) that the amino acid substitutions may mimic the phosphorylation of S20 or S23 but phosphorylation of S20 or S23 does not regulate the initiation of histone mRNA decay.

In order to test which interpretation of the data described above might be correct, I performed qPCR after exposing cells to hydroxyurea for 30 and 60 minutes to measure and compare *HIST1H3B* mRNA decay rates between cell lines. The addition of hydroxyurea resulted in a 70-80% reduction of *HIST1H3B* mRNA after 30 minutes, which progressed to a 90-95% reduction by 60 minutes, in FLAG-SLBP^{WT} control cells as well as FLAG-SLBP^{AA}, FLAG-SLBP^{DD} and FLAG-SLBP^{EE} cells (Figure 4.4B). Based on these data, it appears that phosphorylation of S20 or S23 does not regulate histone mRNA stability as was originally hypothesised.

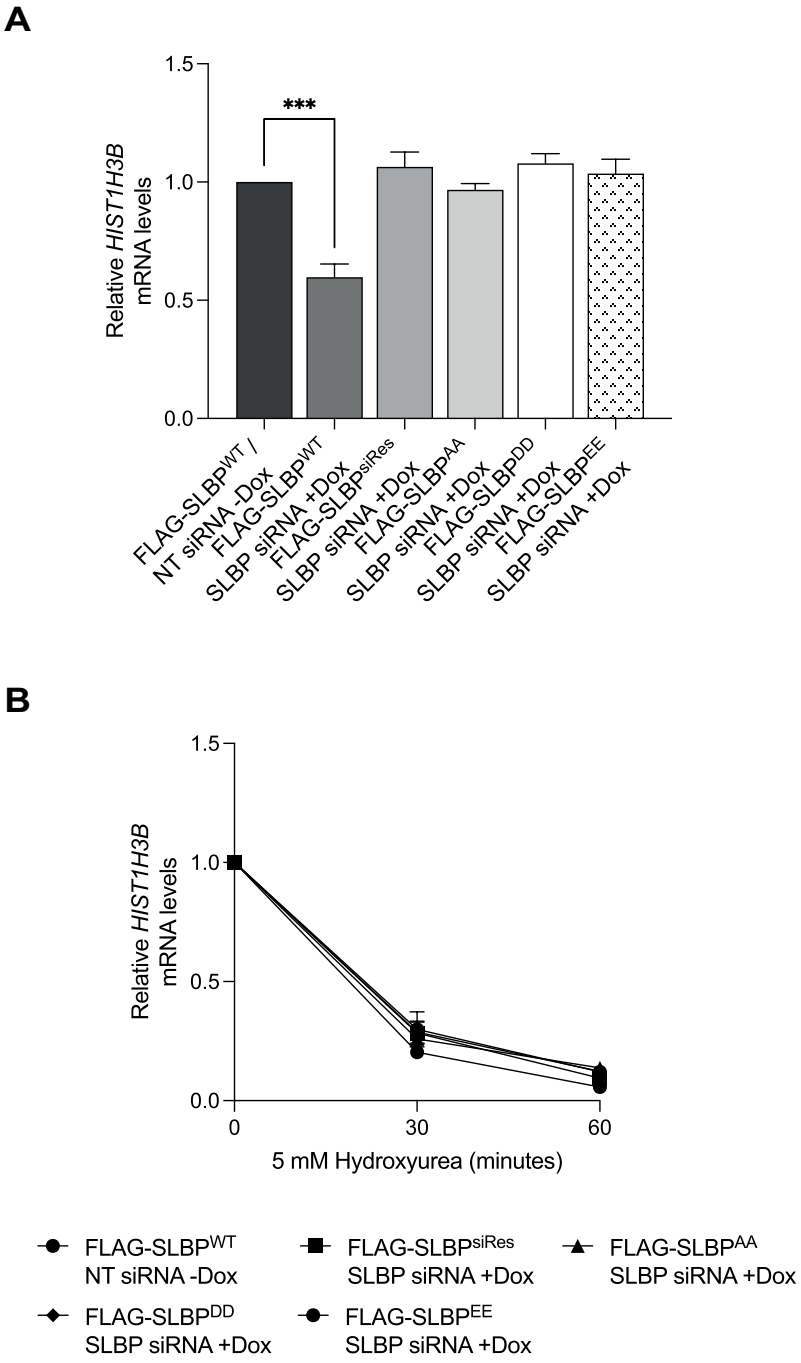

Figure 4.4: Expression of siRNA-resistant FLAG-SLBP S20 or S23 double mutants does not affect the rescue of *HIST1H3B* mRNA transcript levels following siRNA-mediated SLBP knockdown, nor do they affect the rate of hydroxyurea-induced *HIST1H3B* mRNA decay. (A) Asynchronous FLAG-SLBP Flp-In T-REx HeLa cells were transfected with non-targeting (NT) or SLBP siRNA and incubated for 24 hours, with or without 0.5 µg/mL doxycycline for the final 5 hours. cDNA was generated from extracted total RNA and qPCR was performed using *HIST1H3B* primers. **(B)** Asynchronous FLAG-SLBP Flp-In T-REx HeLa cells were treated as in (A) after which 5 mM hydroxyurea was added for 30 and 60 minutes. cDNA was generated from extracted total RNA and qPCR was performed using *HIST1H3B* primers. qPCR samples were tested in triplicate and were quantified and normalised to GAPDH using the $2^{-\Delta\Delta C_T}$ method. *** = $p < .001$. Dunnett's one-way ANOVA. Data are mean ± S.E.M. n = 3 experiments.

4.3 Discussion

Current evidence clearly shows that both S20 and S23 residues in the N-terminus of SLBP are phosphorylated during the course of S phase and, based on the evidence that SLBP polyubiquitination is abolished in non-phosphorylatable S20A/S23A double mutant cells, phospho-S20/S23 is proposed to act as a phosphodegron that regulates SLBP degradation at the end of S phase together with CKII and cyclin A-CDK1-dependent phosphorylation of T61 and T62 (Zheng et al., 2003; Olsen et al., 2006; Krishnan et al., 2012; Zhou et al., 2013). However, recent mass spectrometry data from the Smythe group provides evidence of an enrichment of phosphorylated S20 and S23 in SLBP in cells that have been exposed to hydroxyurea-induced replication stress (Panomwan, 2017). As SLBP is stabilised under conditions of replication stress, the notion that phosphorylation of S20 and S23 acts as a phosphodegron must be incorrect. Rather, the finding in Panomwan (2017) suggests that phosphorylation of S20 and/or S23 is more likely involved in regulating the initiation of replication-dependent histone mRNA decay, perhaps via promoting the recruitment of Pin1 and facilitating the dissociation of SLBP from histone mRNA. Consequently, the objective of the proposed project was to confirm whether phosphorylation of S20 and/or S23 contributes to the regulation of histone mRNA decay and, if so, to identify the kinase responsible for S20/S23 phosphorylation. The aim in this chapter was to generate non-phosphorylatable and phosphomimetic S20 and S23 mutant cell lines and investigate a possible link between the phosphorylation status of S20/S23 and the regulation of hydroxyurea-induced histone mRNA decay using the qPCR assay developed in Chapter 3.

4.3.1 Phosphomimetic S20/S23 mutants display normal histone mRNA transcript levels suggesting that phosphorylation of S20/S23 does not affect histone mRNA stability in the absence of replication stress

Site-directed mutagenesis was conducted in the first instance to produce constructs encoding versions of FLAG-SLBP that include non-phosphorylatable (alanine) or phosphomimetic (aspartic acid/glutamic) amino acid substitutions at positions 20 and/or 23 in place of serine in order to generate novel Flp-In T-REx HeLa cell lines. Western blot analysis showed that the expression levels of both non-phosphorylatable and phosphomimetic FLAG-SLBP S20/S23 mutants were identical

to FLAG-SLBP^{WT} in control cells after 5 hours of culture in media containing the inducer doxycycline. Assuming that both phosphomimetic mutants successfully mimic phosphorylation, this observation suggests that phosphorylation of S20/S23 does not induce SLBP degradation, as was expected. However, it is possible that whilst not being the trigger to induce SLBP degradation per se, phosphorylation of S20 and/or S23 may be a prerequisite for SLBP polyubiquitination if it does not regulate histone mRNA decay, in which case FLAG-SLBP^{AA} might appear stabilised after prolonged exposure to doxycycline, though this was not investigated here.

Analysis of steady-state histone mRNA transcript levels in qPCR rescue experiments showed that all FLAG-SLBP S20/S23 mutants were able to completely rescue SLBP siRNA-induced down-regulation of *HIST1H3B* mRNA. These results were somewhat surprising, as at least one of the S20/S23 phosphomimetic mutants was expected to positively regulate histone mRNA decay, which would have resulted in reduced histone mRNA transcript levels compared to control cells. A possible explanation for this observation might be that phosphorylation of S20/S23 is dynamic and undergoes cycles of phosphorylation and dephosphorylation in order to regulate histone mRNA stability (Gelens and Saurin, 2018). It is also possible that the initiation of histone mRNA decay involves modification of additional residues that are not targeted in the absence of replication stress or that aspartic acid and glutamic acid amino acid substitutions simply fail to mimic phosphorylation. Further qPCR analysis of histone mRNA decay kinetics in S20/S23 mutant cell lines in this and the following chapter suggests that none of these are likely explanations and that the function of S20/S23 *in vivo* is unrelated to the process of histone mRNA decay.

4.3.2 SLBP S20/S23 phosphorylation does not regulate the initiation or the rate of replication-dependent histone mRNA decay in response to hydroxyurea-induced DNA replication stress

If phosphorylation of S20 and/or S23 regulated histone mRNA decay in response to replication stress, then the rate of histone mRNA decay as measured by qPCR should appear reduced in non-phosphorylatable S20/S23 mutants after exposure to hydroxyurea. However, qPCR analyses showed that non-phosphorylatable S20/S23 mutants were able to initiate histone mRNA decay and reduce histone mRNA transcript levels at the same rate and to the same extent as FLAG-SLBP^{WT}

cells. These results were unexpected given our original hypothesis though nonetheless provide conclusive evidence that phosphorylation of S20/S23 does not regulate histone mRNA stability.

Taken together, the data in this chapter appear to show that phosphorylation of S20/S23 regulates neither SLBP stability, histone gene transcription nor histone mRNA decay. How then might phosphorylation of S20 and/or S23 promote SLBP polyubiquitination, as clearly reported in Krishnan et al. (2012)? And why does S20/S23-phosphorylated SLBP accumulate in hydroxyurea-treated cells, as observed in Panomwan (2017)? While by no means conclusive, serendipitous results presented in the following chapter, from what started as an unrelated side project, appear to shed some light on the real function of SLBP S20/S23 in human cells.

Chapter 5

RYKRKL: an evolutionarily conserved SLiM coupling cell cycle progression and the regulation of histone gene transcription

5.1 Introduction

While using the PhosphoNET online tool to identify predicted kinases that might phosphorylate S20 and S23, a glance at the predicted kinase lists for other known and potential SLBP phosphosites revealed that the oncoprotein focal adhesion kinase (FAK) was among the top candidates on the list of kinases that are predicted to phosphorylate a tyrosine residue at position 95. FAK is a non-receptor tyrosine kinase that regulates fundamental cellular processes including cell growth, proliferation and migration by regulating the formation and turnover of integrin-linked focal adhesions at the cell surface and is over-expressed in many human cancers making FAK an attractive therapeutic target (Mitra and Schlaepfer, 2006; Lim, 2013; Yoon et al., 2015). In recent years, novel roles of nuclear-localised FAK have emerged linking FAK signalling with the regulation of gene expression that ultimately promotes cancer cell survival (Lim et al., 2008; Lim, 2013; Serrels et al., 2015). It, therefore, seemed intriguing that FAK was predicted to interact with and phosphorylate SLBP. In support of the notion that Y95 might be post-translationally modified, an *in silico* analysis of tyrosine residue phosphorylation potentials using the NetPhos 3.1 server showed that the phosphorylation potential of Y95 was above the assigned threshold and was the highest phosphorylation potential out of all tyrosines in SLBP (Figure 5.1) (Blom et al., 1999).

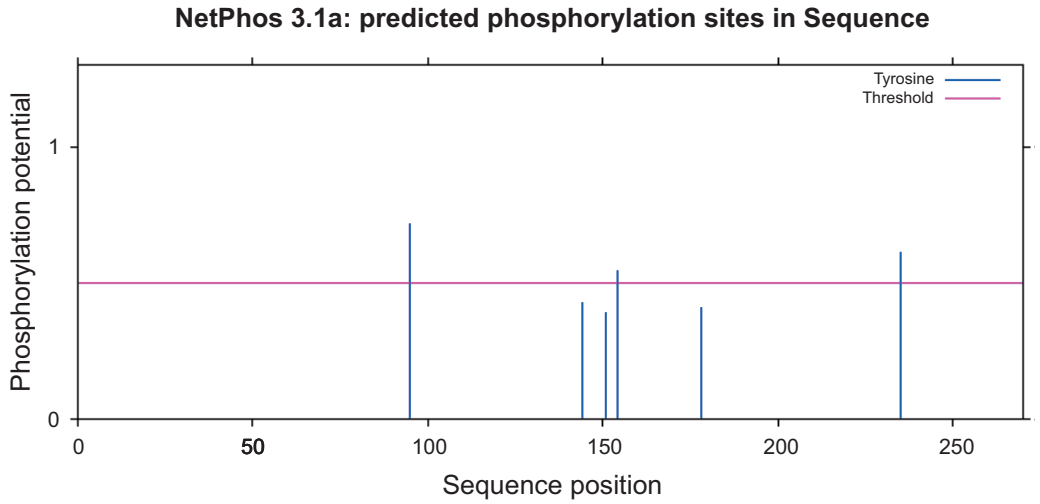

Figure 5.1: SLBP tyrosine phosphorylation potentials. Phosphorylation potential of all tyrosines in SLBP as predicted by the NetPhos 3.1 Server (`http://www.cbs.dtu.dk/services/NetPhos/`; Blom et al., 1999). Blue lines represent the predicted phosphorylation potential of tyrosine residues within $SLBP^{WT}$ on a scale from 0 to 1 (Y-axis). The pink line indicates the 0.5 threshold assigned to the neural network to call a predicted positive tyrosine phosphorylation site. Predicted $SLBP^{WT}$ Y95 phosphorylation potential = 0.715.

Although Y95 is predicted to be phosphorylated, there are no reports in the literature describing the phosphorylation of Y95 or any other tyrosines in SLBP. Furthermore, a survey of ProteomicsDB, an online repository of mass spectrometry data, showed that a peptide containing Y95 has not been observed in any mass spectrometry experiment where peptides derived from SLBP were identified (Figure 5.2) (Schmidt et al., 2018). Inspection of the amino acid sequence surrounding Y95 revealed an abundance of arginine (R) and lysine (K) residues, which are residues that the endopeptidase trypsin preferentially cleaves after. Given the propensity to use trypsin when generating peptides from a protein sample upstream of LC-MS/MS, it is clear how the SLBP Y95 residue has remained elusive in LC-MS/MS analyses, as trypsin would likely cleave after R94 and K96 resulting in the generation of a 2-amino acid peptide ($^{95\text{-}}$YK$^{\text{-}96}$) that would be impossible to assign to a specific protein and would therefore be excluded in any LC-MS/MS analysis. Indeed, an analysis of the raw data in all experiments uploaded to ProteomicsDB that identified SLBP peptides used trypsin to generate peptides prior to LC-MS/MS.

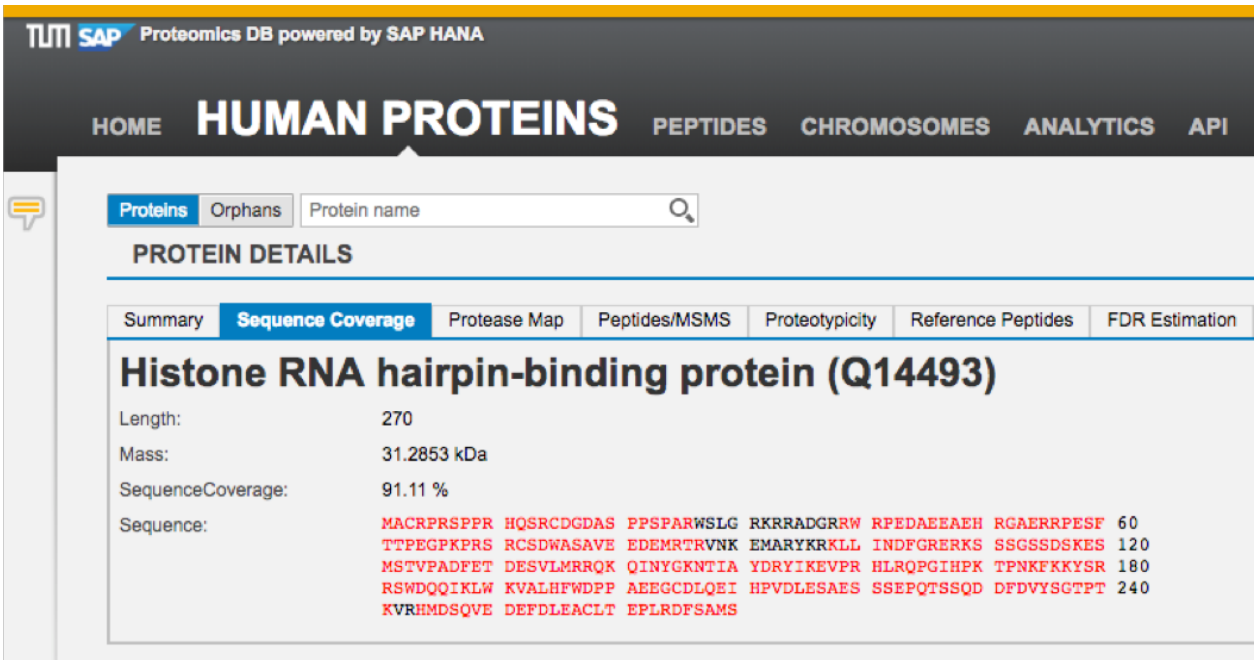

Figure 5.2: SLBP LC-MS/MS cumulative peptide sequence coverage in ProteomicsDB. The cumulative peptide sequence coverage of SLBP (Uniprot ID: Q14493) in data from 720 LC-MS/MS proteomics projects deposited in the ProteomicsDB repository is highlighted in red (91.11%). Regions of SLBP that have not been observed by LC-MS/MS are shown in black. Y95 was not identified in any of the LC-MS/MS projects uploaded to ProteomicsDB at the time of searching (`https://www.proteomicsdb.org/`; Schmidt et al., 2018).

Interestingly, previous reports do show that the amino acids immediately adjacent to Y95 (^{96}-KRKL-^{99}) form one of three nuclear localisation sequences (NLS) that are required for SLBP to cycle between the nucleus and cytoplasm throughout S phase, and that the RKL residues constitute a functional Cy motif (R-x-L) to which cyclins A and F bind in order to regulate SLBP degradation at the end of S phase and in G2 (Figure 5.3) (Erkmann et al., 2005b; Koseoglu et al., 2008; Dankert et al., 2016). Therefore, it seemed plausible that phosphorylation of Y95 by FAK or other kinases, if real, could in some way affect either or both of these processes.

The final observation that hinted Y95 might be phosphorylated and suggested that the wider RYKRKL sequence may itself constitute a functional short linear motif (SLiM) came from an analysis of the evolutionary history of SLBP. Multiple sequence alignments of SLBP amino acid sequences from various eukaryotic model organisms indicated that while the RYKRKL sequence is conserved among mammals, the presence of tyrosine at position 2, the Cy motif, and the overall pattern of charge from an arrangement of basic R and K amino acids, is conserved across vertebrate

species (Figure 5.4).

Despite a lack of experimental evidence, the possibility of FAK or another kinase phosphorylating Y95 in an evolutionarily conserved motif and potentially regulating the activity of SLBP provided an opportunity to conduct a curiosity-driven project alongside work on S20 and S23. Surprisingly, data obtained appeared to suggest that Y95 is not phosphorylated but is nonetheless functional, and showed that the RYKRKL motif and S23 share a functional association that is crucial for the activity of SLBP. The data presented in this chapter provide a novel insight into the cell cycle-dependent regulation of SLBP and provide evidence that suggests the existence of a multi-protein RYKRKL-dependent regulatory network that links cell cycle progression, DNA replication and histone biosynthesis.

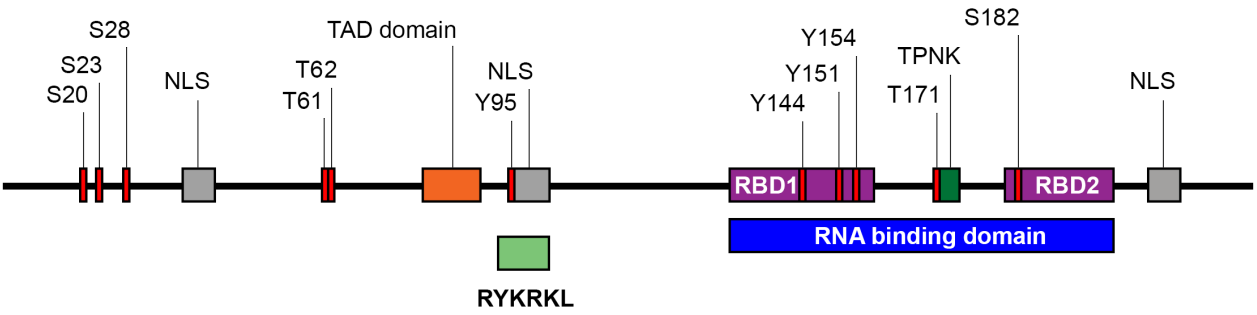

Figure 5.3: Linear representation of SLBP showing the location of the RYKRKL short linear motif. The six amino acid RYKRKL short linear motif is located at amino acid positions 94-99 in human SLBP. It contains amino acids (KRKL) that constitute one of three nuclear localisation signals (NLS) that regulate the nuclear trafficking of SLBP during S phase, and a Cy motif (R-x-L) that provides a docking site for cyclin A and cyclin F at the end of S phase and in G2, respectively, to limit SLBP activity and promote SLBP degradation.

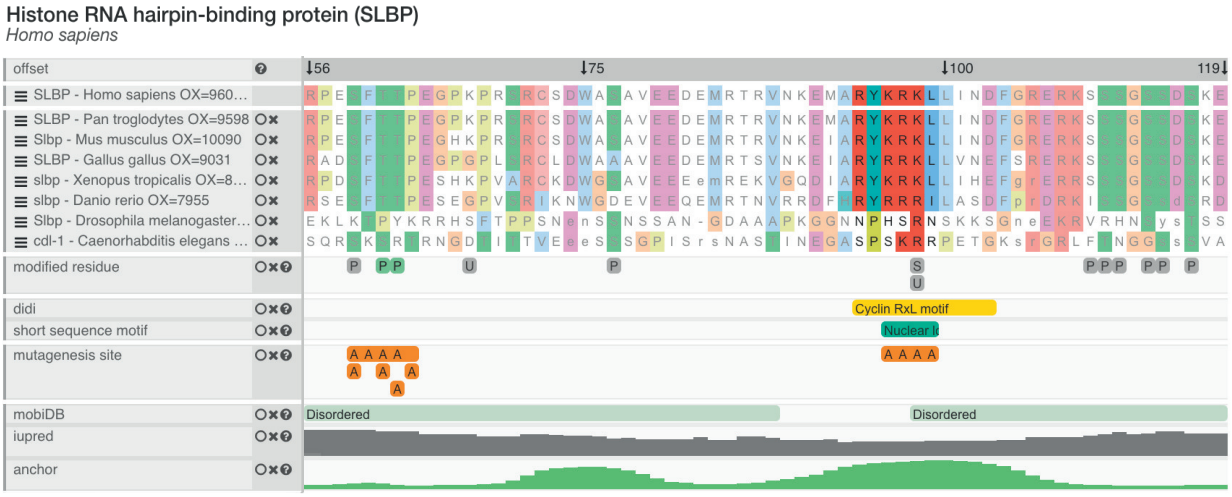

Figure 5.4: Multiple sequence alignment of SLBP amino acid sequences shows evolutionary conservation of the RYKRKL motif. Amino acid sequences of SLBP from human, chimpanzee and common vertebrate and invertebrate model organisms aligned using the ProViz SLiM visualisation tool. The RYKRKL amino acid sequence appears to be conserved among mammals and the overall pattern of charge across the motif is conserved in vertebrates. The motif is absent in invertebrate species. (`http://slim.icr.ac.uk/proviz/`; Jehl et al., 2016).

5.2 Results

5.2.1 *In silico* prediction of SLBP Y95 kinases

I began investigating Y95 and the wider RYKRKL motif by performing an *in silico* analysis using the PhosphoNET online database to identify kinases that are predicted to phosphorylate Y95 based on the local amino acid sequence and known substrate phosphosite amino acid sequence preferences (Safaei et al., 2011). The top 10 predicated kinases with the potential to phosphorylate Y95 according to the PhosphoNET algorithm are shown in Table 5.1. Of these, 5 are plasma membrane-associated receptor tyrosine kinases (RTK) and 5 are cytosolic non-receptor tyrosine kinases (nRTKs, emphasised in bold in Table 5.1), each with diverse cell and tissue expression profiles and no obvious functional association with SLBP, histone mRNA metabolism or intra-S phase checkpoint signalling.

The proto-oncogene gene products ALK (anaplastic lymphoma kinase) and FAK (focal adhesion kinase) are the top two candidate kinases that are predicted to phosphorylate Y95 according to this analysis. ALK is a receptor tyrosine kinase that together with LTK and the insulin receptor (INSR) constitute a distinct RTK superfamily subgroup that transduce specific extracellular signals intracellularly and activate signalling pathways regulating cell survival, growth, proliferation and differentiation. However, in approximately 60% of anaplastic large-cell lymphomas (ALCLs), a genomic translocation event gives rise to the expression of NPM-ALK, a soluble, cytosolic and oncogenic fusion protein comprised of the N-terminal end of nucleophosmin (NPM), derived from the *NPM1* gene on chromosome 5, and the C-terminal catalytic domain of ALK from the *ALK* gene on chromosome 2. NPM-ALK-dependent phosphorylation of AUF1 in ALCL increases the stability of a subset of AUF1 target mRNAs that contain AU-rich elements (AREs) in the 3'-UTR and excess NPM-ALK signalling results in DNA damage and an accumulation of γH2A.X at sites of DSBs (Fawal et al., 2006; Ceccon et al., 2016). In contrast, the non-receptor tyrosine kinase FAK is primarily regulated by integrin signalling and controls fundamental cellular processes, including cell adhesion, migration, cell survival and proliferation, and promotes malignant features of cancer progression, such as cancer stemness, epithelial to mesenchymal transition (EMT) and tumour angiogenesis in a number of human cancer subtypes (Mitra and Schlaepfer, 2006; Lim,

2013; Yoon et al., 2015). Recently, novel roles of nuclear localised FAK have emerged where FAK has been shown to promote cell proliferation via ubiquitin-mediated p53 degradation in addition to regulating *GATA4* and *IL-33* gene transcription to establish a pro-tumourigenic microenvironment (Lim et al., 2008; Lim, 2013; Serrels et al., 2015).

Whilst only a first approach to identify potential SLBP Y95 kinases, the analysis presented in this section suggested that if Y95 is phosphorylated *in vivo*, then it may be targeted for phosphorylation by oncogenic tyrosine kinases in malignant cells specifically, which may provide a selective advantage through the modulation of SLBP activity.

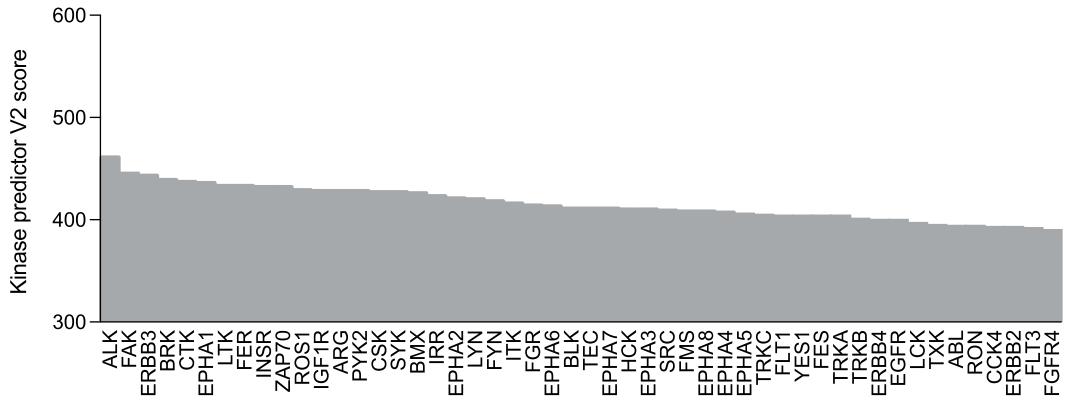

Figure 5.5: Ranked bar chart showing 50 kinases predicted to phosphorylate SLBP Y95. Bar chart showing 50 kinases predicted to phosphorylate SLBP Y95 identified using the PhosphoNET online database. Kinases are ranked by the PhosphoNET kinase predictor V2 score (`http://www.phosphonet.ca/`; Safaei et al., 2011).

#	Kinase	UniProt ID	Kinase predictor V2 score
1	ALK	Q9UM73	463
2	**FAK**	**Q05397**	**447**
3	ERBB3	P21860	445
4	**BRK**	**Q13882**	**441**
5	**CTK (MATK)**	**P42679**	**439**
6	EPHA1	P21709	438
7	LTK	P29376	435
8	**FER**	**P16591**	**435**
9	INSR	P06213	434
10	**ZAP70**	**P43403**	**434**

Table 5.1: SLBP Y95 predicted kinases. Top 10 predicted kinases for SLBP Y95 identified using the PhosphoNET online database (`http://www.phosphonet.ca/`; Safaei et al., 2011). Non-receptor tyrosine kinases (nRTKs) are emphasised in bold.

5.2.2 GluC digestion of FLAG-SLBP^{siRes} to capture RYKRKL containing peptide

To date, peptides containing Y95 or the wider RYKRKL motif have yet to be observed in any LC-MS/MS experiments shared in the Proteomics DB repository (Schmidt et al., 2018). This is due to the presence of arginine (R) and lysine (K) amino acids within the motif and the tendency to use the endopeptidase trypsin when generating peptides from complex protein solutions upstream of LC-MS/MS, which preferentially cleaves a protein's polypeptide backbone after arginine and lysine residues and would therefore give rise to cleavage products that are only one or two amino acids in length and too small to be accurately assigned to a specific protein when interrogating protein databases with obtained mass spectra (Olsen et al., 2004; Fricker, 2015; Swaney et al., 2010). Therefore, in an attempt to capture a peptide containing the RYKRKL motif, I utilised the endopeptidase GluC, which specifically cleaves the polypeptide backbone after glutamic acid (E) residues and is predicted to generate a 16 amino acid peptide with the RYKRKL motif intact ($^{92\text{-}}$MARYKRKLLINDFGRE$^{\text{-}107}$) according to the ExPASy Peptide Cutter online tool (Wilkins et al., 2005).

FLAG-SLBP^{siRes} was immunoprecipitated from 1 mg cell lysate using α-FLAG M2 affinity agarose gel as described in Section 2.2.6.5 and recovered proteins were reduced with 5 mM TCEP, alkylated with 20 mM MMS and digested with 100 ng GluC in 20 µL 1X Glu-C digestion buffer on S-Trap columns for 4 hours at 37°C as in Sections 2.2.7.1 and 2.2.7.2. Mass spectrometry analysis and interrogation of the UniProtKB/Swiss-Prot database using the SEQUEST search algorithm identified 3 out of 11 predicted GluC SLBP cleavage products (27.27%), though failed to capture the desired $^{92\text{-}}$MARYKRKLLINDFGRE$^{\text{-}107}$ peptide (Figure 5.6 and Table 5.2). The specificity of GluC is dependent on the pH and composition of the digestion buffer (Giansanti et al., 2016). At pH 4, the enzyme preferentially cleaves the polypeptide backbone at the C-terminus of glutamic acid (E) residues, whereas at pH 8 it additionally cleaves after aspartic acid (D). The five cleavage sites that give rise to the peptides identified here all occur after an E residue suggesting that the digestion conditions in this experiment were sufficient for optimal GluC specificity and that the poor recovery of GluC SLBP peptides in this experiment is likely due to the short 4 hour GluC digestion incubation time rather than the performance of the enzyme itself (Giansanti et al., 2016; Hansen et al., 2018). Unfortunately, time constraints prevented a thorough optimisation and further

attempts at determining the phosphorylation status of Y95 by LC-MS/MS. In spite of this, qPCR analysis of RYKRKL mutant cell lines presented in the remainder of this chapter provides a novel insight into the function of Y95, the wider RYKRKL motif and SLBP-dependent regulation of histone mRNA.

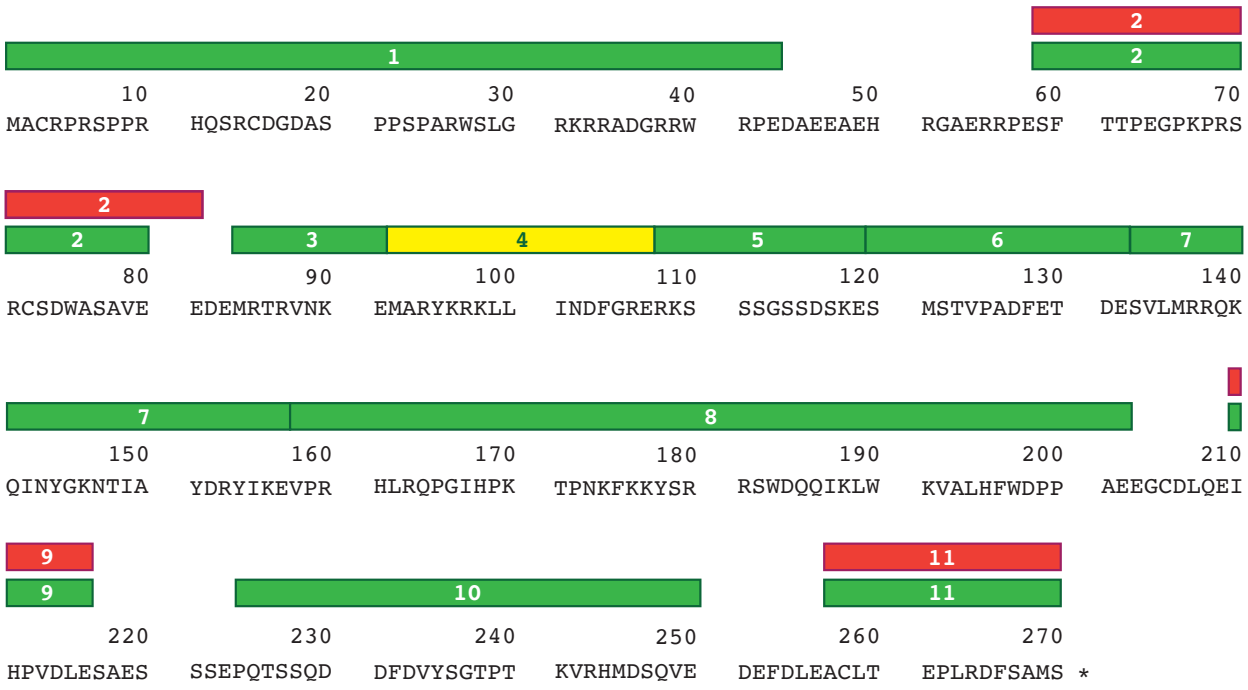

Figure 5.6: SLBP LC-MS/MS peptide coverage obtained after enzymatic digestion with GluC. Predicted SLBP peptides and those identified in LC-MS/MS analysis of FLAG-SLBP^{siRes} immunoprecipitates. Green and yellow peptides are those that are predicted to be generated following enzymatic digestion with GluC according to the ExPASy Peptide Cutter online tool; the 16 amino acid yellow peptide contains the RYKRKL motif and was the desired peptide in this experiment (Wilkins et al., 2005). In red are the 3 peptides identified by LC-MS/MS in this experiment after a 4-hour on-column digestion with 100 ng GluC in 20 µL 1X Glu-C digestion buffer.

Position		Peptide sequence	Charge	Mass-to-charge ratio *(m/z)*	Relative intensity
Start	End				
59	81	SFTTPEGPKPRSRCSDWASAVEE	+3	864.396	0.433
210	216	IHPVDLE	+2	410.714	0.393
257	270	ACLTEPLRDFSAMS	+2	798.364	1.000

Table 5.2: SLBP peptides identified in LC-MS/MS analysis following enzymatic digestion with GluC. Peptide sequence, mass-to-charge ratios and relative intensities of 3 SLBP-derived peptides identified in LC-MS/MS analysis of FLAG-SLBP^{siRes} immunoprecipitates digested with GluC for 4 hours.

5.2.3 Generation and characterisation of FLAG-SLBP^{Y95F} and FLAG-SLBP^{4A} Flp-In T-REx HeLa cell lines

In order to investigate the potential significance of Y95 phosphorylation, I performed site-directed mutagenesis using the pcDNA5/FRT/TO/FLAG-SLBP^{siRes} plasmid listed in Table 2.6 as a template and primers outlined in Section 2.1.3.1 to generate a non-phosphorylatable and RNAi-resistant FLAG-SLBP^{Y95F} mutant containing a phenylalanine (F) amino acid in place of the tyrosine at position 95. In addition, I performed site-directed mutagenesis to mutate the adjacent KRKL amino acids to alanines (A) in order to generate an RNAi-resistant version of the cyclinA/F-binding-impaired and G2-stabilised mutant reported previously (hereafter referred to as FLAG-SLBP^{4A}) for use as a positive control in later experiments (Zheng et al., 2003; Erkmann et al., 2005b; Dankert et al., 2016).

Doxycycline-induced expression of RNAi-resistant FLAG-SLBP^{Y95F} and FLAG-SLBP^{4A} was confirmed by Western blot (Figure 5.7). As the SLBP^{4A} mutant is stabilised and appears in excess after prolonged expression, the duration of doxycycline-induced expression in these experiments was restricted to 5 hours, in keeping with previous experiments described in Chapter 3 and Chapter 4, which confirmed that FLAG-SLBP^{Y95F} and FLAG-SLBP^{4A} protein levels were equal to FLAG-SLBP^{WT} and FLAG-SLBP^{siRes} at this time interval (Figure 5.7A). Expression of FLAG-SLBP^{Y95F} and FLAG-SLBP^{4A} protein at levels equal to FLAG-SLBP^{WT} and FLAG-SLBP^{siRes} in control cells following transfection with SLBP siRNA confirmed that the exogenous FLAG-SLBP^{Y95F} and FLAG-SLBP^{4A} genes in FLAG-SLBP^{Y95F} and FLAG-SLBP^{4A} cell lines are resistant to SLBP siRNA-mediated gene silencing (Figure 5.7B).

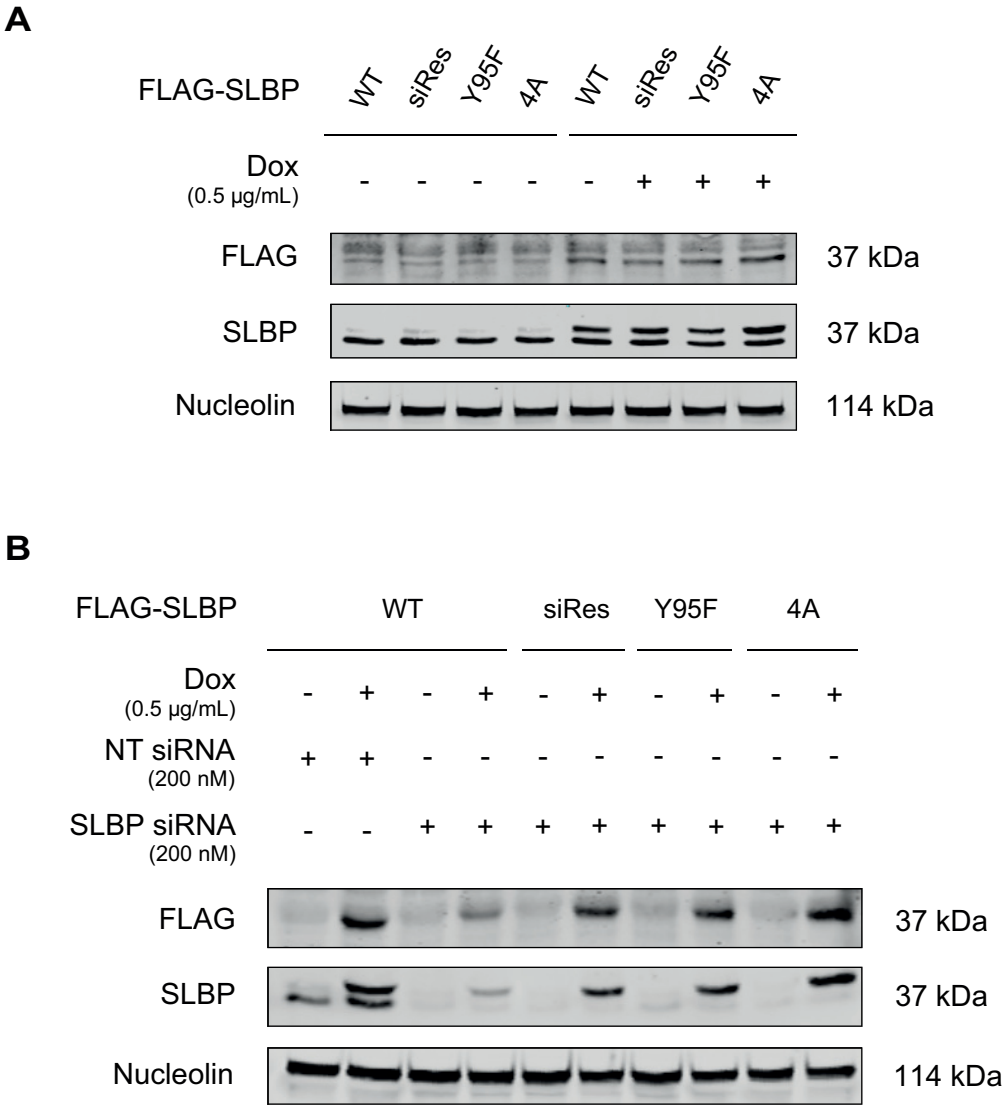

Figure 5.7: Validation of siRNA-resistant FLAG-SLBP^{Y95F} and FLAG-SLBP^{4A} Flp-In T-REx HeLa cell lines. (A) Asynchronous FLAG-SLBP Flp-In T-REx HeLa cells were cultured in media with or without 0.5 µg/mL doxycycline for 5 hours and cell lysates were analysed by Western blot using α-FLAG, α-SLBP and α-nucleolin antibodies. Nucleolin is used as a loading control. **(B)** Asynchronous FLAG-SLBP Flp-In T-REx HeLa cells were transfected with 200 nM non-targeting (NT) or SLBP siRNA for 24 hours, with 0.5 µg/mL doxycycline added to indicated cell populations for the final 5 hours, and cell lysates were analysed by Western blot using α-FLAG, α-SLBP and α-nucleolin antibodies. Nucleolin is used as a loading control.

5.2.3.1 Steady-state *HIST1H3B* mRNA levels and the rate of hydroxyurea-induced *HIST1H3B* mRNA decay are unchanged in FLAG-SLBP^{Y95F} and FLAG-SLBP^{4A} compared to FLAG-SLBP^{WT} after 5 hours of exposure to doxycycline

After generating and validating FLAG-SLBP^{Y95F} and FLAG-SLBP^{4A} cell lines, I then sought to determine what impact, if any, expression of FLAG-SLBP^{Y95F} and FLAG-SLBP^{4A} might have on histone mRNA transcript levels under both steady-state conditions and under conditions of hydroxyurea-induced replication stress. The rationale for the experiments presented in this section was based on the hypothesis that phosphorylation of Y95 may be a mechanism by which cells stabilise SLBP under conditions of replication stress, via the inhibition of cyclin A and cyclin F binding to the Cy motif in the RYKRKL sequence, following Pin1-mediated dissociation of SLBP from replication-dependent histone mRNAs. If this hypothesis is true, the rate of replication-dependent histone mRNA decay would likely be unperturbed in FLAG-SLBP^{Y95F} cells exposed to hydroxyurea, while FLAG-SLBP^{Y95F} protein levels would be reduced when compared to control cells.

Analysis of *HIST1H3B* mRNA levels in FLAG-SLBP^{Y95F} and FLAG-SLBP^{4A} cells following RNAi-mediated knockdown of endogenous SLBP and 5 hours of exposure to doxycycline revealed that expression of FLAG-SLBP^{Y95F} and FLAG-SLBP^{4A} was sufficient to rescue the SLBP siRNA-mediated downregulation of *HIST1H3B* mRNA (Figure 5.8A). This result indicates that neither Y95 nor the presence of the cyclin binding motif is required for replication-dependent histone gene transcription, as expected. I next measured the rate of hydroxyurea-induced *HIST1H3B* mRNA decay in FLAG-SLBP^{Y95F} and FLAG-SLBP^{4A} cells and showed that FLAG-SLBP^{Y95F} and FLAG-SLBP^{4A} expressing cells were able to perform histone mRNA decay with similar decay kinetics as FLAG-SLBP^{WT} and FLAG-SLBP^{siRes} cells (Figure 5.8B), confirming that neither Y95 nor the presence of the cyclin binding motif is required for replication-dependent histone mRNA decay. Unfortunately, time constraints prevented me from performing the crucial and relatively simple experiment to assay FLAG-SLBP^{Y95F} protein stability by Western blot following exposure to hydroxyurea and future work will be required to address this.

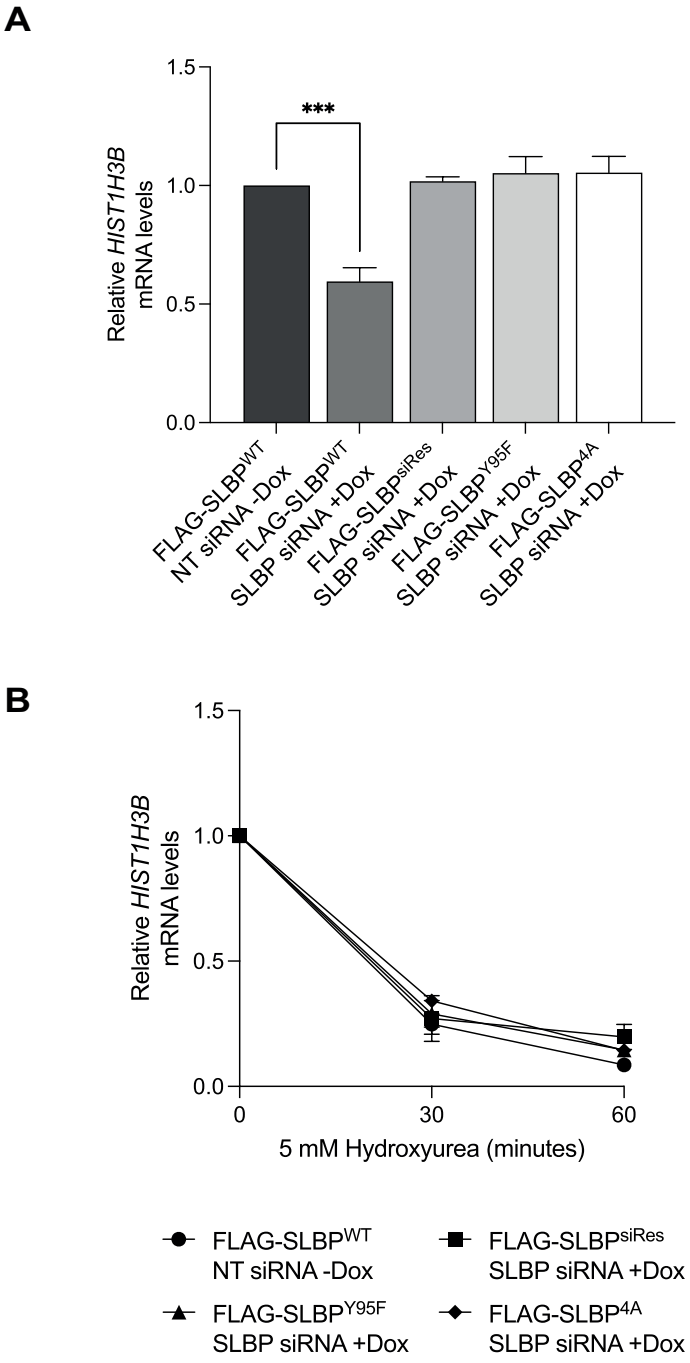

Figure 5.8: Expression of siRNA-resistant FLAG-SLBP^{Y95F} or FLAG-SLBP^{4A} does not affect the rescue of *HIST1H3B* mRNA transcript levels following siRNA-mediated SLBP knock-down, nor do they affect the rate of hydroxyurea-induced *HIST1H3B* mRNA decay. (A) Asynchronous FLAG-SLBP Flp-In T-REx HeLa cells were transfected with non-targeting (NT) or SLBP siRNA and incubated for 24 hours, with or without 0.5 μg/mL doxycycline for the final 5 hours. cDNA was generated from extracted total RNA and qPCR was performed using *HIST1H3B* primers. **(B)** Asynchronous FLAG-SLBP Flp-In T-REx HeLa cells were treated as in (A) after which 5 mM hydroxyurea was added for 30 and 60 minutes. cDNA was generated from extracted total RNA and qPCR was performed using *HIST1H3B* primers. qPCR samples were tested in triplicate and were quantified and normalised to *GAPDH* using the $2^{-\Delta\Delta C_T}$ method. *** = $p < .001$. Dunnett's one-way ANOVA. Data are mean ± S.E.M. n = 3 experiments.

5.2.3.2 Exposure to doxycycline for 24 hours leads to the presence of a stabilised and hyperphosphorylated FLAG-SLBP^{4A} protein that promotes the expression of *H2AFX* and *HIST1H3B* mRNA in G2

The experiments presented so far in this chapter suggest that SLBP Y95 is not implicated in the regulation of replication-dependent histone mRNA expression or the rate of histone mRNA decay, despite the fact that Y95 is predicted to be phosphorylated according to an *in silico* analysis using the NetPhos 3.1 server (Figure 5.1) (Blom et al., 1999). In light of these results, I directed attention towards further understanding the function of the RYKRKL motif in relation to the regulation of histone mRNA metabolism when SLBP is stabilised into G2.

Shortly before starting this project, Dankert et al. (2016) identified cyclin F as the E3 ubiquitin ligase that polyubiquitinates SLBP and marks the protein for degradation by the ubiquitin-proteasome system in G2. The authors showed that the Cy motif in the RYKRKL sequence is essential for cyclin F binding to SLBP as mutation of R97 and L99 to alanines abolished the interaction between cyclin F and SLBP. Expression of FLAG-SLBP$^{RL97/99AA}$ in G2 led to an increased association of *H2AFX* mRNA with polyribosomes, increased *H2AFX* mRNA translation and an increase in histone H2A.X being deposited into chromatin, which sensitises cells to genotoxic stress and results in sustained γH2A.X signalling and increased apoptosis when cells are exposed to the potent DNA-damaging agent neocarzinostatin. However, it was not clear if the observed increase in *H2AFX* mRNA translation was due to an increase in *H2AFX* gene transcription or increased translational efficiency. As it was previously demonstrated in this project that SLBP regulates the expression of *H2AFX* in addition to replication-dependent histone genes (Figure 3.12), I sought to determine whether prolonged expression of the stabilised FLAG-SLBP^{4A} mutant leads to increased expression of *H2AFX* and *HIST1H3B* genes as measured by qPCR.

I first replicated the findings in Zheng et al. (2003) and Erkmann et al. (2005b) showing that SLBP^{4A} is stabilised and hyperphosphorylated by culturing asynchronous FLAG-SLBP^{4A} cells in the presence of doxycycline for 24 hours and analysing cell lysates by Western blot, with FLAG-SLBP^{Y95F} analysed alongside for comparison (Figure 5.9A). Consistent with published observations, the prolonged expression of FLAG-SLBP^{4A} resulted in increased α-FLAG and α-SLBP band intensities, indicating increased FLAG-SLBP^{4A} protein abundance, and the emergence of an

additional band corresponding to the presence of hyperphosphorylated SLBP, which was absent in FLAG-SLBP^{WT} and FLAG-SLBP^{Y95F} cells (Figure 5.9A) (Zheng et al., 2003; Erkmann et al., 2005b). Quantification of the overall exogenous SLBP signal intensities (specifically the upper band(s) in the α-SLBP immunoblot) showed that there was a 10-fold increase in FLAG-SLBP^{4A} protein after culturing asynchronous cells in media with doxycycline for 24 hours (Figure 5.9B).

As there was such a marked increase in FLAG-SLBP^{4A} abundance in asynchronous cells after 24 hours of culture in media containing doxycycline, I generated cDNA from RNA that was extracted from asynchronous cells cultured under the same conditions and performed qPCR in order to measure and compare *H2AFX* and *HIST1H3B* mRNA transcript levels in FLAG-SLBP^{Y95F}, FLAG-SLBP^{4A} and control cells. qPCR analysis revealed a statistically significant 20% increase in both *H2AFX* (p = .014) and *HIST1H3B* (p = .001) mRNA transcript levels in FLAG-SLBP^{4A} cells, while mRNA transcript levels for both genes in FLAG-SLBP^{Y95F} cells remained comparable to the levels seen in control cells (Figure 5.9C and D). Dankert et al. (2016) demonstrated that when SLBP is stabilised into G2, the increased histone mRNA translation is specific to *H2AFX* as there was no increased association of replication-dependent *HIST1H3H* mRNA with polyribosomes. The data presented here suggest that the increased *H2AFX* mRNA translation in G2, as reported in Dankert et al. (2016), is driven by an increase in *H2AFX* gene expression that is attributed to the presence of stabilised FLAG-SLBP^{4A} in G2. Furthermore, the data presented here suggest that expression of FLAG-SLBP^{4A} also increases the expression of canonical histone genes though, as reported in Dankert et al. (2016), the mRNAs transcribed from canonical histone genes in G2 remain untranslated, presumably due to the necessary factors required for replication-dependent histone mRNA processing and translation being absent or inhibited outside of S phase.

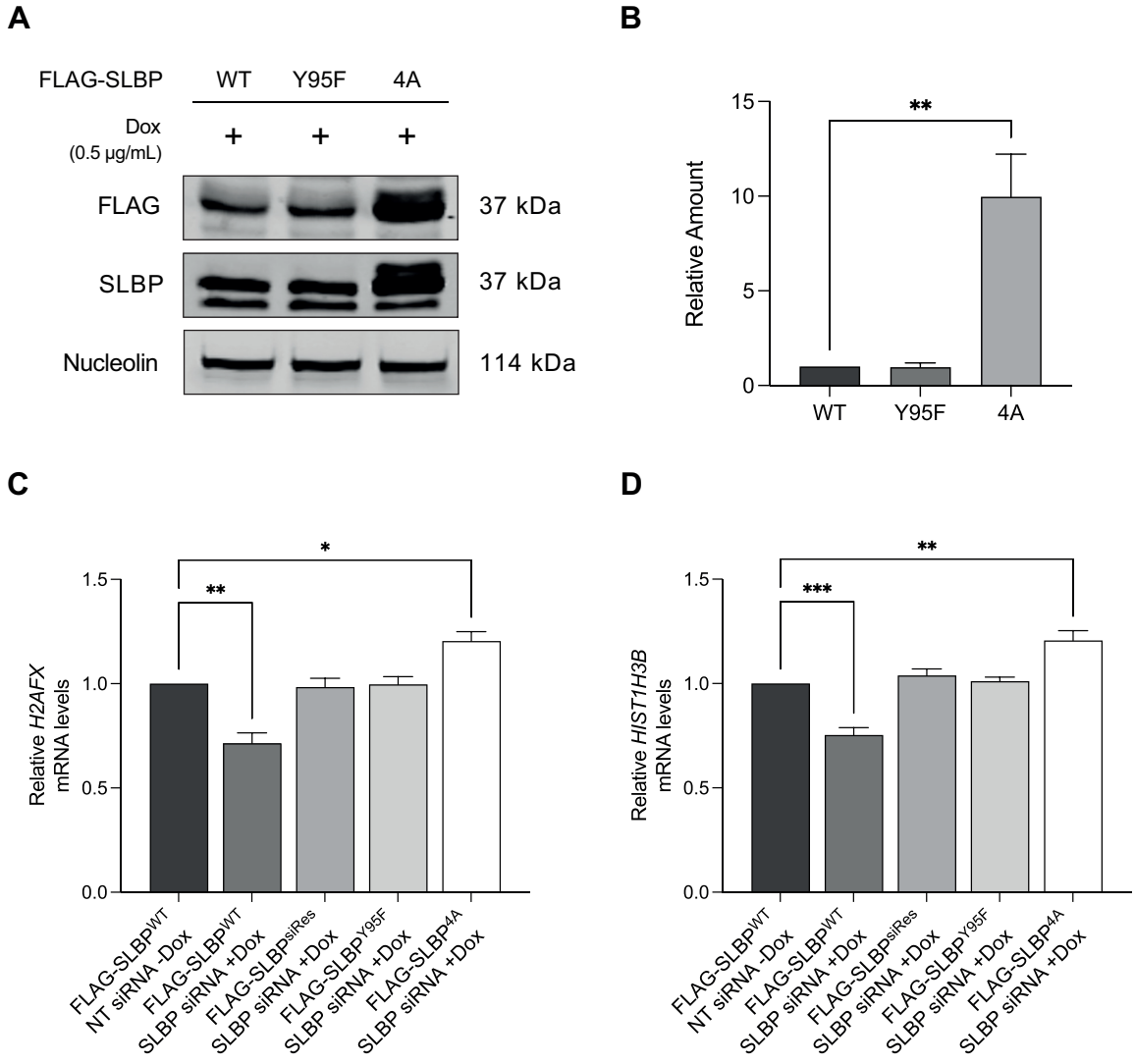

Figure 5.9: FLAG-SLBP^{4A} is stabilised after 24 hours of culture in media containing doxycycline and increases the mRNA transcript levels of both *H2AFX* and *HIST1H3B*. **(A)** Asynchronous FLAG-SLBP Flp-In T-REx HeLa cells were cultured in media containing 0.5 µg/mL doxycycline for 24 hours and cell lysates were analysed by Western blot using α-FLAG, α-SLBP and α-nucleolin antibodies. Nucleolin is used as a loading control. **(B)** Relative quantification of FLAG-SLBP bands in SLBP immunoblot (upper band) in (A). **(C)** Asynchronous FLAG-SLBP Flp-In T-REx HeLa cells were transfected with non-targeting (NT) or SLBP siRNA and incubated for 24 hours with or without 0.5 µg/mL doxycycline. cDNA was generated from extracted total RNA and qPCR was performed using *H2AFX* or **(D)** *HIST1H3B* primers. qPCR samples in (C) and (D) were tested in triplicate and were quantified and normalised to *GAPDH* using the $2^{-\Delta\Delta C_T}$ method. * = $p < .05$, ** = $p < .01$, *** = $p < .001$. Dunnett's one-way ANOVA. Data in are mean $\pm$ S.E.M. n = 3 or 4 experiments.

5.2.3.3 Analysis of hyperphosphorylated FLAG-SLBP^{4A} reveals a functional link between the RYKRKL motif and S23 that regulates *HIST1H3B* and *H2AFX* gene transcription

Degradation of SLBP at the end of S phase is a multistep process that requires the dissociation of SLBP from histone mRNA, phosphorylation of T61 by CKII, binding of cyclin A/CDK1 to the Cy motif within the RYKRKL sequence and the subsequent phosphorylation of T62 by CDK1 (Zheng et al., 2003; Krishnan et al., 2012). SLBP that is phosphorylated on T61 and T62 then serves as a substrate for cyclin F, which also binds via the Cy motif and is the E3 ubiquitin ligase that polyubiquitinates SLBP and marks the protein for degradation by the ubiquitin-proteasome system in G2 (Dankert et al., 2016). Interestingly, the stabilised FLAG-SLBP^{4A} protein, in which the KRKL amino acids are mutated to alanines, appears to be hyperphosphorylated as evidenced by the presence of additional SLBP bands that migrate more slowly through SDS-PAGE gels when FLAG-SLBP^{4A} cell lysates are analysed by Western blot (Figure 5.9A) (Zheng et al., 2003; Erkmann et al., 2005b). Hyperphosphorylated FLAG-SLBP^{4A} is almost certainly phosphorylated on T61, as phosphorylation of T61 by CKII at the end of S phase is independent of cyclin A binding (Zheng et al., 2003), and is likely to be phosphorylated on multiple other residues in addition to T61. Given the predicted phosphorylation potential of Y95, it is possible that Y95 is one of the residues that is phosphorylated in the stabilised FLAG-SLBP^{4A} protein.

To investigate whether Y95 might be one of the residues contributing to the emergence of hyperphosphorylated SLBP in FLAG-SLBP^{4A} cells, I first returned to the NetPhos 3.1 server to determine the predicted phosphorylation potential of Y95 when the KRKL amino acids in the RYKRKL sequence are mutated to alanines. Interestingly, the analysis showed that the phosphorylation potential of Y95 rose from 0.715 to 0.856 in SLBP^{4A}, adding weight to the notion that Y95 may be phosphorylated in FLAG-SLBP^{4A} cells exposed to doxycycline for 24 hours (Figure 5.10). To investigate further, I performed site-directed mutagenesis using the pcDNA5/FRT/TO/FLAG-SLBP^{4A} plasmid as a template and primers outlined in Section 2.1.3.1 to generate a new FLAG-SLBP$^{Y95F/4A}$ mutant to be used in a repeat of the experiment shown in Figure 5.9A. If Y95 is one of the residues that is phosphorylated in FLAG-SLBP^{4A} cells after prolonged expression of FLAG-SLBP^{4A}, then the signal intensity of the additional band seen in Figure 5.9A would appear to be reduced when repeating the experiment with lysates from FLAG-SLBP$^{Y95F/4A}$ cells. Despite

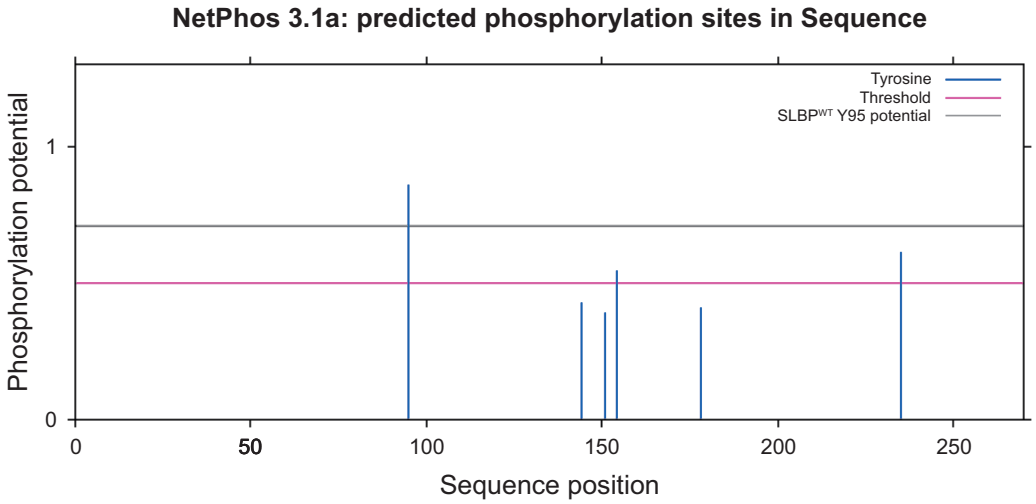

Figure 5.10: SLBP^{4A} tyrosine phosphorylation potentials. Phosphorylation potential of tyrosines in SLBP^{4A} as predicted by the NetPhos 3.1 Server (`http://www.cbs.dtu.dk/services/NetPhos/`; Blom et al., 1999). Blue lines represent the predicted phosphorylation potential of tyrosine residues within SLBP^{4A} on a scale from 0 to 1 (Y-axis). The pink line indicates the 0.5 threshold assigned to the neural network to call a predicted positive tyrosine phosphorylation site. The grey line represents the predicted phosphorylation potential of Y95 in SLBP^{WT} (0.715). Predicted SLBP^{4A} Y95 phosphorylation potential = 0.856.

the data reported in Chapter 4 that suggest neither S20 nor S23 is involved in regulating SLBP or histone mRNA stability, I additionally performed site-directed mutagenesis to generate FLAG-SLBP$^{S20A/4A}$ and FLAG-SLBP$^{S23A/4A}$ cell lines to test alongside FLAG-SLBP$^{Y95F/4A}$.

Asynchronous cells were cultured as before in media containing doxycycline for 24 hours before lysates were harvested and analysed by Western blot. As in Figure 5.9A, prolonged exposure to doxycycline resulted in the presence of stabilised and phosphorylated FLAG-SLBP^{4A} (Figure 5.11, compare lanes 1 and 3). Surprisingly, the observed band intensity for FLAG-SLBP^{Y95F} appeared to be lower than that seen in FLAG-SLBP^{WT} (compare lanes 1 and 2). As the FLAG-SLBP^{Y95F} signal after 24 hours of exposure to doxycycline was quantified after three repeats in Figure 5.9A and statistical analysis showed no significant difference between FLAG-SLBP^{WT} and FLAG-SLBP^{Y95F}, the reduced FLAG-SLBP^{Y95F} signal in this experiment is most likely due to a pipetting error when adding doxycycline to FLAG-SLBP^{Y95F} cells. Analysis of FLAG-SLBP$^{Y95F/4A}$ cells showed that FLAG-SLBP$^{Y95F/4A}$ protein abundance was increased to the same extent as FLAG-SLBP^{4A} after 24 hours of exposure to doxycycline and the intensity of the hyperphosphorylated FLAG-SLBP$^{Y95F/4A}$

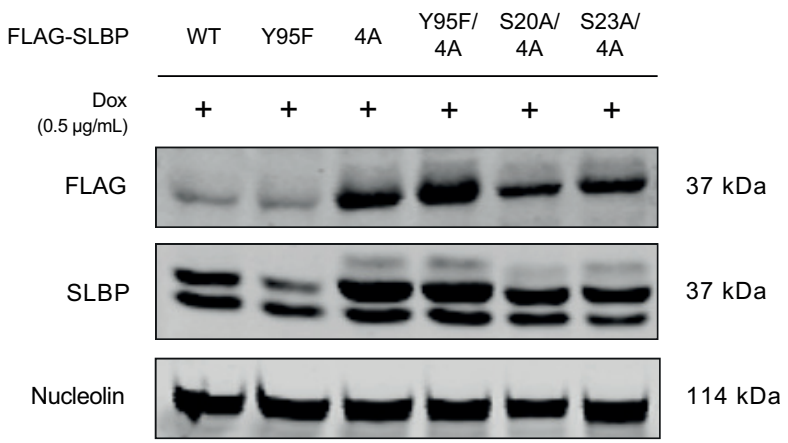

Figure 5.11: Western blot analysis of FLAG-SLBP protein levels in FLAG-SLBP^{Y95F}, FLAG-SLBP$^{S20A/4A}$ and FLAG-SLBP$^{S23A/4A}$ cells cultured for 24 hours in doxycycline containing media. Asynchronous FLAG-SLBP Flp-In T-REx HeLa cells were cultured in media containing 0.5 µg/mL doxycycline for 24 hours and cell lysates were analysed by Western blot using α-FLAG, α-SLBP and α-nucleolin antibodies. Nucleolin is used as a loading control. The low signal for FLAG-SLBP^{Y95F} in lane 2 of the α-SLBP immunoblot (top band) is likely due to a pipetting error when adding doxycycline to FLAG-SLBP^{Y95F} cells. n = 1.

band (top band in the α-SLBP immunoblot) was comparable to that seen in FLAG-SLBP^{4A}, indicating that Y95 is not one of the residues targeted for phosphorylation in FLAG-SLBP^{4A} under these conditions (compare lanes 3 and 4). Interestingly, in FLAG-SLBP$^{S20A/4A}$ and FLAG-SLBP$^{S23A/4A}$, the band intensities for FLAG-SLBP (middle bands in the α-SLBP immunoblot) and FLAG appeared to be reduced compared to FLAG-SLBP^{4A} and FLAG-SLBP$^{Y95F/4A}$ (Figure 5.11, compare lanes 5 and 6 with 3 and 4). Whilst this experiment was conducted only once and therefore lacks a statistical analysis, the result was intriguing as it suggests that the increased stability of FLAG-SLBP^{4A} and FLAG-SLBP$^{Y95F/4A}$ is, at least in part, dependent on S20 and S23, which appears to contradict reports in the literature that phosphorylation of S20 and/or S23 acts as a phosphodegron promoting SLBP degradation at the end of S phase (Krishnan et al., 2012; Djakbarova et al., 2014; Thapar, 2015).

Given the increase in *HIST1H3B* and *H2AFX* mRNA transcript levels observed in cells expressing stabilised FLAG-SLBP^{4A}, I repeated the experiment in Figure 5.9C and D with FLAG-SLBP$^{Y95/4A}$, FLAG-SLBP$^{S20A/4A}$ and FLAG-SLBP$^{S23A/4A}$ cells with the expectation that *HIST1H3B*

and *H2AFX* mRNA transcript levels would likely appear reduced in FLAG-SLBP$^{S20A/4A}$ and FLAG-SLBP$^{S23A/4A}$ cells compared to FLAG-SLBP^{4A} and would appear similar to levels in control cells. Instead, the qPCR analysis showed that *HIST1H3B* and *H2AFX* mRNA transcript levels in FLAG-SLBP$^{S20A/4A}$ and FLAG-SLBP$^{Y95F/4A}$ cells were reduced to FLAG-SLBP^{WT} levels, and that, surprisingly, FLAG-SLBP$^{S23A/4A}$ cells failed to rescue SLBP siRNA-dependent downregulation of *HIST1H3B* and *H2AFX* mRNA (Figure 5.12).

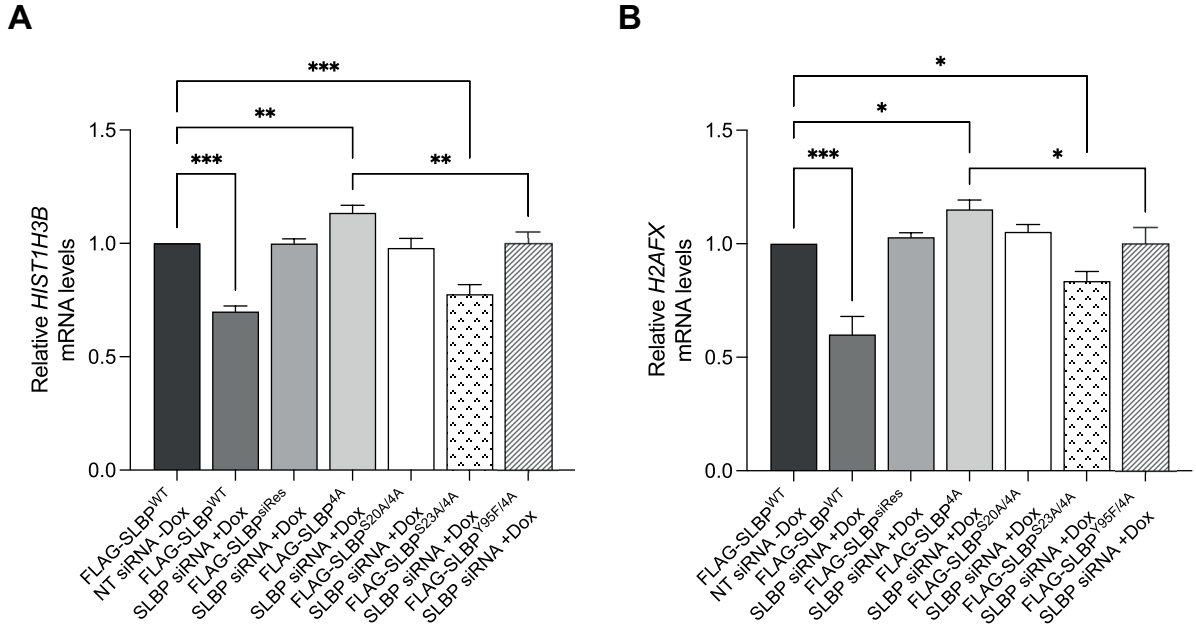

Figure 5.12: *HIST1H3B* and *H2AFX* mRNA transcript levels in FLAG-SLBP$^{S20A/4A}$, FLAG-SLBP$^{S23A/4A}$ and FLAG-SLBP$^{Y95F/4A}$ Flp-In T-REx HeLa cells cultured for 24 hours in doxycycline containing media. Asynchronous FLAG-SLBP Flp-In T-REx HeLa cells were transfected with non-targeting (NT) or SLBP siRNA and incubated for 24 hours with or without 0.5 μg/mL doxycycline. cDNA was generated from extracted total RNA and qPCR was performed using **(A)** *HIST1H3B* or **(B)** *H2AFX* primers. qPCR samples were tested in triplicate and were quantified and normalised to *GAPDH* using the $2^{-\Delta\Delta C_T}$ method. * = $p < .05$, ** = $p < .01$, *** = $p < .001$. Dunnett's one-way ANOVA. Data are mean ± S.E.M. n = 4 or 5 experiments.

The data presented in Figure 5.11 and Figure 5.12 appear to suggest that S20 and S23 both contribute to the increase in SLBP stability when cyclins A and F are unable to bind to FLAG-SLBP^{4A} to promote its degradation at the end of S phase and that the observed increase in *HIST1H3B* and *H2AFX* mRNA transcript levels in cells expressing stabilised FLAG-SLBP^{4A} is dependent on both S20 and Y95. Furthermore, these data, along with those from Chapter 4 showing that the non-phosphorylatable FLAG-SLBP^{S23A} mutant is able to rescue SLBP siRNA-mediated histone mRNA downregulation, indicate that SLBP-dependent regulation of histone gene transcription involves both S23 and the RYKRKL motif.

5.2.4 AlphaFold analysis suggests an intramolecular hydrogen bond links Y95 and N173 in the TPNK motif to facilitate SLBP domain tethering

Data presented in Figure 5.12 show that expression of stabilised FLAG-SLBP^{4A} (^{94}-RYAAAA-^{99}) results in an increase in histone mRNA transcript levels but the expression of stable FLAG-SLBP$^{Y95F/4A}$ (^{94}-RFAAAA-^{99}) does not. The signal intensities of the hyperphosphorylated FLAG-SLBP^{4A} and FLAG-SLBP$^{Y95F/4A}$ bands in Figure 5.11 appear equal, which indicates the absence of a negatively charged phosphate group on Y95 in FLAG-SLBP^{4A} and suggests that the increased histone mRNA transcript levels in FLAG-SLBP^{4A} cells are likely due to a structural function of Y95. As such, I queried AlphaFold to obtain the predicted *in vivo* 3D structure of SLBP in order to locate Y95 and the wider RYKRKL motif (Figure 5.13) (Jumper et al., 2021).

According to the predicted 3D structure, the RYKRKL motif forms part of the C-terminal end of an α-helix that appears to be in close proximity to the TPNK motif and RNA binding domain (RBD) (Figure 5.13A). Closer inspection of this region in the 3D structure revealed the presence of a hydrogen bond linking the Y95 side chain with N173 in the TPNK motif (Figure 5.13B). It appears that this hydrogen bond is the only intramolecular interaction linking the α-helix that contains the RYKRKL motif with the TPNK motif and the RBDs and serves to tether these regions of the protein. Therefore, it is possible that the increased histone mRNA levels observed in stabilised FLAG-SLBP^{4A} cells are in part due to FLAG-SLBP^{4A} existing in a tethered configuration at a time when the protein would otherwise be degraded by cyclins A and F.

Given that dissociation of SLBP and histone mRNA requires dephosphorylation of T171 by PP2A and Pin1-mediated prolyl isomerisation of P172, it seems plausible that isomerisation of P172 might provide sufficient energy to break the hydrogen bond linking Y95 and N173 and might therefore act as a molecular switch to change SLBP from an RYKRKL-TPNK-RBD tethered-to-untethered configuration as part of the process to dissociate SLBP from histone mRNA. It is also plausible that tethering the RYKRKL and TPNK motifs may serve to sequester the TPNK motif and make it inaccessible to PP2A and PIN1. While the precise nature of the structural function of Y95 remains to be elucidated, it is becoming increasingly clear that the wider RYKRKL motif is a multifunctional SLiM that is crucial for the proper regulation of SLBP function and histone mRNA metabolism.

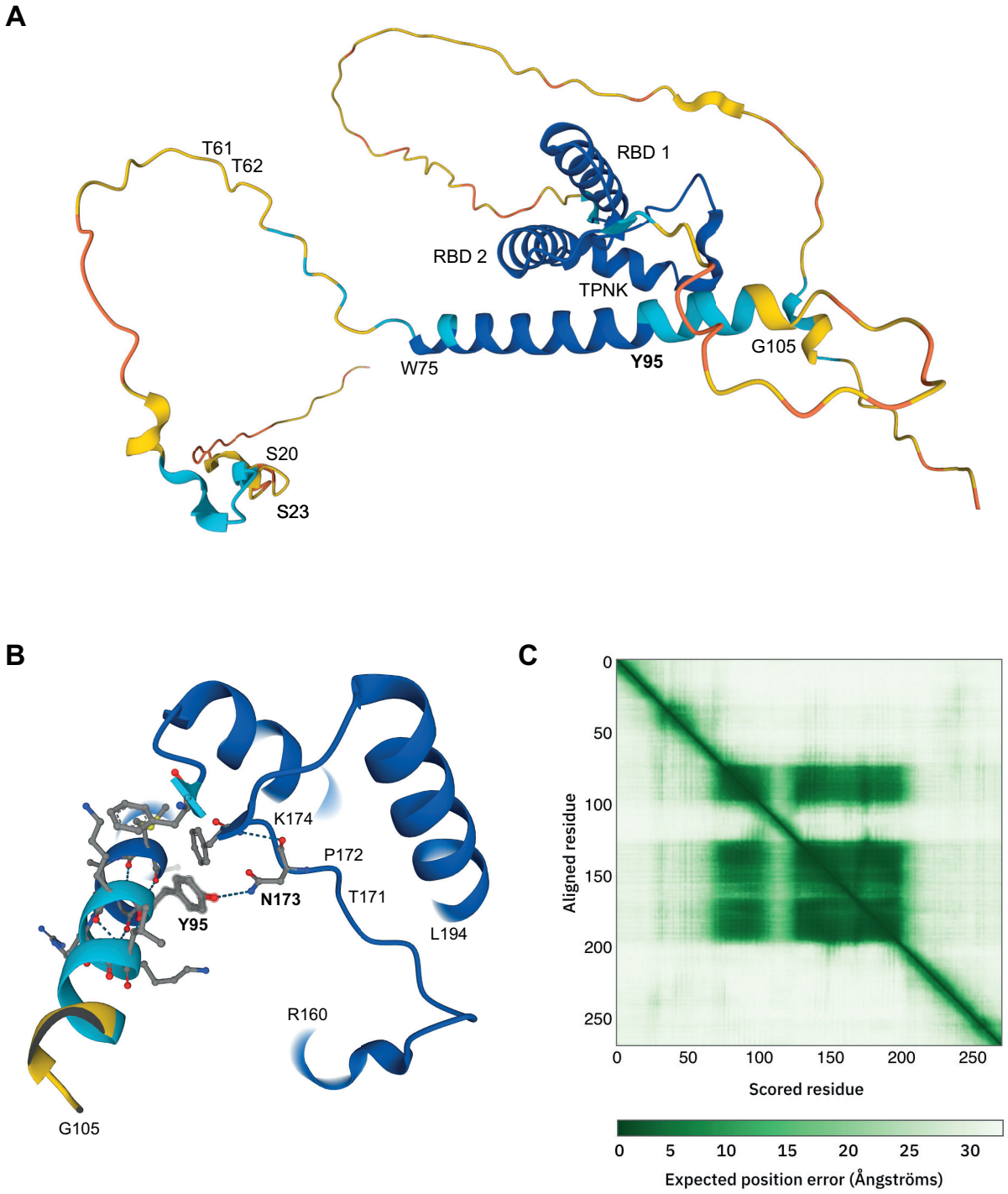

Figure 5.13: AlphaFold analysis indicates that Y95 and N173 in the TPNK motif interact via hydrogen bonding. AlphaFold structural prediction of **(A)** full-length SLBP and **(B)** a region of SLBP showing the RYKRKL-TPNK-RBD interaction, with **(C)** the AlphaFold predicted aligned error. The full-length folded structure shows an N-terminal disordered region containing phosphosites S20, S23, T61, T62 and a central alpha-helix containing the RYKRKL motif that is positioned in close proximity to RBD1, RBD2 and the TPNK motif (A). The four domains appear to be tethered via a hydrogen bond that links Y95 with N173 in the TPNK motif (B). The formation or breakage of this hydrogen bond is presumably sensitive to the phosphorylation status of T171 and Pin1-mediated P172 prolyl-isomerisation suggesting that the RYRKRKL and RBD domains switch between a tethered and untethered conformation whenever SLBP and histone mRNAs associate or dissociate. (`https://alphafold.ebi.ac.uk/`; Jumper et al., 2021)

5.2.5 Other RYKRKL containing proteins

The data presented in this chapter are consistent with previous reports in the literature showing that elements of the RYKRKL motif are crucial for SLBP degradation and provide new evidence revealing a link between the RYKRKL motif, the phosphorylation status of S23 in the N-terminus of SLBP and the regulation of histone gene transcription (Zheng et al., 2003; Erkmann et al., 2005b; Dankert et al., 2016). As mentioned previously, the functional SLBP RYKRKL motif is evolutionarily conserved among vertebrates, suggesting that the presence of the RYKRKL motif in SLBP may provide a selective advantage in vertebrate species. Short linear motifs (SLiMs) act as binding sites for interacting partners and are often present in multiple proteins, allowing a single protein to bind to multiple targets that may or may not be functionally related (Van Roey et al., 2014). As such, I performed an *in silico* analysis using the SLiMSearch4 online tool to identify additional human proteins that contain the RYKRKL motif which is present and functional in SLBP (Figure 5.14; Krystkowiak and Davey, 2017).

Surprisingly, RNF20 and RNF40 are the only other human proteins that contain the complete RYKRKL motif. RNF20 and RNF40 are the two subunits of the E3 ubiquitin ligase BRE1, which together with the E2 ubiquitin ligase UBE2A, monoubiquitinate histone H2B on lysine 120 to form H2BK120ub1 (Kim et al., 2005). H2BK120ub1 is a crucial histone modification promoting transcriptional elongation at a subset of highly expressed RNA Polymerase II-transcribed genes in-

SLiMSearch4

Protein Name	Peptide	Length	Start	End	Metazoa	QFO	Disorder score
Histone RNA hairpin-binding protein (SLBP)	nkemaRYKRKLlindf	6	94	99	0.315	0.186	0.387
E3 ubiquitin-protein ligase BRE1A (RNF20)	kgevlRYKRKLreaqs	6	496	501	0.129	0.088	0.464
E3 ubiquitin-protein ligase BRE1B (RNF40)	kgdaqRYKRKLrevqa	6	503	508	0.036	0.009	0.554

Figure 5.14: Other RYKRKL motif-containing proteins identified using the SLiMSearch4 online tool. Other human proteins that contain the RYKRKL SLiM identified using the SLiMSearch4 online tool. (`http://slim.icr.ac.uk/slimsearch/`; Krystkowiak and Davey, 2017)

volved in the regulation of cell cycle progression, DNA replication and the DNA damage response, including early cyclins that drive the G1/S phase transition, p53, and interestingly, the replication-dependent histones H2A and H2B (Shema et al., 2008; Chernikova et al., 2012). In addition to its role in RNA Polymerase II transcriptional elongation, BRE1 is recruited to replication origins by the ssDNA binding factor RPA and is present on active replication forks where H2BK120ub1 promotes replication fork progression and the assembly and stability of nucleosomes in newly replicated DNA (Trujillo and Osley, 2012; Liu et al., 2021).

Monoubiquitination of H2B by BRE1 during transcription is regulated by CDK9, a constitutively expressed cyclin-dependent kinase that, together with cyclin T or K, constitutes the catalytic and regulatory subunits of the positive transcription elongation factor complex, P-TEFb (Garriga et al., 2003; Anshabo et al., 2021). CDK9 phosphorylates RNA Polymerase II on serine 2 and UBE2A on serine 120 in order to promote the recruitment of BRE1 and the subsequent monoubiquitination of histone H2B (Shchebet et al., 2012). Given the well-recognised role P-TEFb plays in multiple pathological processes, including cancer, cardiovascular diseases, and viral replication, CDK9 is an attractive therapeutic target and a number of small molecule inhibitors targeting CDK9 have entered clinical trials (Johnsen, 2012; Franco et al., 2018; Anshabo et al., 2021). However, many of the small molecule inhibitors developed to date against CDK9 target the highly conserved ATP-binding site and, as such, tend to target multiple CDKs and/or proteins kinases, leading to considerable off-target effects (Anshabo et al., 2021). The presence of the RYKRKL motif in both RNF20 and RNF40 (BRE1) raises the distinct possibility that P-TEFb might interact with SLBP and BRE1 via the Cy motif and one or more S/T-P motifs, of which there are a total of five in RNF20/40, in order to regulate H2BK120ub1 levels and histone gene transcription. Therefore, it is possible that inhibition of cyclin/CDK binding to BRE1 and/or SLBP via the RYKRKL motif and an associated S/T-P motif may prove to be a more favourable therapeutic strategy compared to the use of CDK9 kinase inhibitors. Surprisingly, an *in silico* prediction of synthetic lethality revealed a positive synthetic lethal association between RNF20 and PARP1, and both RNF20 and RNF40 with HRAS, KRAS and NRAS proteins (Figure 5.15) (Wang et al., 2022). If this is correct, then targeted pharmacological inhibition of cyclin/CDK binding to BRE1 in tumour cells, in combination with systemic PARP and/or RAS inhibition, may provide therapeutic benefit in the clinic.

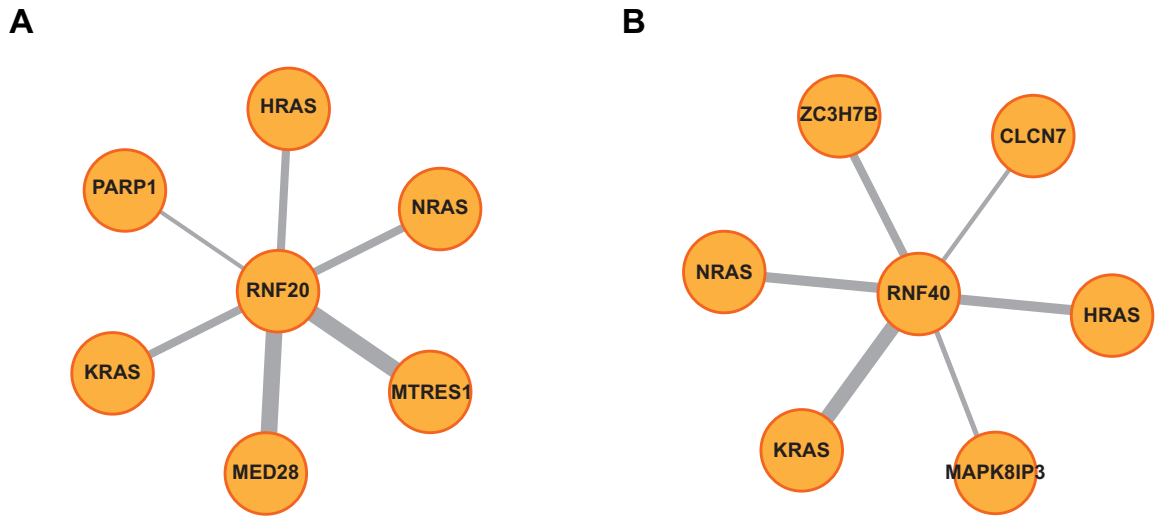

Figure 5.15: SynLethDB analysis predicts a synthetic lethal association between RNF20 and PARP1, and RNF20/40 and RAS. Genes identified using the SynLethDB database that are predicted to be synthetically lethal with loss of **(A)** RNF20 and **(B)** RNF40. The thickness of the grey connecting lines represents the strength of the SynLethDB statistical score assigned to a predicted synthetic lethal relationship (`http://synlethdb.sist.shanghaitech.edu.cn/`; Wang et al., 2022).

Interestingly, data reported in Pirngruber et al. (2009a,b) showing an increase in polyadenylated *HIST1H2AC* and *HIST1H2BD* mRNA in CDK9 and RNF20/40 knockdown cells provides evidence of a connection between P-TEFb-UBE2A-BRE1-H2BK120ub1 signalling and the regulation of replication-dependent histone mRNA 3'-UTR processing by the SLBP-U7 snRNP complex. However, although the activity of P-TEFb and H2BK120ub1 has previously been linked to the transcription and processing of replication-dependent histone mRNAs, the molecular mechanisms that link P-TEFb, H2BK120ub1 and SLBP activity remain unknown. Although by no means conclusive, the data presented in this chapter suggest that the RYKRKL SLiM evolved as a docking site for P-TEFb, cyclin A/CDK1 and cyclin F on RNF20, RNF40 and SLBP, which may have established a system of regulation that coordinates cell cycle progression, histone gene transcription, histone mRNA 3'UTR processing and histone mRNA translation in vertebrate species.

5.3 Discussion

Y95 in human SLBP is a centrally located tyrosine residue that is predicted to be phosphorylated according to *in silico* analyses of its phosphorylation potential and of the local amino acid sequence around the residue. An *in silico* prediction of the kinase(s) that might phosphorylate Y95 identified ALK and FAK among the top predicted kinases. Given that Y95 is located immediately adjacent to amino acids ^{96}-KRKL-^{99}, which form a known NLS that contributes towards the nuclear-cytoplasmic trafficking of SLBP (Erkmann et al., 2005b), and contains a known cyclin A and cyclin F binding site that is important for the regulation of SLBP degradation at the end of S phase and in G2 (Koseoglu et al., 2008; Dankert et al., 2016), a hypothesis was developed whereby phosphorylation of Y95, by ALK, FAK or other kinases, might affect one or both of these processes under certain conditions. Further evidence from an analysis of the evolutionary history of SLBP revealed that the amino acids RYKRKL are evolutionarily conserved in mammals and that the tyrosine residue and the overall pattern of charge across the six amino acid motif are conserved in vertebrates. Therefore, it appeared that RYKRKL may constitute a multifunctional short linear motif (SLiM) whose activity may be regulated by reversible phosphorylation.

As such, my aim in this chapter was to investigate the phosphorylation status of Y95 and determine whether there may be additional unexplored functions of the RYKRKL motif in SLBP. Although I was unable to identify a peptide containing the Y95 residue by LC-MS/MS, additional experiments suggested that Y95 is not post-translationally modified by phosphorylation, at least under the conditions tested here. However, Y95 was shown to have a structural function that contributes towards the normal function of SLBP. Moreover, it was demonstrated for the first time that the RYKRKL motif, in conjunction with S23, likely acts as a binding site for a currently unidentified cyclin/CDK complex that is essential for the initiation of histone gene transcription in S phase. Furthermore, an analysis of the amino acid sequences of all human proteins revealed that only two other proteins contain an RYKRKL motif, RNF20 and RNF40, which are subunits of an E3 ubiquitin ligase (BRE1) that is functionally related to SLBP.

5.3.1 Prolonged expression of FLAG-SLBP^{4A} results in the stabilisation of FLAG-SLBP^{4A} past S phase and aberrant transcription of *HIST1H3B* and *H2AFX* in G2

In order to investigate the phosphorylation status and function of Y95, site-directed mutagenesis was undertaken to incorporate a non-phosphorylatable tyrosine-to-phenylalanine substitution at position 95 (Y95F) in FLAG-SLBP Flp-In T-REx HeLa cells. In addition, a cell line in which the $^{96\text{-}}$KRKL$^{\text{-}99}$ amino acids were substituted with alanines (FLAG-SLBP^{4A}), which has previously been shown to be defective for cyclin A and cyclin F binding, was generated to serve as a positive control (Koseoglu et al., 2008; Dankert et al., 2016). Western blot analysis showed that after 5 hours of doxycycline-induced gene expression, the protein levels of FLAG-SLBP^{Y95F} and FLAG-SLBP^{4A} appeared equal to that seen in control FLAG-SLBP^{WT} cells but that after 24 hours, the abundance of FLAG-SLBP^{4A} protein was 10-fold higher than both FLAG-SLBP^{WT} and FLAG-SLBP^{Y95F}, which is consistent with previous reports regarding the stability of SLBP when cyclin A or cyclin F binding is impaired (Koseoglu et al., 2008; Dankert et al., 2016).

qPCR analysis showed that *HIST1H3B* mRNA transcript levels were equal in FLAG-SLBP^{WT}, FLAG-SLBP^{Y95F} and FLAG-SLBP^{4A} cells after 5 hours of exposure to doxycycline and that both FLAG-SLBP^{Y95F} and FLAG-SLBP^{4A} cell lines were able to initiate histone mRNA decay in response to hydroxyurea. Dankert et al. (2016) reported that stabilisation of FLAG-SLBP^{4A} past the end of S phase and into G2 resulted in increased translation of *H2AFX* mRNA, leading to increased deposition of the variant histone H2A.X into chromatin in G2, which sensitises cells to DNA damage and results in increased apoptosis upon genotoxic stress. As it was shown in Dankert et al. (2016) that histone mRNA decay at the end of S phase proceeds unperturbed in FLAG-SLBP^{4A} cells, it follows that the observed increase in *H2AFX* mRNA translation in G2 is either due to increased translational efficiency of basal G2 *H2AFX* mRNA or is due an increase in *H2AFX* gene expression. Given the results in Chapter 3 showing that SLBP directly regulates *HIST1H3B* and *H2AFX* gene expression, I repeated the qPCR analysis using material from cells that had been cultured in doxycycline-media for 24 hours in order to assess whether histone mRNA levels were increased in cells with stabilised FLAG-SLBP^{4A}. Under these conditions, the levels of both *HIST1H3B* and *H2AFX* mRNA increased by $\sim$20% in FLAG-SLBP^{4A} cells compared to FLAG-SLBP^{WT} and FLAG-SLBP^{Y95F}, suggesting that stabilised FLAG-SLBP^{4A} promotes the aberrant

expression of *HIST1H3B* and *H2AFX* genes in G2. It is important to note that these experiments were conducted with asynchronous cells and therefore the increased histone mRNA levels observed here in FLAG-SLBP^{4A} cells include histone mRNA that is normally present in S phase. Further qPCR analysis using synchronised cells would provide a more accurate insight into the dynamics of aberrant histone gene transcription in FLAG-SLBP^{4A} cells.

5.3.2 Stabilised and hyperphosphorylated FLAG-SLBP^{4A} is not phosphorylated on Y95

Consistent with previous reports, the stabilised FLAG-SLBP^{4A} protein appears as multiple bands when analysed by Western blot (Zheng et al., 2003; Erkmann et al., 2005b), which is indicative of hyperphosphorylation as the negatively charged phosphate groups result in a protein that migrates more slowly through an SDS-PAGE gel. Due to the *in silico* analyses predicting that Y95 is phosphorylated and that the phosphorylation potential for Y95 is increased in FLAG-SLBP^{4A}, it was hypothesised that Y95 may be one of the residues that are phosphorylated when FLAG-SLBP^{4A} is stabilised. Therefore, site-directed mutagenesis was conducted to generate a FLAG-SLBP$^{Y95F/4A}$ mutant in order to compare signal intensities of hyperphosphorylated SLBP in FLAG-SLBP^{4A} and FLAG-SLBP$^{Y95F/4A}$ cells that had been cultured in doxycycline-media for 24 hours. Surprisingly, signal intensities of hyperphosphorylated SLBP were identical in FLAG-SLBP^{4A} and FLAG-SLBP$^{Y95F/4A}$ cells, indicating that Y95 is not phosphorylated in stabilised FLAG-SLBP^{4A}.

5.3.3 Phosphorylation of both S20 and S23 contribute towards the stability of FLAG-SLBP^{4A} after prolonged FLAG-SLBP^{4A} expression

As the original aim of this project concerned S20 and S23 in the N-terminus of SLBP and as there are multiple lines of evidence showing that S20 and S23 are phosphorylated during S phase, site-directed mutagenesis was conducted to generate non-phosphorylatable S20 and S23 cell lines that contained the 4A mutation in the RYKRKL motif in addition to FLAG-SLBP$^{Y95F/4A}$. Surprisingly, Western blot analysis of FLAG-SLBP protein levels after prolonged doxycycline-induced expression showed that both FLAG-SLBP$^{S20A/4A}$ and FLAG-SLBP$^{S23A/4A}$ appeared to be stabilised though

not to the same extent as FLAG-SLBP^{4A} or FLAG-SLBP$^{Y95F/4A}$. Additionally, the hyperphosphorylated band that was present in FLAG-SLBP$^{S20A/4A}$ and FLAG-SLBP$^{S23A/4A}$ appeared fainter than that observed in FLAG-SLBP^{4A} or FLAG-SLBP$^{Y95F/4A}$ cells. Although this experiment was only conducted once and therefore lacks statistical analysis, these results appear to confirm that both S20 and S23 are phosphorylated residues in the stabilised FLAG-SLBP^{4A} protein.

The observation that FLAG-SLBP$^{S20A/4A}$ and FLAG-SLBP$^{S23A/4A}$ protein did not appear to be stabilised to the same extent as FLAG-SLBP^{4A} and FLAG-SLBP$^{Y95F/4A}$ suggests that S20 and S23 may contribute towards the observed stability of FLAG-SLBP^{4A} and FLAG-SLBP$^{Y95F/4A}$. This result appears to contradict the conclusion made in Krishnan et al. (2012) that states phosphorylation of S20 and S23 regulates SLBP polyubiquitination and degradation. However, based on the results in this chapter, it seems likely that post-translational modification of S20 and S23 is an early event in S phase that may serve to inhibit FEM1-mediated degradation of SLBP, thereby stabilising SLBP as cells transition from G1 to S phase. Further analysis of FLAG-SLBP$^{S20A/4A}$, FLAG-SLBP$^{S23A/4A}$ and FLAG-SLBP^{4A} protein stability as a function of time in synchronised cells would provide the necessary evidence to test this hypothesis.

5.3.4 A structural function of Y95 promotes aberrant histone gene transcription in cells expressing stabilised FLAG-SLBP^{4A}

Analysis of histone mRNA levels in the various 4A mutants described in this chapter showed that *HIST1H3B* and *H2AFX* mRNA levels were equal to FLAG-SLBP^{WT} levels in both FLAG-SLBP$^{Y95F/4A}$ and FLAG-SLBP$^{S20A/4A}$ cells. Given that Y95 is not phosphorylated, this observation suggests that S20 and a structural function of Y95 contribute towards the increased histone mRNA transcript levels observed in FLAG-SLBP^{4A} cells.

As tyrosine contains a hydroxyl group in its side chain, it is capable of forming hydrogen bonds with other hydroxyl group-containing amino acids. Interestingly, an analysis of the predicted 3D AlphaFold structure of SLBP showed that the C-terminal RBD domain of SLBP is folded back towards the central region and appears to be tethered to the RYKRKL motif via a hydrogen bond that

is formed between Y95 and N173 in the TPNK motif. Although only a prediction, AI-driven AlphaFold structures are considered to be highly accurate and in light of data presented in this chapter, it appears that the predicted hydrogen bond between Y95 and N173 may be a real intramolecular interaction *in vivo* that allows SLBP to switch between a tethered and untethered conformation in order to regulate the function of SLBP.

5.3.5 The RYKRKL motif and S23 are essential for histone gene transcription

Strikingly, qPCR analysis of histone mRNA transcript levels showed that FLAG-SLBP$^{S23A/4A}$ cells failed to rescue SLBP siRNA-mediated histone mRNA downregulation. As SLBP knockdown results in an accumulation of cells in S phase and a reduced rate of cell proliferation, due to the reduced ability to supply histone proteins during DNA replication, it is likely that FLAG-SLBP$^{S23A/4A}$ cells phenocopy SLBP-knockdown cells, however, time constraints precluded further analysis of the cell cycle profile of FLAG-SLBP$^{S23A/4A}$ cells.

The RYKRKL motif contains a canonical Cy motif (R-x-L), which is the minimum consensus sequence for cyclin binding (Chen et al., 1996; Schulman et al., 1998). As previously reported, both cyclin A/CDK1 and cyclin F interact with SLBP via this motif, though neither interacts with SLBP until late in S phase or in G2. Koseoglu et al. (2008) and Dankert et al. (2016) showed that the mutation of KRKL to alanines is sufficient to abolish the interaction between cyclins A and F with SLBP, which results in SLBP stabilisation. Given that the interaction between cyclin A, cyclin F and SLBP is inhibited in FLAG-SLBP^{4A} cells and that histone mRNA levels in FLAG-SLBP^{4A} cells appear equal to that seen in FLAG-SLBP^{WT} after 5 hours of doxycycline-induced expression, it is clear that the failure to rescue histone mRNA in FLAG-SLBP$^{S23A/4A}$ cells is not due to inhibited cyclin A or F binding. Although not the case for cyclin A/CDK1 binding to SLBP, a bi-partite mode of interaction, where cyclin A binds to a Cy motif and an additional subunit (e.g. Cks1) binds to a distal phosphosite, is a common mechanism to regulate and promote cyclin A/CDK1/2 binding to particular S phase substrates (Takeda et al., 2001; Stevenson-Lindert et al., 2003; Kõivomägi et al., 2013; Örd et al., 2019; Faustova et al., 2021). Therefore, based on this and the observation

in FLAG-SLBP$^{S23A/4A}$ cells, it is highly likely that a currently unidentified cyclin/CDK complex interacts with SLBP via the RYKRKL motif and S23 during early S phase in order to regulate histone gene transcription.

5.3.6 RNF20 and RNF40 (BRE1) are the only other human proteins that contain an RYKRKL motif and are functionally related to SLBP

Analysis of the human proteome revealed that only two other proteins contain the RYKRKL motif, these being RNF20 and RNF40. RNF20 and RNF40 are two subunits that form the E3 ubiquitin ligase BRE1, which specifically monoubiquitinates histone H2B on lysine 120 to form the histone modification H2BK120ub1 (Kim et al., 2005; Turco et al., 2015). H2BK120ub1 is required for the expression of a subset of RNA Polymerase II transcribed genes that are involved in the regulation of cell cycle progression, DNA replication and the DNA damage response, including the expression of cyclins and the replication-dependent histones H2A and H2B (Kim et al., 2005; Shema et al., 2008; Chernikova et al., 2012; Trujillo and Osley, 2012; Liu et al., 2021). Given its role in regulating H2A and H2B expression in humans, BRE1 can be considered to be functionally related to SLBP, in that it contributes towards the regulation of histone biosynthesis. Indeed, in the fission yeast *S. pombe*, a simple eukaryotic cell system that lacks SLBP, the expression of replication-dependent histones is regulated solely at the level of transcription through the activity of BRE1 (Pagé et al., 2016), though yeast BRE1 lacks the RYKRKL motif.

Monoubiquitination of H2B by BRE1 is regulated by CDK9, the catalytic subunit of the positive transcription elongation factor, P-TEFb (Pirngruber et al., 2009a; Sansó et al., 2012; Shchebet et al., 2012). The presence of the RYKRKL motif in vertebrate species raises the possibility that the cognate cyclin for CDK9 may interact with the Cy motifs in RNF20 and RNF40 in order for P-TEFb to bind to BRE1 and regulate its activity, however, there is currently no experimental evidence to support this hypothesis.

Interestingly, knockdown of P-TEFb has been shown to result in an increase of polyadenylated histone mRNA, suggesting a role for P-TEFb in the regulation of 3'UTR processing of histone

mRNAs and a possible interaction with SLBP (Pirngruber et al., 2009b). Therefore, it seems likely that P-TEFb may be the cyclin/CDK complex that binds to the RYKRKL motif and S23 in SLBP during S phase as part of a coordinated RYKRKL-dependent regulatory network that governs histone gene transcription and histone mRNA processing, thereby linking both of these processes with cell cycle progression from G1 to S phase. Unfortunately, testing this hypothesis was beyond the scope of this project, though it would be interesting to establish whether it is correct. If it is correct, then the results presented in this chapter suggest that pharmacological inhibition of P-TEFb or other cyclin/CDKs binding to RYKRKL in SLBP and BRE1 may negatively regulate cell proliferation, DNA replication and histone biosynthesis. Furthermore, an *in silico* prediction of synthetic lethality between RNF20/RNF40 with PARP1 and RAS suggests that targeted pharmacological inhibition of cyclin/CDKs binding to BRE1 in malignant cells, combined with PARP1 or RAS inhibition, may lead to therapeutic benefit in the clinic. With the recent development and approval of a novel KRAS inhibitor, RAS is no longer considered an "undruggable" target, making this a distinct possibility (Cox et al., 2014; Kessler et al., 2019; Huang et al., 2021).

Chapter 6

Concluding discussion and future perspectives

6.1 General discussion

The supply of histone proteins during S phase of the cell cycle is essential for the proper packaging of newly replicated DNA into chromatin and as such, the process of histone biosynthesis and the rate of DNA replication are tightly coordinated (Mariño-Ramírez et al., 2005). Imbalances in the supply of histone proteins and the rate of DNA replication can lead to genomic instability, which can prove deleterious to the survival of the cell (Celona et al., 2011). Often during the course of DNA replication, the replication machinery encounters physical obstacles or may be subject to decreased nucleotide supply, which ultimately impedes replication fork progression and slows the rate of DNA replication. During such instances of replication stress, the production of new histones is halted in order to prevent an accumulation of free histones, which can also be detrimental to the cell (Gunjan and Verreault, 2003; Gunjan et al., 2005; Maya Miles et al., 2018). The cell achieves this via the tightly regulated process of histone mRNA decay that ensures that the molecular mRNA instructions from which histones proteins are translated are rapidly degraded during periods of replication stress or at the end of S phase (Kaygun and Marzluff, 2005; Marzluff et al., 2008; Mullen and Marzluff, 2008; Koseoglu et al., 2010).

Histone mRNA decay is a multistep process that requires a number of cellular factors, including stem-loop binding protein (SLBP), which is the only protein that binds directly to the

stem-loop structure in the 3'UTR of histone mRNA and acts as the master regulator of histone mRNA metabolism (Kaygun and Marzluff, 2005; Marzluff et al., 2008; Mullen and Marzluff, 2008; Koseoglu et al., 2010). In the case of replication stress and histone mRNA decay, the activated intra-S phase checkpoint results in the RNA-binding domain (RBD) of SLBP dissociating from the histone mRNA stem-loop, which allows degradation components to degrade histone mRNA in both 5'-3' and 3'-5' directions, however, the precise molecular mechanisms that link intra-S phase checkpoint signalling and histone mRNA decay are not clear.

It was demonstrated in Panomwan (2017) that phosphorylation of S20 and S23 residues in the N-terminus of SLBP is elevated in cells exposed to hydroxyurea, a chemical that induces replication stress via the depletion of the nucleotide pool required to synthesise new DNA. This observation contradicts the conclusion in Krishnan et al. (2012) that suggests phosphorylation of S20/S23 acts as a phosphodegron to regulate SLBP degradation, as SLBP remains stable under conditions of replication stress. Instead, the finding in Panomwan (2017) suggested that phosphorylation of S20 and/or S23 may be required to initiate the dissociation of SLBP and histone mRNA in order to facilitate histone mRNA decay. Therefore, the aim of this project was to establish whether phosphorylation of S20 and/or S23 affects histone mRNA decay and, if so, to identify the kinase that phosphorylates these residues and thereby links activated intra-S phase checkpoint signalling and histone mRNA decay.

Surprisingly, data acquired in this project showed that histone mRNA decay proceeds as normal in non-phosphorylatable S20 and S23 mutant cell lines and that histone mRNA transcript levels were unchanged compared to wild-type cells in phosphomimetic S20 and S23 mutants. These findings unexpectedly indicated that the phosphorylation of S20 and S23 is not involved in the regulation of histone mRNA stability, despite the apparent increase in S20/S23 phosphorylation in cells exposed to replication stress.

Interestingly, during the course of this work, it was realised that a centrally located tyrosine residue in SLBP (Y95), in a stretch of basic amino acids with the sequence RYKRKL, was predicted to be phosphorylated by *in silico* analyses, though a peptide containing the residue had not been observed in previously published LC-MS/MS experiments and therefore there was no evi-

dence to confirm its phosphorylation. As the Y95 amino acid is located immediately adjacent to KRKL residues that have been shown to regulate nuclear-cytoplasmic trafficking and SLBP degradation, it was hypothesised that phosphorylation of Y95, if indeed a real event *in vivo*, may control either or both of these processes. Mass spectrometry was performed on FLAG-SLBP^{siRes} peptides that were digested using the endopeptidase GluC, which was expected to generate a 16-amino acid peptide containing Y95, though this attempt was unsuccessful in capturing a Y95-containing peptide. Nevertheless, additional experiments described in this thesis provide novel insights into the mechanism underlying SLBP-dependent regulation of histone gene expression in mammalian cells, involving S20, S23 and the RYKRKL motif.

6.1.1 SLBP S20/S23 contribute to the regulation of histone mRNA transcript levels but not via replication stress-induced histone mRNA decay

In the work presented here, I have shown that phosphorylation of S20 and S23 is not involved in the regulation of histone mRNA decay, as was originally hypothesised, as non-phosphorylatable S20/S23 cell lines were able to initiate and carry out histone mRNA decay and phosphomimetic S20/S23 mutants expressed histone mRNA transcripts at the same level as control cells. While it is possible that the aspartic acid and glutamic acid amino acid substitutions in the phosphomimetic cell lines fail to mimic the phosphorylation of S20 or S23, the result from non-phosphorylatable S20/S23 cell lines is sufficient to prove that phosphorylation of these residues is unrelated to histone mRNA decay.

Instead, S20 and S23 appear to independently contribute towards the regulation of histone mRNA transcript levels but not through the regulation of histone mRNA decay. The mechanism by which S20 influences histone mRNA transcript levels remains unclear and requires further investigation, though data presented here suggest that the aberrant expression of *HIST1H3B* and *H2AFX* in FLAG-SLBP^{4A} cells is dependent on S20. However, in the case of S23, the data clearly show that it acts in concert with the RYKRKL motif to regulate the expression of histone genes, as mutation of both S23 and KRKL to alanines abrogates the ability of FLAG-SLBP^{siRes} to rescue SLBP siRNA-mediated histone mRNA downregulation. In light of this finding, together with the known

mechanism of cyclin A/CDK-substrate binding described in Kõivomägi et al. (2013) and Örd et al. (2019), it appears possible that a currently unidentified cyclin/CDK complex might interact with SLBP at the onset of S phase to promote SLBP activation, which may be a step that is required for the initiation of histone gene transcription. This hypothesis will require further testing as it may help to further explain how the activation of histone gene transcription is linked to the transition from G1 to S phase.

6.1.2 The evolutionarily conserved RYKRKL motif is multifunctional and coordinates SLBP function in S phase

Previously, residues in the RYKRKL motif have been shown to contribute towards the nuclear-cytoplasmic trafficking of SLBP and also to provide a binding site for cyclins A and F, which regulate SLBP degradation at the end of S phase and in G2, respectively.

In this thesis, I have presented evidence that suggests additional roles for the RYKRKL motif that are critical for the normal function of SLBP. Based on these data it appears that a currently unidentified factor likely interacts with the RYKRKL motif and S23 in order to regulate the expression of histone genes during S phase. Furthermore, it has been shown that Y95 in the RYKRKL motif has a structural function that increases histone mRNA transcript levels in cells expressing the stabilised FLAG-SLBP^{4A} mutant. Analysis of the SLBP AlphaFold structural prediction suggests that Y95 forms a hydrogen bond with N173 in the TPNK motif, which if true, would tether the TPNK motif and RBDs to the RYKRKL motif. Switching between a tethered and untethered conformation could be part of the mechanism by which SLBP regulates its affinity for histone mRNA.

Given the conservation of the RYKRKL motif in vertebrate species and the fundamental SLBP processes that the motif is implicated in, it seems that the RYKRKL motif is central to the regulation of SLBP function, however, the precise molecular details remain to be elucidated and requires further detailed investigation.

6.2 Future perspectives

Following the completion of this project, it is clear that there remain significant gaps in our current understanding of SLBP regulation and function, and indeed, this project has opened more questions than it originally aimed to answer. In light of the novel findings that the RYKRKL is an evolutionarily conserved SLiM and the unanswered question regarding the initiation of histone mRNA decay, the immediate next steps that could be undertaken to further investigate the regulation of histone mRNA metabolism in mammalian cells are:

1. The identification of the proposed cyclin/CDK complex that interacts with RYKRKL and S23 during S phase in order to regulate histone gene transcription
2. Assessing the cell cycle profile of FLAG-SLBP$^{S23A/4A}$ cells in comparison to wild-type and knockdown cells to confirm a cell cycle defect in mutant cells deficient for histone biosynthesis
3. Optimisation of FLAG-SLBP enzymatic digestions with GluC upstream of LC-MS/MS to capture the 16-amino acid peptide containing Y95 to determine if the residue is phosphorylated under normal conditions and under conditions of stress or DNA damage (e.g. +HU, +UV, +chemical DNA damaging agents)
4. Identification of the kinase(s) responsible for S20 phosphorylation and determining the context under which it is targeted
5. Identification of the signal that induces Pin1-mediated SLBP and histone mRNA dissociation in order to facilitate histone mRNA decay in response to replication stress
6. Characterisation of the RYKRKL motifs in RNF20 and RNF40 to determine if the motif is functional in RNF20/40 as it is in SLBP

It is anticipated that data from the proposed experiments listed above will provide answers to the research questions that remain unanswered following the completion of this project and will

provide clarity and increase our understanding regarding the detailed molecular mechanisms underlying SLBP-dependent regulation of histone mRNA metabolism. Crucially, analysis of the function of the RYKRKL motifs in RNF20 and RNF40, along with identification of the cyclin/CDK complexes that bind to RNF20/40 and SLBP, could confirm the existence of a coordinated system of regulation that links cell cycle progression with histone gene transcription, histone mRNA processing and histone protein synthesis, which would be of considerable interest within the cell cycle, histone mRNA metabolism and SLiM research fields, in addition to pharmaceutical companies seeking to develop novel therapeutics that promote synthetic lethality as a means to selectively target and kill cancer cells in the clinic.

References

Agami, R. and Bernards, R. (2000). Distinct initiation and maintenance mechanisms cooperate to induce G1 cell cycle arrest in response to DNA damage. *Cell*, 102(1):55–66.

Aguilera, A. and García-Muse, T. (2013). Causes of genome instability. *Annual Review of Genetics*, 47:1–32.

Alexander, J. L. and Orr-Weaver, T. L. (2016). Replication fork instability and the consequences of fork collisions from rereplication. *Genes & Development*, 30(20):2241–2252.

Anderson, M. W., Reynolds, S. H., You, M., and Maronpot, R. M. (1992). Role of proto-oncogene activation in carcinogenesis. *Environmental Health Perspectives*, 98:13–24.

Anshabo, A. T., Milne, R., Wang, S., and Albrecht, H. (2021). CDK9: a comprehensive review of its biology, and its role as a potential target for anti-cancer agents. *Frontiers in Oncology*, 11:678559.

Appella, E. and Anderson, C. W. (2001). Post-translational modifications and activation of p53 by genotoxic stresses. *European Journal of Biochemistry*, 268(10):2764–2772.

Arora, M., Moser, J., Phadke, H., Basha, A. A., and Spencer, S. L. (2017). Endogenous replication stress in mother cells leads to quiescence of daughter cells. *Cell Reports*, 19(7):1351–1364.

Aubrey, B. J., Kelly, G. L., Janic, A., Herold, M. J., and Strasser, A. (2018). How does p53 induce apoptosis and how does this relate to p53-mediated tumour suppression? *Cell Death & Differentiation*, 25(1):104–113.

Ausió, J. (2006). Histone variants-the structure behind the function. *Briefings in Functional Genomics & Proteomics*, 5(3):228–243.

Azzouz, T. N., Gruber, A., and Schümperli, D. (2005). U7 snRNP-specific Lsm11 protein: dual binding contacts with the 100 kDa zinc finger processing factor (ZFP100) and a ZFP100-independent function in histone RNA 3' end processing. *Nucleic Acids Research*, 33(7):2106–2117.

Bansal, N., Zhang, M., Bhaskar, A., Itotia, P., Lee, E., Shlyakhtenko, L. S., Lam, T. T., Fritz, A., Berezney, R., Lyubchenko, Y. L., Stafford, W. F., and Thapar, R. (2013). Assembly of the SLIP1-SLBP complex on histone mRNA requires heterodimerization and sequential binding of SLBP followed by SLIP1. *Biochemistry*, 52(3):520–536.

Barnum, K. J. and O'Connell, M. J. (2014). Cell cycle regulation by checkpoints. *Methods in Molecular Biology*, 1170:29–40.

Bartek, J., Lukas, C., and Lukas, J. (2004). Checking on DNA damage in S phase. *Nature Reviews Molecular Cell Biology*, 5(10):792–804.

Bartek, J. and Lukas, J. (2003). Chk1 and Chk2 kinases in checkpoint control and cancer. *Cancer Cell*, 3(5):421–429.

Berkovich, E., Monnat, R. J. J., and Kastan, M. B. (2007). Roles of ATM and NBS1 in chromatin structure modulation and DNA double-strand break repair. *Nature Cell Biology*, 9(6):683–690.

Biterge, B. and Schneider, R. (2014). Histone variants: key players of chromatin. *Cell and Tissue Research*, 356(3):457–466.

Blom, N., Gammeltoft, S., and Brunak, S. (1999). Sequence and structure-based prediction of eukaryotic protein phosphorylation sites. *Journal of Molecular Biology*, 294:1351–1362.

Bonner, W. M., Mannironi, C., Orr, A., Pilch, D. R., and Hatch, C. L. (1993). Histone H2A.X gene transcription is regulated differently than transcription of other replication-linked histone genes. *Molecular and Cellular Biology*, 13(2):984–992.

Bradford, M. M. (1976). A rapid and sensitive method for the quantitation of microgram quantities of protein utilizing the principle of protein-dye binding. *Analytical Biochemistry*, 254:248–254.

Brooks, L. r., Lyons, S. M., Mahoney, J. M., Welch, J. D., Liu, Z., Marzluff, W. F., and Whitfield,

M. L. (2015). A multiprotein occupancy map of the mRNP on the 3' end of histone mRNAs. *RNA*, 21(11):1943–1965.

Burnette, W. (1981). "Western blotting": Electrophoretic transfer of proteins from sodium dodecyl sulfate-polyacrylamide gels to unmodified nitrocellulose and radiographic detection with antibody and radioiodinated protein A. *Analytical Biochemistry*, 112:195–203.

Castedo, M., Perfettini, J.-L., Roumier, T., Andreau, K., Medema, R., and Kroemer, G. (2004). Cell death by mitotic catastrophe: a molecular definition. *Oncogene*, 23(16):2825–2837.

Ceccon, M., Merlo, M. E. B., Mologni, L., Poggio, T., Varesio, L. M., Menotti, M., Bombelli, S., Rigolio, R., Manazza, A. D., Di Giacomo, F., Ambrogio, C., Giudici, G., Casati, C., Mastini, C., Compagno, M., Turner, S. D., Gambacorti-Passerini, C., Chiarle, R., and Voena, C. (2016). Excess of NPM-ALK oncogenic signaling promotes cellular apoptosis and drug dependency. *Oncogene*, 35(29):3854–3865.

Celona, B., Weiner, A., Di Felice, F., Mancuso, F. M., Cesarini, E., Rossi, R. L., Gregory, L., Baban, D., Rossetti, G., Grianti, P., Pagani, M., Bonaldi, T., Ragoussis, J., Friedman, N., Camilloni, G., Bianchi, M. E., and Agresti, A. (2011). Substantial histone reduction modulates genomewide nucleosomal occupancy and global transcriptional output. *PLoS Biology*, 9(6):e1001086.

Chen, J., Saha, P., Kornbluth, S., Dynlacht, B. D., and Dutta, A. (1996). Cyclin-binding motifs are essential for the function of p21CIP1. *Molecular and Cellular Biology*, 16(9):4673–4682.

Chen, Z. and Cole, P. A. (2015). Synthetic approaches to protein phosphorylation. *Current Opinion in Chemical Biology*, 28:115–122.

Chernikova, S. B., Razorenova, O. V., Higgins, J. P., Sishc, B. J., Nicolau, M., Dorth, J. A., Chernikova, D. A., Kwok, S., Brooks, J. D., Bailey, S. M., Game, J. C., and Brown, J. M. (2012). Deficiency in mammalian histone H2B ubiquitin ligase Bre1 (Rnf20/Rnf40) leads to replication stress and chromosomal instability. *Cancer Research*, 72(8):2111–2119.

Choe, J., Kim, K. M., Park, S., Lee, Y. K., Song, O.-K., Kim, M. K., Lee, B.-G., Song, H. K., and Kim, Y. K. (2013). Rapid degradation of replication-dependent histone mRNAs largely occurs on mRNAs bound by nuclear cap-binding proteins 80 and 20. *Nucleic Acids Research*, 41(2):1307–1318.

Chomczynski, P. and Sacchi, N. (1987). Single-step method of RNA isolation by acid guanidinium thiocyanate-phenol-chloroform extraction. *Analytical Biochemistry*, 162(1):156–159.

Ciardo, D., Goldar, A., and Marheineke, K. (2019). On the interplay of the DNA replication program and the intra-S Phase checkpoint pathway. *Genes*, 10(2).

Cortez, D. (2015). Preventing replication fork collapse to maintain genome integrity. *DNA Repair*, 32:149–157.

Cox, A. D., Fesik, S. W., Kimmelman, A. C., Luo, J., and Der, C. J. (2014). Drugging the undruggable RAS: Mission possible? *Nature Reviews Drug Discovery*, 13(11):828–851.

Cox, M. M. (1983). The FLP protein of the yeast 2-microns plasmid: expression of a eukaryotic genetic recombination system in *Escherichia coli*. *Proceedings of the National Academy of Sciences of the United States of America*, 80(14):4223–4227.

Craig, N. L. (1988). The mechanism of conservative site-specific recombination. *Annual Review of Genetics*, 22(1):77–105.

Cullen, B. R. (2006). Enhancing and confirming the specificity of RNAi experiments. *Nature Methods*, 3(9):677–681.

Danckwardt, S., Hentze, M. W., and Kulozik, A. E. (2008). 3' end mRNA processing: molecular mechanisms and implications for health and disease. *EMBO Journal*, 27(3):482–498.

Dankert, J. F., Rona, G., Clijsters, L., Geter, P., Skaar, J. R., Bermudez-Hernandez, K., Sassani, E., Fenyö, D., Ueberheide, B., Schneider, R., and Pagano, M. (2016). Cyclin F-mediated degradation of SLBP limits H2A.X accumulation and apoptosis upon genotoxic stress in G2. *Molecular Cell*, 64(3):507–519.

Djakbarova, U., Marzluff, W. F., and Köseoğlu, M. M. (2014). Translation regulation and proteasome mediated degradation cooperate to keep stem-loop binding protein low in G1-phase. *Journal of Cellular Biochemistry*, 115(3):523–530.

Dominski, Z., Erkmann, J. A., Yang, X., Sànchez, R., and Marzluff, W. F. (2002). A novel zinc finger protein is associated with U7 snRNP and interacts with the stem-loop binding protein in the histone pre-mRNP to stimulate 3'-end processing. *Genes & Development*, 16(1):58–71.

Dominski, Z. and Marzluff, W. F. (1999). Formation of the 3' end of histone mRNA. *Gene*, 239(1):1–14.

Dominski, Z., Yang, X.-c., and Marzluff, W. F. (2005). The polyadenylation factor CPSF-73 is involved in histone-pre-mRNA processing. *Cell*, 123(1):37–48.

Ehlert, F., Bierbaum, P., and Schorr, J. (1993). Importance of DNA quality for transfection efficiency. *Biotechniques*, 14(4):546.

Elledge, S. J., Zhou, Z., and Allen, J. B. (1992). Ribonucleotide reductase: regulation, regulation, regulation. *Trends in Biochemical Sciences*, 17(3):119–123.

Erkmann, J. A., Sànchez, R., Treichel, N., Marzluff, W. F., and Kutay, U. (2005a). Nuclear export of metazoan replication-dependent histone mRNAs is dependent on RNA length and is mediated by TAP. *RNA*, 11(1):45–58.

Erkmann, J. A., Wagner, E. J., Dong, J., Zhang, Y., Kutay, U., and Marzluff, W. F. (2005b). Nuclear import of the stem-loop binding protein and localization during the cell cycle. *Molecular Biology of the Cell*, 16(6):2960–2971.

Faustova, I., Bulatovic, L., Matiyevskaya, F., Valk, E., Örd, M., and Loog, M. (2021). A new linear cyclin docking motif that mediates exclusively S-phase CDK-specific signaling. *The EMBO Journal*, 40(2):e105839.

Fawal, M., Armstrong, F., Ollier, S., Dupont, H., Touriol, C., Monsarrat, B., Delsol, G., Payrastre, B., and Morello, D. (2006). A "liaison dangereuse" between AUF1/hnRNPD and the oncogenic tyrosine kinase NPM-ALK. *Blood*, 108(8):2780–2788.

Fire, A., Xu, S., Montgomery, M. K., Kostas, S. A., Driver, S. E., and Mello, C. C. (1998). Potent and specific genetic interference by double-stranded RNA in Caenorhabditis elegans. *Nature*, 391(6669):806–811.

Fiszer-Kierzkowska, A., Vydra, N., Wysocka-Wycisk, A., Kronekova, Z., Jarzab, M., Lisowska, K. M., and Krawczyk, Z. (2011). Liposome-based DNA carriers may induce cellular stress response and change gene expression pattern in transfected cells. *BMC Molecular Biology*, 12:27.

Franco, L. C., Morales, F., Boffo, S., and Giordano, A. (2018). CDK9: A key player in cancer and other diseases. *Journal of Cellular Biochemistry*, 119(2):1273–1284.

Fricker, L. D. (2015). Limitations of mass spectrometry-based peptidomic approaches. *Journal of the American Society for Mass Spectrometry*, 26(12):1981–1991.

Furuta, T., Takemura, H., Liao, Z.-Y., Aune, G. J., Redon, C., Sedelnikova, O. A., Pilch, D. R., Rogakou, E. P., Celeste, A., Chen, H. T., Nussenzweig, A., Aladjem, M. I., Bonner, W. M., and Pommier, Y. (2003). Phosphorylation of histone H2AX and activation of Mre11, Rad50, and Nbs1 in response to replication-dependent DNA double-strand breaks induced by mammalian DNA topoisomerase I cleavage complexes. *Journal of Biological Chemistry*, 278(22):20303–20312.

Garriga, J., Bhattacharya, S., Calbó, J., Marshall, R. M., Truongcao, M., Haines, D. S., and Graña, X. (2003). CDK9 is constitutively expressed throughout the cell cycle, and its steady-state expression is independent of SKP2. *Molecular and Cellular Biology*, 23(15):5165–5173.

Gelens, L. and Saurin, A. T. (2018). Exploring the function of dynamic phosphorylation-dephosphorylation cycles. *Developmental Cell*, 44(6):659–663.

Gérard, C. and Goldbeter, A. (2014). The balance between cell cycle arrest and cell proliferation: control by the extracellular matrix and by contact inhibition. *Interface Focus*, 4(3):20130075.

Giansanti, P., Tsiatsiani, L., Low, T. Y., and Heck, A. J. R. (2016). Six alternative proteases for mass spectrometry–based proteomics beyond trypsin. *Nature Protocols*, 11(5):993–1006.

Gick, O., Krämer, A., Keller, W., and Birnstiel, M. L. (1986). Generation of histone mRNA 3' ends by endonucleolytic cleavage of the pre-mRNA in a snRNP-dependent in vitro reaction. *EMBO Journal*, 5(6):1319–1326.

Gordon, Erlinda, M., Ravicz, Joshua, R., Liu, S., Chawla, Sant, P., and Hall, Frederick, L. (2018). Cell cycle checkpoint control: The cyclin G1/Mdm2/p53 axis emerges as a strategic target for broad-spectrum cancer gene therapy - A review of molecular mechanisms for oncologists. *Molecular & Clinical Oncology*, 9(2):115–134.

Griesbach, E., Schlackow, M., Marzluff, W. F., and Proudfoot, N. J. (2021). Dual RNA 3'-end processing of H2A.X messenger RNA maintains DNA damage repair throughout the cell cycle. *Nature Communications*, 12(1):359.

Gruber, J. J., Olejniczak, S. H., Yong, J., La Rocca, G., Dreyfuss, G., and Thompson, C. B. (2012). Ars2 promotes proper replication-dependent histone mRNA 3' end formation. *Molecular Cell*, 45(1):87–98.

Gunjan, A., Paik, J., and Verreault, A. (2005). Regulation of histone synthesis and nucleosome assembly. *Biochimie*, 87(7):625–635.

Gunjan, A. and Verreault, A. (2003). A Rad53 kinase-dependent surveillance mechanism that regulates histone protein levels in *S. cerevisiae*. *Cell*, 115(5):537–549.

Guo, Z., Qian, L., Liu, R., Dai, H., Zhou, M., Zheng, L., and Shen, B. (2008). Nucleolar localization and dynamic roles of flap endonuclease 1 in ribosomal DNA replication and damage repair. *Molecular and Cellular Biology*, 28(13):4310–4319.

Hakem, R. (2008). DNA-damage repair; the good, the bad, and the ugly. *EMBO Journal*, 27(4):589–605.

Hansen, K., Szarka, S., Escoffier, E., Berthet, A., Venet, J., Collet-Brose, J., Hepburn, S., Wright, M., Wheller, R., Nelson, R., and Kay, R. G. (2018). Glu-C, an alternative digestive enzyme for the quantitative LC-MS/MS analysis of an IgG-based antibody biotherapeutic. *Bioanalysis*, 10(13):997–1007.

Harashima, H., Dissmeyer, N., and Schnittger, A. (2013). Cell cycle control across the eukaryotic kingdom. *Trends in Cell Biology*, 23(7):345–356.

Harper, J. W. and Elledge, S. J. (2007). The DNA damage response: ten years after. *Molecular Cell*, 28(5):739–745.

Harris, M. E., Böhni, R., Schneiderman, M. H., Ramamurthy, L., Schümperli, D., and Marzluff, W. F. (1991). Regulation of histone mRNA in the unperturbed cell cycle: evidence suggesting control at two posttranscriptional steps. *Molecular and Cellular Biology*, 11(5):2416–2424.

He, W.-X., Wu, M., Liu, Z., Li, Z., Wang, Y., Zhou, J., Yu, P., Zhang, X.-J., Zhou, L., and Gui, J.-F. (2018). Oocyte-specific maternal Slbp2 is required for replication-dependent histone storage and early nuclear cleavage in zebrafish oogenesis and embryogenesis. *RNA*, 24(12):1738–1748.

Henikoff, S. and Smith, M. M. (2015). Histone variants and epigenetics. *Cold Spring Harbor Perspectives in Biology*, 7(1):a019364.

Huang, L., Guo, Z., Wang, F., and Fu, L. (2021). KRAS mutation: from undruggable to druggable in cancer. *Signal Transduction and Targeted Therapy*, 6(1):386.

Hume, S., Dianov, G. L., and Ramadan, K. (2020). A unified model for the G1/S cell cycle transition. *Nucleic Acids Research*, 48(22):12483–12501.

Ishigaki, Y., Li, X., Serin, G., and Maquat, L. E. (2001). Evidence for a pioneer round of mRNA translation: mRNAs subject to nonsense-mediated decay in mammalian cells are bound by CBP80 and CBP20. *Cell*, 106(5):607–617.

Ishii, K. J. and Akira, S. (2006). Innate immune recognition of, and regulation by, DNA. *Trends in Immunology*, 27(11):525–532.

Iyer, D. R. and Rhind, N. (2017). The intra-S checkpoint responses to DNA damage. *Genes (Basel)*, 8(2).

Jehl, P., Manguy, J., Shields, D. C., Higgins, D. G., and Davey, N. E. (2016). ProViz—a web-based visualization tool to investigate the functional and evolutionary features of protein sequences. *Nucleic Acids Research*, 44(W1):W11–W15.

Johnsen, S. (2012). The enigmatic role of H2Bub1 in cancer. *FEBS Letters*, 586:1592–601.

Jumper, J., Evans, R., Pritzel, A., Green, T., Figurnov, M., Ronneberger, O., Tunyasuvunakool, K., Bates, R., Žídek, A., Potapenko, A., Bridgland, A., Meyer, C., Kohl, S. A. A., Ballard, A. J., Cowie, A., Romera-Paredes, B., Nikolov, S., Jain, R., Adler, J., Back, T., Petersen, S., Reiman, D., Clancy, E., Zielinski, M., Steinegger, M., Pacholska, M., Berghammer, T., Bodenstein, S., Silver, D., Vinyals, O., Senior, A. W., Kavukcuoglu, K., Kohli, P., and Hassabis, D. (2021). Highly accurate protein structure prediction with AlphaFold. *Nature*, 596(7873):583–589.

Kastan, M. B. and Bartek, J. (2004). Cell-cycle checkpoints and cancer. *Nature*, 432(7015):316–323.

Kaygun, H. and Marzluff, W. F. (2005). Regulated degradation of replication-dependent histone mRNAs requires both ATR and Upf1. *Nature Structural & Molecular Biology*, 12(9):794–800.

Kerzendorfer, C., Hannes, F., Colnaghi, R., Abramowicz, I., Carpenter, G., Vermeesch, J. R., and O'Driscoll, M. (2012). Characterizing the functional consequences of haploinsufficiency of NELF-A (WHSC2) and SLBP identifies novel cellular phenotypes in Wolf-Hirschhorn syndrome. *Human Molecular Genetics*, 21(10):2181–2193.

Kessler, D., Gmachl, M., Mantoulidis, A., Martin, L. J., Zoephel, A., Mayer, M., Gollner, A., Covini, D., Fischer, S., Gerstberger, T., Gmaschitz, T., Goodwin, C., Greb, P., Häring, D., Hela, W., Hoffmann, J., Karolyi-Oezguer, J., Knesl, P., Kornigg, S., Koegl, M., Kousek, R., Lamarre, L., Moser, F., Munico-Martinez, S., Peinsipp, C., Phan, J., Rinnenthal, J., Sai, J., Salamon, C., Scherbantin, Y., Schipany, K., Schnitzer, R., Schrenk, A., Sharps, B., Siszler, G., Sun, Q., Waterson, A., Wolkerstorfer, B., Zeeb, M., Pearson, M., Fesik, S. W., and McConnell, D. B. (2019). Drugging an undruggable pocket on KRAS. *Proceedings of the National Academy of Sciences of the United States of America*, 116(32):15823–15829.

Kim, J., Hake, S. B., and Roeder, R. G. (2005). The human homolog of yeast BRE1 functions as a transcriptional coactivator through direct activator interactions. *Molecular Cell*, 20(5):759–770.

Kõivomägi, M., Örd, M., Iofik, A., Valk, E., Venta, R., Faustova, I., Kivi, R., Balog, E. R. M., Rubin, S. M., and Loog, M. (2013). Multisite phosphorylation networks as signal processors for Cdk1. *Nature Structural & Molecular Biology*, 20(12):1415–1424.

Köpper, F., Bierwirth, C., Schön, M., Kunze, M., Elvers, I., Kranz, D., Saini, P., Menon, M. B., Walter, D., Sørensen, C. S., Gaestel, M., Helleday, T., Schön, M. P., and Dobbelstein, M. (2013). Damage-induced DNA replication stalling relies on MAPK-activated protein kinase 2 activity. *Proceedings of the National Academy of Sciences of the United States of America*, 110(42):16856–16861.

Koseoglu, M. M., Dong, J., and Marzluff, W. F. (2010). Coordinate regulation of histone mRNA

metabolism and DNA replication: cyclin A/cdk1 is involved in inactivation of histone mRNA metabolism and DNA replication at the end of S phase. *Cell Cycle*, 9(19):3857–3863.

Koseoglu, M. M., Graves, L. M., and Marzluff, W. F. (2008). Phosphorylation of threonine 61 by cyclin a/Cdk1 triggers degradation of stem-loop binding protein at the end of S phase. *Molecular and Cellular Biology*, 28(14):4469–4479.

Krishnan, N., Lam, T. T., Fritz, A., Rempinski, D., O'Loughlin, K., Minderman, H., Berezney, R., Marzluff, W. F., and Thapar, R. (2012). The prolyl isomerase Pin1 targets stem-loop binding protein (SLBP) to dissociate the SLBP-histone mRNA complex linking histone mRNA decay with SLBP ubiquitination. *Molecular and Cellular Biology*, 32(21):4306–4322.

Krude, T. (1995). Chromatin: nucleosome assembly during DNA replication. *Current Biology*, 5(11):1232–1234.

Krystkowiak, I. and Davey, N. E. (2017). SLiMSearch: a framework for proteome-wide discovery and annotation of functional modules in intrinsically disordered regions. *Nucleic Acids Research*, 45(W1):W464–W469.

Laemmli, U. K. (1970). Cleavage of structural proteins during the assembly of the head of bacteriophage T4. *Nature*, 227(5259):680–685.

Lee, J.-H. and Paull, T. T. (2005). ATM activation by DNA double-strand breaks through the Mre11-Rad50-Nbs1 complex. *Science*, 308(5721):551–554.

Lim, S.-T., Chen, X. L., Lim, Y., Hanson, D. A., Vo, T.-T., Howerton, K., Larocque, N., Fisher, S. J., Schlaepfer, D. D., and Ilic, D. (2008). Nuclear FAK promotes cell proliferation and survival through FERM-enhanced p53 degradation. *Molecular Cell*, 29(1):9–22.

Lim, S.-T. S. (2013). Nuclear FAK: a new mode of gene regulation from cellular adhesions. *Molecules & Cells*, 36(1):1–6.

Liu, G., Yan, J., Wang, X., Chen, J., Wang, X., Dong, Y., Zhang, S., Gan, X., Huang, J., and Chen, X. (2021). RPA-mediated recruitment of Bre1 couples histone H2B ubiquitination to DNA replication and repair. *Proceedings of the National Academy of Sciences of the United States of America*, 118(8).

Liu, Y., Parry, J. A., Chin, A., Duensing, S., and Duensing, A. (2008). Soluble histone H2AX is induced by DNA replication stress and sensitizes cells to undergo apoptosis. *Molecular Cancer*, 7:61.

Livak, K. J. and Schmittgen, T. D. (2001). Analysis of relative gene expression data using real-time quantitative PCR and the $2^{-\Delta\Delta C_T}$ method. *Methods*, 25(4):402–408.

Llopis, A., Salvador, N., Ercilla, A., Guaita-Esteruelas, S., Barrantes, I. d. B., Gupta, J., Gaestel, M., Davis, R. J., Nebreda, A. R., and Agell, N. (2012). The stress-activated protein kinases p38α/β and JNK1/2 cooperate with Chk1 to inhibit mitotic entry upon DNA replication arrest. *Cell Cycle*, 11(19):3627–3637.

Löbrich, M. and Jeggo, P. A. (2007). The impact of a negligent G2/M checkpoint on genomic instability and cancer induction. *Nature Reviews Cancer*, 7(11):861–869.

Lykke-Andersen, S., Rouvière, J. O., and Jensen, T. H. (2021). ARS2/SRRT: at the nexus of RNA polymerase II transcription, transcript maturation and quality control. *Biochemical Society Transactions*, 49(3):1325–1336.

Malumbres, M. (2014). Cyclin-dependent kinases. *Genome Biology*, 15(6):122.

Mannironi, C., Bonner, W. M., and Hatch, C. L. (1989). H2A.X. a histone isoprotein with a conserved C-terminal sequence, is encoded by a novel mRNA with both DNA replication type and polyA 3' processing signals. *Nucleic Acids Research*, 17(22):9113–9126.

Maréchal, A. and Zou, L. (2013). DNA damage sensing by the ATM and ATR kinases. *Cold Spring Harbor Perspectives in Biology*, 5(9).

Mariño-Ramírez, L., Kann, M. G., Shoemaker, B. A., and Landsman, D. (2005). Histone structure and nucleosome stability. *Expert Reviews of Proteomics*, 2(5):719–729.

Martin, F., Schaller, A., Eglite, S., Schümperli, D., and Müller, B. (1997). The gene for histone RNA hairpin binding protein is located on human chromosome 4 and encodes a novel type of RNA binding protein. *EMBO Journal*, 16(4):769–778.

Martire, S. and Banaszynski, L. A. (2020). The roles of histone variants in fine-tuning chromatin organization and function. *Nature Reviews Molecular Cellular Biology*, 21(9):522–541.

Marzluff, W. F. and Duronio, R. J. (2002). Histone mRNA expression: multiple levels of cell cycle regulation and important developmental consequences. *Current Opinion in Cell Biology*, 14(6):692–699.

Marzluff, W. F., Gongidi, P., Woods, K. R., Jin, J., and Maltais, L. J. (2002). The human and mouse replication-dependent histone genes. *Genomics*, 80(5):487–498.

Marzluff, W. F. and Koreski, K. P. (2017). Birth and death of histone mRNAs. *Trends in Genetics*, 33(10):745–759.

Marzluff, W. F., Wagner, E. J., and Duronio, R. J. (2008). Metabolism and regulation of canonical histone mRNAs: life without a poly(A) tail. *Nature Reviews Genetics*, 9(11):843–854.

Matthews, H. K., Bertoli, C., and de Bruin, R. A. M. (2022). Cell cycle control in cancer. *Nature Reviews Molecular Cell Biology*, 23(1):74–88.

Mattijssen, S., Kozlov, G., Fonseca, B. D., Gehring, K., and Maraia, R. J. (2021). LARP1 and LARP4: up close with PABP for mRNA 3' poly(A) protection and stabilization. *RNA Biology*, 18(2):259–274.

Maya Miles, D., Peñate, X., Sanmartín Olmo, T., Jourquin, F., Muñoz Centeno, M. C., Mendoza, M., Simon, M.-N., Chavez, S., and Geli, V. (2018). High levels of histones promote whole-genome-duplications and trigger a Swe1$^{\mathrm{WEE1}}$-dependent phosphorylation of Cdc28$^{\mathrm{CDK1}}$. *eLife*, 7:e35337.

Mellacheruvu, D., Wright, Z., Couzens, A. L., Lambert, J.-P., St-Denis, N. A., Li, T., Miteva, Y. V., Hauri, S., Sardiu, M. E., Low, T. Y., Halim, V. A., Bagshaw, R. D., Hubner, N. C., Al-Hakim, A., Bouchard, A., Faubert, D., Fermin, D., Dunham, W. H., Goudreault, M., Lin, Z.-Y., Badillo, B. G., Pawson, T., Durocher, D., Coulombe, B., Aebersold, R., Superti-Furga, G., Colinge, J., Heck, A. J. R., Choi, H., Gstaiger, M., Mohammed, S., Cristea, I. M., Bennett, K. L., Washburn, M. P., Raught, B., Ewing, R. M., Gingras, A.-C., and Nesvizhskii, A. I. (2013). The CRAPome: a contaminant repository for affinity purification-mass spectrometry data. *Nature Methods*, 10(8):730–736.

Mitra, S. K. and Schlaepfer, D. D. (2006). Integrin-regulated FAK-Src signaling in normal and cancer cells. *Current Opinion in Cell Biology*, 18(5):516–523.

Molinari, M. (2000). Cell cycle checkpoints and their inactivation in human cancer. *Cell Proliferation*, 33(5):261–274.

Morimoto, M. and Boerkoel, C. F. (2013). The role of nuclear bodies in gene expression and disease. *Biology (Basel)*, 2(3):976–1033.

Mullen, T. E. and Marzluff, W. F. (2008). Degradation of histone mRNA requires oligouridylation followed by decapping and simultaneous degradation of the mRNA both 5' to 3' and 3' to 5'. *Genes & Development*, 22(1):50–65.

Müller, B., Blackburn, J., Feijoo, C., Zhao, X., and Smythe, C. (2007). DNA-activated protein kinase functions in a newly observed S phase checkpoint that links histone mRNA abundance with DNA replication. *Journal of Cell Biology*, 179(7):1385–1398.

Murray, A. W. (2004). Recycling the cell cycle: cyclins revisited. *Cell*, 116(2):221–234.

Nizami, Z., Deryusheva, S., and Gall, J. G. (2010). The Cajal body and histone locus body. *Cold Spring Harbor Perspectives in Biology*, 2(7):1–12.

Nurse, P. (1990). Universal control mechanism regulating onset of M-phase. *Nature*, 344(6266):503–508.

Olsen, J. V., Blagoev, B., Gnad, F., Macek, B., Kumar, C., Mortensen, P., and Mann, M. (2006). Global, in vivo, and site-specific phosphorylation dynamics in signaling networks. *Cell*, 127(3):635–648.

Olsen, J. V., Ong, S.-E., and Mann, M. (2004). Trypsin cleaves exclusively C-terminal to arginine and lysine residues. *Molecular & Cellular Proteomics*, 3(6):608–614.

Örd, M., Möll, K., Agerova, A., Kivi, R., Faustova, I., Venta, R., Valk, E., and Loog, M. (2019). Multisite phosphorylation code of CDK. *Nature Structural & Molecular Biology*, 26(7):649–658.

O'Sullivan, C., Christie, J., Pienaar, M., Gambling, J., Nickerson, P. E. B., Alford, S. C., Chow, R. L., and Howard, P. L. (2015). Mutagenesis of ARS2 domains to assess possible roles in cell cycle progression and microRNA and replication-dependent histone mRNA biogenesis. *Molecular and Cellular Biology*, 35(21):3753–3767.

Pagé, V., Grabowski, D., Allis, C. D., and Tanny, J. C. (2016). Histone gene expression is regulated by histone H2B ubiquitylation in fission yeast. *bioRxiv*, page 094565.

Paleologou, K. E., Schmid, A. W., Rospigliosi, C. C., Kim, H.-Y., Lamberto, G. R., Fredenburg, R. A., Lansbury, P. T. J., Fernandez, C. O., Eliezer, D., Zweckstetter, M., and Lashuel, H. A. (2008). Phosphorylation at Ser-129 but not the phosphomimics S129E/D inhibits the fibrillation of alpha-synuclein. *Journal of Biological Chemistry*, 283(24):16895–16905.

Panomwan, P. (2017). *Analysis of the mechanism of DNA damage and replication arrest-induced histone mRNA decay*. PhD thesis, The University of Sheffield.

Paull, T. T., Rogakou, E. P., Yamazaki, V., Kirchgessner, C. U., Gellert, M., and Bonner, W. M. (2000). A critical role for histone H2AX in recruitment of repair factors to nuclear foci after DNA damage. *Current Biology*, 10(15):886–895.

Persad, S., Attwell, S., Gray, V., Mawji, N., Deng, J. T., Leung, D., Yan, J., Sanghera, J., Walsh, M. P., and Dedhar, S. (2001). Regulation of protein kinase B/Akt-serine 473 phosphorylation by integrin-linked kinase: critical roles for kinase activity and amino acids arginine 211 and serine 343. *Journal of Biological Chemistry*, 276(29):27462–27469.

Pillai, R. S., Grimmler, M., Meister, G., Will, C. L., Lührmann, R., Fischer, U., and Schümperli, D. (2003). Unique Sm core structure of U7 snRNPs: assembly by a specialized SMN complex and the role of a new component, Lsm11, in histone RNA processing. *Genes & Development*, 17(18):2321–2333.

Pillai, R. S., Will, C. L., Lührmann, R., Schümperli, D., and Müller, B. (2001). Purified U7 snRNPs lack the Sm proteins D1 and D2 but contain Lsm10, a new 14 kDa Sm D1-like protein. *EMBO Journal*, 20(19):5470–5479.

Pirngruber, J., Shchebet, A., and Johnsen, S. (2009a). Insights into the function of the human P-TEFb component CDK9 in the regulation of chromatin modifications and co-transcriptional mRNA processing. *Cell Cycle*, 8:3636–42.

Pirngruber, J., Shchebet, A., Schreiber, L., Shema, E., Minsky, N., Chapman, R. D., Eick, D., Aylon, Y., Oren, M., and Johnsen, S. A. (2009b). CDK9 directs H2B monoubiquitination and

controls replication-dependent histone mRNA 3'-end processing. *EMBO Reports*, 10(8):894–900.

Poon, R. Y., Jiang, W., Toyoshima, H., and Hunter, T. (1996). Cyclin-dependent kinases are inactivated by a combination of p21 and Thr-14/Tyr-15 phosphorylation after UV-induced DNA damage. *Journal of Biological Chemistry*, 271(22):13283–13291.

Potter-Birriel, J. M., Gonsalvez, G. B., and Marzluff, W. F. (2021). A region of SLBP outside the mRNA-processing domain is essential for deposition of histone mRNA into the *Drosophila* egg. *Journal of Cell Science*, 134(3).

Pronobis, M. I., Deuitch, N., and Peifer, M. (2016). The miraprep: a protocol that uses a miniprep kit and provides maxiprep yields. *PLOS ONE*, 11(8):1–12.

Reinhardt, H. C. and Yaffe, M. B. (2009). Kinases that control the cell cycle in response to DNA damage: Chk1, Chk2, and MK2. *Current Opinion in Cell Biology*, 21(2):245–255.

Rogakou, E. P., Pilch, D. R., Orr, A. H., Ivanova, V. S., and Bonner, W. M. (1998). DNA double-stranded breaks induce histone H2AX phosphorylation on serine 139. *Journal of Biological Chemistry*, 273(10):5858–5868.

Safaei, J., Ma, J., Gupta, A., Stacho, L., and Pelech, S. (2011). Prediction of 492 human protein kinase substrate specificities. *Proteome Science*, 9(Suppl 1):1–13.

Sansó, M., Lee, K. M., Viladevall, L., Jacques, P.-É., Pagé, V., Nagy, S., Racine, A., St Amour, C. V., Zhang, C., Shokat, K. M., Schwer, B., Robert, F., Fisher, R. P., and Tanny, J. C. (2012). A positive feedback loop links opposing functions of P-TEFb/Cdk9 and histone H2B ubiquitylation to regulate transcript elongation in fission yeast. *PLOS Genetics*, 8(8):1–17.

Sarma, K. and Reinberg, D. (2005). Histone variants meet their match. *Nature Reviews Molecular Cellular Biology*, 6(2):139–149.

Schafer, K. A. (1998). The cell cycle: a review. *Veterinary Pathology*, 35(6):461–478.

Schmidt, T., Samaras, P., Frejno, M., Gessulat, S., Barnert, M., Kienegger, H., Krcmar, H., Schlegl, J., Ehrlich, H.-C., Aiche, S., Kuster, B., and Wilhelm, M. (2018). ProteomicsDB. *Nucleic Acids Research*, 46(D1):D1271–D1281.

Schulman, B. A., Lindstrom, D. L., and Harlow, E. (1998). Substrate recruitment to cyclin-dependent kinase 2 by a multipurpose docking site on cyclin A. *Proceedings of the National Academy of Sciences of the United States of America*, 95(18):10453–10458.

Segurado, M. and Tercero, J. A. (2009). The S-phase checkpoint: targeting the replication fork. *Biology of the Cell*, 101(11):617–627.

Senkel, S., Waldner, C., Ryffel, G. U., and Thomas, H. (2009). Improved conditional expression systems resulting in physiological level of HNF4alpha expression confirm HNF4alpha induced apoptosis in the pancreatic beta-cell line INS-1. *BMC Research Notes*, 2:210.

Serra-Cardona, A. and Zhang, Z. (2018). Replication-Coupled Nucleosome Assembly in the Passage of Epigenetic Information and Cell Identity. *Trends in Biochemical Sciences*, 43(2):136–148.

Serrels, A., Lund, T., Serrels, B., Byron, A., McPherson, R. C., von Kriegsheim, A., Gómez-Cuadrado, L., Canel, M., Muir, M., Ring, J. E., Maniati, E., Sims, A. H., Pachter, J. A., Brunton, V. G., Gilbert, N., Anderton, S. M., Nibbs, R. J. B., and Frame, M. C. (2015). Nuclear FAK controls chemokine transcription, Tregs, and evasion of anti-tumor immunity. *Cell*, 163(1):160–173.

Shaltiel, I. A., Krenning, L., Bruinsma, W., and Medema, R. (2015). The same, only different – DNA damage checkpoints and their reversal throughout the cell cycle. *Journal of Cell Science*, 128(4):607–620.

Shchebet, A., Karpiuk, O., Kremmer, E., Eick, D., and Johnsen, S. A. (2012). Phosphorylation by cyclin-dependent kinase-9 controls ubiquitin-conjugating enzyme-2A function. *Cell Cycle*, 11(11):2122–2127.

Shema, E., Tirosh, I., Aylon, Y., Huang, J., Ye, C., Moskovits, N., Raver-Shapira, N., Minsky, N., Pirngruber, J., Tarcic, G., Hublarova, P., Moyal, L., Gana-Weisz, M., Shiloh, Y., Yarden, Y., Johnsen, S. A., Vojtesek, B., Berger, S. L., and Oren, M. (2008). The histone H2B-specific ubiquitin ligase RNF20/hBRE1 acts as a putative tumor suppressor through selective regulation of gene expression. *Genes & Development*, 22(19):2664–2676.

Shi, Y. (2003). Mammalian RNAi for the masses. *Trends in Genetics*, 19(1):9–12.

Stark, G. R. and Taylor, W. R. (2006). Control of the G2/M transition. *Molecular Biotechnology*, 32(3):227–248.

Stepanenko, A. A. and Heng, H. H. (2017). Transient and stable vector transfection: pitfalls, off-target effects, artifacts. *Mutation Research - Reviews in Mutation Research*, 773:91–103.

Stevenson-Lindert, L. M., Fowler, P., and Lew, J. (2003). Substrate specificity of CDK2-cyclin A. What is optimal? *Journal of Biological Chemistry*, 278(51):50956–50960.

Sullivan, K. D., Mullen, T. E., Marzluff, W. F., and Wagner, E. J. (2009). Knockdown of SLBP results in nuclear retention of histone mRNA. *RNA*, 15(3):459–472.

Swaney, D. L., Wenger, C. D., and Coon, J. J. (2010). Value of using multiple proteases for large-scale mass spectrometry-based proteomics. *Journal of Proteome Research*, 9(3):1323–1329.

Szczesny, R. J., Kowalska, K., Klosowska-Kosicka, K., Chlebowski, A., Owczarek, E. P., Warkocki, Z., Kulinski, T. M., Adamska, D., Affek, K., Jedroszkowiak, A., Kotrys, A. V., Tomecki, R., Krawczyk, P. S., Borowski, L. S., and Dziembowski, A. (2018). Versatile approach for functional analysis of human proteins and efficient stable cell line generation using FLP-mediated recombination system. *PLOS ONE*, 13(3):1–29.

Szklarczyk, D., Gable, A. L., Nastou, K. C., Lyon, D., Kirsch, R., Pyysalo, S., Doncheva, N. T., Legeay, M., Fang, T., Bork, P., Jensen, L. J., and von Mering, C. (2020). The STRING database in 2021: customizable protein–protein networks, and functional characterization of user-uploaded gene/measurement sets. *Nucleic Acids Research*, 49(D1):D605–D612.

Takeda, D. Y., Wohlschlegel, J. A., and Dutta, A. (2001). A bipartite substrate recognition motif for cyclin-dependent kinases. *Journal of Biological Chemistry*, 276(3):1993–1997.

Talbert, P. B. and Henikoff, S. (2021). Histone variants at a glance. *Journal of Cell Science*, 134(6).

Taylor, S. C., Nadeau, K., Abbasi, M., Lachance, C., Nguyen, M., and Fenrich, J. (2019). The ultimate qPCR Experiment: producing publication quality, reproducible data the first time. *Trends in Biotechnology*, 37(7):761–774.

Thapar, R. (2015). Roles of prolyl isomerases in RNA-mediated gene expression. *Biomolecules*, 5:974–999.

Thomas, H., Senkel, S., Erdmann, S., Arndt, T., Turan, G., Klein-Hitpass, L., and Ryffel, G. U. (2004). Pattern of genes influenced by conditional expression of the transcription factors HNF6, HNF4α and HNF1β in a pancreatic β-cell line. *Nucleic Acids Research*, 32(19):1–12.

Thomas, P. D., Ebert, D., Muruganujan, A., Mushayahama, T., Albou, L.-P., and Mi, H. (2022). PANTHER: Making genome-scale phylogenetics accessible to all. *Protein Science*, 31(1):8–22.

Torres, J. Z., Miller, J. J., and Jackson, P. K. (2009). High-throughput generation of tagged stable cell lines for proteomic analysis. *Proteomics*, 9(10):2888–2891.

Townley-Tilson, W. H. D., Pendergrass, S. A., Marzluff, W. F., and Whitfield, M. L. (2006). Genome-wide analysis of mRNAs bound to the histone stem-loop binding protein. *RNA*, 12(10):1853–1867.

Trujillo, K. M. and Osley, M. A. (2012). A role for H2B ubiquitylation in DNA replication. *Molecular Cell*, 48(5):734–746.

Tubbs, A. and Nussenzweig, A. (2017). Endogenous DNA damage as a source of genomic instability in cancer. *Cell*, 168(4):644–656.

Turco, E., Gallego, L. D., Schneider, M., and Köhler, A. (2015). Monoubiquitination of histone H2B is intrinsic to the Bre1 RING domain-Rad6 interaction and augmented by a second Rad6-binding site on Bre1. *Journal of Biological Chemistry*, 290(9):5298–5310.

Turner, K. J., Hoyle, J., Valdivia, L. E., Cerveny, K. L., Hart, W., Mangoli, M., Geisler, R., Rees, M., Houart, C., Poole, R. J., Wilson, S. W., and Gestri, G. (2019). Abrogation of stem loop binding protein (Slbp) function leads to a failure of cells to transition from proliferation to differentiation, retinal coloboma and midline axon guidance deficits. *PLOS ONE*, 14(1):1–24.

Van Roey, K., Uyar, B., Weatheritt, R. J., Dinkel, H., Seiler, M., Budd, A., Gibson, T. J., and Davey, N. E. (2014). Short linear motifs: ubiquitous and functionally diverse protein interaction modules directing cell regulation. *Chemical Reviews*, 114(13):6733–6778.

von Moeller, H., Lerner, R., Ricciardi, A., Basquin, C., Marzluff, W. F., and Conti, E. (2013). Structural and biochemical studies of SLIP1-SLBP identify DBP5 and eIF3g as SLIP1-binding proteins. *Nucleic Acids Research*, 41(16):7960–7971.

Wagner, E. J., Berkow, A., and Marzluff, W. F. (2005). Expression of an RNAi-resistant SLBP restores proper S-phase progression. *Biochemical Society Transactions*, 33(Pt 3):471–473.

Walther, T. N., Wittop Koning, T. H., Schümperli, D., and Müller, B. (1998). A 5'-3' exonuclease activity involved in forming the 3' products of histone pre-mRNA processing *in vitro*. *RNA*, 4(9):1034–1046.

Wang, J., Wu, M., Huang, X., Wang, L., Zhang, S., Liu, H., and Zheng, J. (2022). SynLethDB 2.0: a web-based knowledge graph database on synthetic lethality for novel anticancer drug discovery. *Database*, 2022.

Wang, Z. F., Whitfield, M. L., Ingledue, T. C. r., Dominski, Z., and Marzluff, W. F. (1996). The protein that binds the 3' end of histone mRNA: a novel RNA-binding protein required for histone pre-mRNA processing. *Genes & Development*, 10(23):3028–3040.

Ward, I. M. and Chen, J. (2001). Histone H2AX is phosphorylated in an ATR-dependent manner in response to replicational stress. *Journal of Biological Chemistry*, 276(51):47759–47762.

Ward, R. J., Alvarez-Curto, E., and Milligan, G. (2011). Using the Flp-In™ T-Rex™ system to regulate GPCR expression. *Methods in Molecular Biology*, pages 21–37.

Whitfield, M. L., Zheng, L. X., Baldwin, A., Ohta, T., Hurt, M. M., and Marzluff, W. F. (2000). Stem-loop binding protein, the protein that binds the 3' end of histone mRNA, is cell cycle regulated by both translational and posttranslational mechanisms. *Molecular and Cellular Biology*, 20(12):4188–4198.

Wilhelm, T., Magdalou, I., Barascu, A., Técher, H., Debatisse, M., and Lopez, B. S. (2014). Spontaneous slow replication fork progression elicits mitosis alterations in homologous recombination-deficient mammalian cells. *Proceedings of the National Academy of Sciences of the United States of America*, 111(2):763–768.

Wilkins, M. R., Gasteiger, E., Bairoch, A., Sanchez, J. C., Williams, K. L., Appel, R. D., and Hochstrasser, D. F. (2005). Protein identification and analysis tools in the ExPASy server. In J. M. Walker, editor, *The Proteomics Protocols Handbook*, volume 112 of *Springer Protocols Handbooks*, pages 531–552. Humana Press, Totowa, NJ, USA.

Wong, M. L. and Medrano, J. F. (2005). Real-time PCR for mRNA quantitation. *BioTechniques*, 39(1):75–85.

Yang, R., Gaidamakov, S. A., Xie, J., Lee, J., Martino, L., Kozlov, G., Crawford, A. K., Russo, A. N., Conte, M. R., Gehring, K., and Maraia, R. J. (2011). La-related protein 4 binds poly(A), interacts with the poly(A)-binding protein MLLE domain via a variant PAM2w motif, and can promote mRNA stability. *Molecular and Cellular Biology*, 31(3):542–556.

Yang, X.-C., Burch, B. D., Yan, Y., Marzluff, W. F., and Dominski, Z. (2009). FLASH, a proapoptotic protein involved in activation of caspase-8, is essential for 3' end processing of histone pre-mRNAs. *Molecular Cell*, 36(2):267–278.

Yoon, H., Dehart, J. P., Murphy, J. M., and Lim, S.-T. S. (2015). Understanding the roles of FAK in cancer: inhibitors, genetic models, and new insights. *Journal of Histochemistry & Cytochemistry*, 63(2):114–128.

Zeman, M. K. and Cimprich, K. A. (2014). Causes and consequences of replication stress. *Nature Cell Biology*, 16(1):2–9.

Zhao, J., Kennedy, B. K., Lawrence, B. D., Barbie, D. A., Matera, A. G., Fletcher, J. A., and Harlow, E. (2000). NPAT links cyclin E-Cdk2 to the regulation of replication-dependent histone gene transcription. *Genes & Development*, 14(18):2283–2297.

Zhao, X., McKillop-Smith, S., and Müller, B. (2004). The human histone gene expression regulator HBP/SLBP is required for histone and DNA synthesis, cell cycle progression and cell proliferation in mitotic cells. *Journal of Cell Science*, 117(25):6043–6051.

Zheng, L., Dominski, Z., Yang, X.-C., Elms, P., Raska, C. S., Borchers, C. H., and Marzluff, W. F. (2003). Phosphorylation of stem-loop binding protein (SLBP) on two threonines triggers degradation of SLBP, the sole cell cycle-regulated factor required for regulation of histone mRNA processing, at the end of S phase. *Molecular and Cellular Biology*, 23(5):1590–1601.

Zhou, B.-B. S. and Elledge, S. J. (2000). The DNA damage response: putting checkpoints in perspective. *Nature*, 408(6811):433–439.

Zhou, H., Di Palma, S., Preisinger, C., Peng, M., Polat, A. N., Heck, A. J. R., and Mohammed, S. (2013). Toward a comprehensive characterization of a human cancer cell phosphoproteome. *Journal of Proteome Research*, 12(1):260–271.

Appendices

A Recipes

Medium	Components
T-REx HeLa cell culture medium	450 ml Dulbecco's Modified Eagle's Culture Medium (DMEM) 50 ml (10%) Foetal bovine serum (FBS) 5 ml penicillin / streptomycin solution 2 ml hygromycin B
2× freezing medium	90% FBS 10% Dimethyl sulfoxide (DMSO)
Buffers	**Components**
1× RIPA buffer	20 mM Tris-HCl (pH 7.5) 150 mM NaCl 1 mM EDTA 1 mM EGTA 1% (v/v) NP-40 substitute 1% (w/v) sodium deoxycholate 2.5 mM sodium pyrophosphate 1 mM β-glycerophosphate 1 mM sodium orthovanadate + 1× protease inhibitor cocktail before use
1× A2220 immunoprecipitation buffer	50 mM Tris-HCl (pH 7.5) 150 mM NaCl 1 mM EDTA 1% (v/v) Triton X-100 1 mM β-glycerophosphate 1 mM sodium orthovanadate + 1× protease inhibitor cocktail before use
25× protease inhibitor cocktail	1 x Complete Mini EDTA-free protease inhibitor cocktail tablet 2 mL phosphate-buffered saline (PBS)

Buffers	Components
4X SDS-PAGE loading buffer	100 mM Tris-HCl (pH 6.8) 4% (w/v) sodium dodecyl sulphate (SDS) 20% (v/v) glycerol 400 mM dithiothreitol (DTT)
1× SDS-PAGE running buffer	25 mM Tris-HCl (pH 8.3) 192 mM glycine 0.1% (w/v) SDS
1× gel transfer buffer	25 mM Tris-HCl (pH 8.3) 192 mM glycine 20% (v/v) methanol
1× Tris-buffered saline (TBS)	20 mM Tris-HCl (pH 7.4) 137 mM NaCl
1× Tris-buffered saline + Tween-20 (TBST)	20 mM Tris-HCl (pH 7.4) 137 mM NaCl 0.1% (v/v) Tween-20
1× Western blot blocking buffer	1× TBS 5% (w/v) skimmed milk powder or BSA
1× Western blot antibody buffer	1× TBST 5% (w/v) skimmed milk powder or BSA
1× Western blot wash buffer	1× TBST 5% (w/v) skimmed milk powder or BSA
1× Tris-acetate EDTA (TAE)	40 mM Tris-acetate 20 mM acetic acid 0.5 mM EDTA (pH 8.0)
5× DNA loading buffer	0.25% (w/v) bromophenol blue 0.25% (w/v) xylene cyanol FF 30% (v/v) glycerol

N.B. All solutions made with distilled water (dH_2O) unless otherwise stated.

B FLAG-SLBP^{WT} cDNA sequence

```
  1 ATGGATTACA AGGATGACGA TGACAAGCTG GCCTGCCGCC CGCGAAGCCC
 51 GCCGAGGCAT CAGAGCCGCT GCGACGGTGA CGCCAGCCCG CCGTCCCCCG
101 CGCGATGGAG CCTGGGACGG AAGCGCAGAG CCGACGGCAG GCGCTGGAGG
151 CCCGAAGACG CCGAGGAGGC AGAGCACCGC GGCGCCGAGC GCAGACCCGA
201 GAGCTTTACC ACTCCTGAAG GCCCTAAACC CCGTTCCAGA TGCTCTGACT
251 GGGCAAGTGC AGTTGAAGAA GATGAAATGA GGACCAGAGT TAACAAAGAA
301 ATGGCAAGAT ATAAAAGGAA ACTCCTCATC AATGACTTTG GAAGAGAGAG
351 AAAATCATCA TCAGGAAGTT CTGATTCAAA GGAGTCTATG TCTACTGTGC
401 CGGCTGACTT TGAGACAGAT GAAAGTGTCC TAATGAGGAG ACAGAAGCAG
451 ATCAACTATG GGAAGAACAC AATTGCCTAC GATCGTTATA TTAAAGAAGT
501 CCCAAGACAC CTTCGACAAC CTGGCATTCA TCCCAAGACC CCTAATAAAT
551 TTAAGAAGTA TAGTCGACGT TCATGGGACC AGCAAATCAA ACTCTGGAAG
601 GTGGCTCTGC ATTTTTGGGA TCCTCCAGCG GAAGAAGGAT GTGATTTGCA
651 AGAAATACAC CCTGTAGACC TTGAATCTGC AGAAAGCAGC TCCGAGCCCC
701 AGACCAGCTC TCAGGATGAC TTTGATGTGT ACTCTGGCAC ACCCACCAAG
751 GTGAGACACA TGGACAGTCA AGTGGAGGAT GAGTTTGATT TGGAAGCTTG
801 TTTAACTGAA CCCTTGAGAG ACTTCTCAGC CATGAGCTAA
```

N.B. FLAG tag sequence is highlighted in green.

C FLAG-SLBP^{siRes} cDNA sequence

```
  1 ATGGATTACA AGGATGACGA TGACAAGCTG GCCTGCCGCC CGCGAAGCCC
 51 GCCGAGGCAT CAGAGCCGCT GCGACGGTGA CGCCAGCCCG CCGTCCCCCG
101 CGCGATGGAG CCTGGGACGG AAGCGCAGAG CCGACGGCAG GCGCTGGAGG
151 CCCGAAGACG CCGAGGAGGC AGAGCACCGC GGCGCCGAGC GCAGACCCGA
201 GAGCTTTACC ACTCCTGAAG GCCCTAAACC CCGTTCCAGA TGCTCTGACT
251 GGGCAAGTGC AGTTGAAGAA GATGAAATGA GGACCAGAGT TAACAAAGAA
301 ATGGCAAGAT ATAAAAGGAA ACTCCTCATC AATGACTTTG GAAGGGAGCG
351 AAAATCATCA TCAGGAAGTT CTGATTCAAA GGAGTCTATG TCTACTGTGC
401 CGGCTGACTT TGAGACAGAT GAAAGTGTCC TAATGAGGAG ACAGAAGCAG
451 ATCAACTATG GGAAGAACAC AATTGCCTAC GATCGTTATA TTAAAGAAGT
501 CCCAAGACAC CTTCGACAAC CTGGCATTCA TCCCAAGACC CCTAATAAAT
551 TTAAGAAGTA TAGTCGACGT TCATGGGACC AGCAAATCAA ACTCTGGAAG
601 GTGGCTCTGC ATTTTTGGGA TCCTCCAGCG GAAGAAGGAT GTGATTTGCA
651 AGAAATACAC CCTGTAGACC TTGAATCTGC AGAAAGCAGC TCCGAGCCCC
701 AGACCAGCTC TCAGGATGAC TTTGATGTGT ACTCTGGCAC ACCCACCAAG
751 GTGAGACACA TGGACAGTCA AGTGGAGGAT GAGTTTGATT TGGAAGCTTG
801 TTTAACTGAA CCCTTGAGAG ACTTCTCAGC CATGAGCTAA
```

N.B. FLAG tag sequence is highlighted in green. Two silent mutations (A345G and A349C) conferring siRNA resistance are highlighted in yellow.

D FLAG-SLBP^{siRes} LC-MS/MS data

Accession number	Protein	Gene ID	Rel. Intensity
G3V279	Enhancer of rudimentary homolog	ERH	8.559
E7EX17	Eukaryotic translation initiation factor 4B	EIF4B	3.705
P54105	Methylosome subunit pICln	CLNS1A	3.423
P59044	NLR Family Pyrin Domain Containing 6	NLRP6	1.905
Q60FE5	Filamin-A	FLNA	1.748
P63220	40S ribosomal protein S21	RPS21	1.283
H3BT13	Small nuclear ribonucleoprotein Sm D3	SNRPD3	1.228
H0YN88	40S ribosomal protein S17	RPS17	1.121
F8W8D3	Histone RNA hairpin-binding protein	SLBP	1
P25398	40S ribosomal protein S12	RPS12	0.865
K7ENH0	Eukaryotic translation initiation factor 3 subunit G	EIF3G	0.812
A0A087WVQ9	Elongation factor 1-alpha 1;Putative elongation factor 1-alpha-like 3	EEF1A1	0.806
Q9Y2W1	Thyroid hormone receptor-associated protein 3	THRAP3	0.766
A0A0D9SF54	Spectrin alpha chain	SPTAN1	0.724
Q9BRS2	Serine/threonine-protein kinase RIO1	RIOK1	0.663
Q15233	Non-POU domain-containing octamer-binding protein	NONO	0.662
G3V153	**Caprin-1**	**CAPRIN1**	0.652
A0A0A0MR52	Eukaryotic translation initiation factor 4 gamma 1	EIF4G1	0.466
P62158	Calmodulin	CALM1	0.413
Q13501	Sequestosome-1	SQSTM1	0.412
P67936	Tropomyosin alpha-4 chain;Tropomyosin alpha-3 chain	TPM4	0.404
P19338	**Nucleolin**	**NCL**	0.326
E7EPK0	LIM and calponin homology domains-containing protein 1	LIMCH1	0.31
P24534	Elongation factor 1-beta	EEF1B2	0.3
Q15208	Serine/threonine-protein kinase 38	STK38	0.297
Q580R0	Uncharacterized protein C2orf27	C2orf27A	0.294
P62857	40S ribosomal protein S28	RPS28	0.29
F8VQE1	LIM domain and actin-binding protein 1	LIMA1	0.27
P98179	RNA-binding protein 3	RBM3	0.267
O00303	Eukaryotic translation initiation factor 3 subunit F	EIF3F	0.254
A8MT87	Phenylethanolamine N-methyltransferase	PNMT	0.246
H3BTP7	60S ribosomal protein L4	RPL4	0.24
E9PPJ0	Splicing factor 3B subunit 2	SF3B2	0.237
P30050	60S ribosomal protein L12	RPL12	0.233
Q9NQ92	Coordinator of PRMT5 and differentiation stimulator	COPRS	0.231
P63261	Actin	ACTG1	0.23
E9PK09	Bcl-2-associated transcription factor 1	BCLAF1	0.229
H0Y711	Methylosome protein 50	WDR77	0.229
A0A087WUZ3	Spectrin beta chain	SPTBN1	0.221
H7C3A1	**Serrate RNA effector molecule homolog**	**SRRT**	0.216
H0Y9X0	Protein furry homolog-like	FRYL	0.214

Accession number	Protein names	Gene ID	Rel. Abundance
H0YJD3	Protein arginine N-methyltransferase 5;Protein arginine N-methyltransferase 5	PRMT5	0.212
B1ALA7	Ribose-phosphate pyrophosphokinase 1;Ribose-phosphate pyrophosphokinase 3	PRPS1	0.205
Q14152	Eukaryotic translation initiation factor 3 subunit A	EIF3A	0.204
X6RLN4	**La-related protein 4**	**LARP4**	0.198
O43852	Calumenin	CALU	0.196
E5RH50	La-related protein 1	LARP1	0.195
P35579	Myosin-9	MYH9	0.186
D6R9B6	40S ribosomal protein S3a	RPS3A	0.179
Q9P219	Protein Daple	CCDC88C	0.176
E9PQZ1	Elongation factor 1-delta	EEF1D	0.174
H3BRC9	Lysine–tRNA ligase	KARS	0.173
A0A087X2B6	Cell cycle and apoptosis regulator protein 2	CCAR2	0.172
J3KSR8	Serine/arginine-rich splicing factor 1	SRSF1	0.164
Q15459	Splicing factor 3A subunit 1	SF3A1	0.163
K7EKJ7	Polypyrimidine tract-binding protein 1	PTBP1	0.159
A0A087WUK2	Heterogeneous nuclear ribonucleoprotein D-like	HNRNPDL	0.138
O43167	Zinc finger and BTB domain-containing protein 24	ZBTB24	0.138
P19474	E3 ubiquitin-protein ligase TRIM21	TRIM21	0.134
F8WJN3	Cleavage and polyadenylation specificity factor subunit 6	CPSF6	0.131
Q8NC51	**Plasminogen activator inhibitor 1 RNA-binding protein**	**SERBP1**	0.13
A0A0A0MR66	RNA-binding protein 10	RBM10	0.129
P00558	Phosphoglycerate kinase 1	PGK1	0.127
E7EWK3	**ATP-dependent RNA helicase DHX36**	**DHX36**	0.125
K7EML2	RNA-binding protein 42	RBM42	0.125
A0A0C4DGV5	Zinc finger Ran-binding domain-containing protein 2	ZRANB2	0.125
Q5VZU9	Tripeptidyl-peptidase 2	TPP2	0.121
P41567	Eukaryotic translation initiation factor 1	EIF1	0.12
H3BV01	Pre-mRNA-splicing factor ATP-dependent RNA helicase PRP16	DHX38	0.119
A6NMS2	Ribose-phosphate pyrophosphokinase 2	PRPS2	0.118
P55072	Transitional endoplasmic reticulum ATPase	VCP	0.115
A0A0J9YVV8	Microtubule-associated protein;Microtubule-associated protein 4	MAP4	0.113
H3BQC6	Ubiquitin carboxyl-terminal hydrolase 10	USP10	0.108
Q15293	Reticulocalbin-1	RCN1	0.103
C9JL25	60 kDa heat shock protein	HSPD1	0.102
O75643	U5 small nuclear ribonucleoprotein 200 kDa helicase	SNRNP200	0.101
F6UXX1	Heterogeneous nuclear ribonucleoprotein Q	SYNCRIP	0.099
Q9UH99	SUN domain-containing protein 2	SUN2	0.099
Q9BUA3	Spindlin Interactor And Repressor Of Chromatin Binding	SPINDOC	0.097
P00966	Argininosuccinate synthase	ASS1	0.09
H0Y8R1	**G-rich sequence factor 1**	**GRSF1**	0.076
G3V1Y7	Myosin light polypeptide 6	MYL6	0.07
P11021	78 kDa glucose-regulated protein	HSPA5	0.069
P55884	Eukaryotic translation initiation factor 3 subunit B	EIF3B	0.069

Accession number	Protein names	Gene ID	Rel. Abundance
A0A0U1RQV4	Rho-associated protein kinase 1	ROCK1	0.067
G3V4Y7	Kinectin	KTN1	0.064
Q99459	**Cell division cycle 5-like protein**	**CDC5L**	0.063
P53618	Coatomer subunit beta	COPB1	0.063
H0YEV2	Src substrate cortactin	CTTN	0.06
F8W0U6	Dynactin subunit 2	DCTN2	0.055
Q5W0B1	RING finger protein 219	RNF219	0.055
Q5T4S7	E3 ubiquitin-protein ligase UBR4	UBR4	0.049
Q07065	**Cytoskeleton-associated protein 4**	**CKAP4**	0.044
C9JHK9	ATP-binding cassette sub-family F member 2	ABCF2	0.043
E7ENZ3	T-complex protein 1 subunit epsilon	CCT5	0.033
A0A0G2JQJ7	Microtubule-associated protein tau	MAPT	0.029
Q01804	OTU domain-containing protein 4	OTUD4	0.029
Q06323	Proteasome activator complex subunit 1	PSME1	0.024
A0A087X0K8	Probable G-protein coupled receptor 179	GPR179	0.021

FLAG-SLBP^{siRes} interacting proteins identified by LC-MS/MS. List of 98 proteins identified in LC-MS/MS analysis of a single FLAG-SLBP^{siRes} immunoprecipitation eluate digested with Glu-C for 4 hours ranked by ion intensity of the most abundant peptide from the identified protein relative to the ion intensity of the most abundant SLBP peptide. Shaded red are proteins identified in control affinity purification experiments using α-FLAG M2 affinity agarose gel analysed by mass spectrometry and are considered as contaminants (Mellacheruvu et al., 2013). SLBP is highlighted in yellow. In bold text are proteins identified as FLAG-SLBP^{WT} interactors in Panomwan (2017).